2. Spatial Pattern Formation with Reaction Diffusion Systems

2.1 Role of Pattern in Biology

Embryology is that part of biology which is concerned with the formation and development of the embryo from fertilization until birth. Development of the embryo is a sequential process and follows a ground plan, which is usually laid down very early in gestation. In humans, for example, it is set up roughly by the 5th week. There are many books on the subject; the one by Slack (1983) is a readable account of the early stages of development from egg to embryo. Morphogenesis, the part of embryology with which we are mainly concerned, is the development of pattern and form. How the developmental ground plan is established is unknown as are the mechanisms which produce the spatial patterning necessary for specifying the various organs.[1]

The following chapters and most of this one will be devoted to mechanisms which can generate spatial pattern and form, and which have been proposed as possible pattern formation processes in a variety of developmental situations. Wave phenomena create spatial patterns, of course, but these are spatio-temporal patterns. Here we shall be concerned with the formation of steady state spatially heterogeneous spatial patterns. In this chapter we introduce and analyse reaction diffusion pattern formation mechanisms mainly with developmental biology in mind. Section 2.7, however, is concerned with an ecological aspect of pattern formation, which suggests a possible strategy for pest control—the mathematical analysis is different but directly relevant to many embryological situations.

The questions we would like to answer, or, more realistically, get any enlightenment about, are legion. For example, are there any general patterning principles that are shared by bacteria, which can form complex patterns and wolf packs when they mark

[1] Professor Jean-Pierre Aubin in his book on *Mutational and Morphological Analysis* notes that the adjective *morphological* is due to Goethe (1749–1832). Goethe spent a lot of time thinking and writing about biology (the discipline 'biology' dates from 1802). Aubin goes on to describe Goethe's theory of plant evolution that hypothesizes that most plants come from one archetypal plant. Except for Geoffroy St. Hilaire, a distinguished early 19th century French biologist who wrote extensively about teratologies, or monsters (see Chapter 7), it was not taken seriously. Goethe was very bitter about it and complained about the difficulties in trying to work in a discipline other than one's own: it is still a problem. Goethe's work had some reevaluation in the 20th century, primarily by historians of science (see, for example, Lenoir 1984, Brady 1984 and other references there).

out territory? Spatial patterns are ubiquitous in the biomedical sciences and understanding how they are formed is without question one of the major fundamental scientific challenges. In the rest of the book we shall study a variety of pattern formation mechanisms which generate pattern in a variety of diverse areas.

Cell division starts after fertilisation. When sufficient cell division has taken place in a developing embryo the key problem is how the homogeneous mass of cells are spatially organised so that the sequential process of development can progress. Cells differentiate, in a biological sense, according to where they are in the spatial organisation. They also move around in the embryo. This latter phenomenon is an important element in morphogenesis and has given rise to a new approach to the generation of pattern and form discussed in some detail in Chapter 6.

It is impossible not to be fascinated and enthralled with the wealth, diversity and beauty of pattern in biology. Figure 2.1 shows only four examples. How such patterns, and millions of others, were laid down is still unknown although considerable progress has been made in several different fronts such as in the early patterning in the embryo of the fruit fly, spatial patterning in slime moulds and bacterial patterns discussed in Chapter 5. The patterning problems posed by only the few patterns in Figure 2.1 are quite diverse.

As a footnote to Figure 2.1(c), note the antennae on the moth. These antennae very effectively collect molecules of the chemical odorant, called a pheromone called bombykol, which is exuded by the female to attract the male. In the case of the silk moth the male, which cannot fly, can detect the pheromone from the female as far away as a kilometre and can move up the concentration gradient towards the female. The filtering efficiency of such antennae, which collect, and in effect count, the molecules, poses a very different and interesting mathematical biology patterning problem to those discussed in this book, namely, how such a filter antenna should be designed to be most efficient. This specific problem—an interesting fluid mechanics and diffusion one—was discussed in detail by Murray (1977).

The fundamental importance of pattern and form in biology is self-evident. Our understanding is such that whatever pattern we observe in the animal world, it is almost certain that the process that produced it is still unknown. Pattern formation studies have often been criticized for their lack of inclusion of genes in the models. But then the criticism can be levelled at any modelling abstraction of a complex system to a relatively simple one. It should be remembered that the generation of pattern and form, particularly in development, is usually a long way from the level of the genome. Of course genes play crucial roles and the mechanisms must be genetically controlled; the genes, however, themselves cannot create the pattern. They only provide a blueprint or recipe, for the pattern generation. Many of the evolving patterns could hardly have been anticipated solely by genetic information. Another of the major problems in biology is how genetic information is physically translated into the necessary pattern and form. Much of the research in developmental biology, both experimental and theoretical, is devoted to trying to determine the underlying mechanisms which generate pattern and form in early development. The detailed discussion in these next few chapters discusses some of the mechanisms which have been proposed and gives an indication of the role of mathematical modelling in trying to unravel the underlying mechanisms involved in morphogenesis.

(a)

(b)

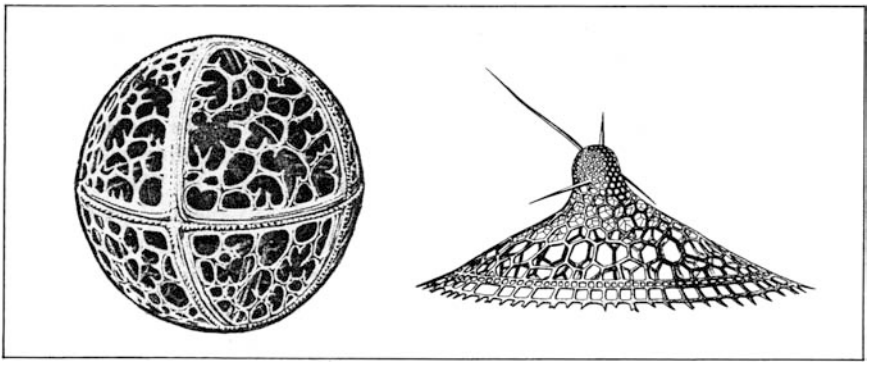

(c)

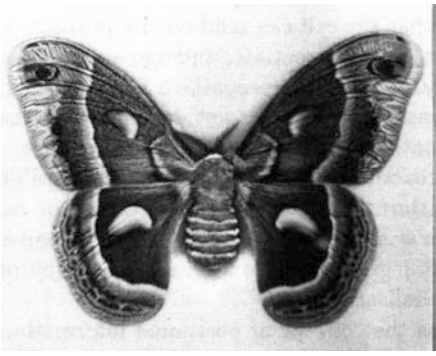

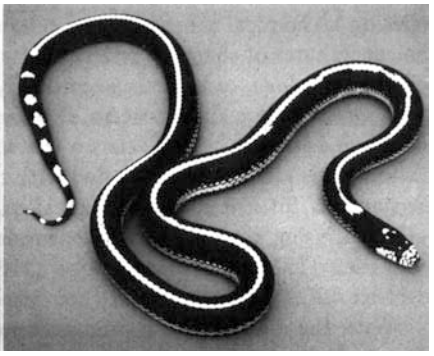

(d)

Figure 2.1. (**a**) Leopard (*Panthera pardus*) in the Serengeti National Park, Tanzania. Note the individual spot structure. (Photograph courtesy of Hans Kruuk) (**b**) Radiolarians (*Trissocyclus spaeridium* and *Eucecryphalus genbouri*). These are small marine organisms—protozoa—of the order of a millimeter across. (After Haekel 1862, 1887) The structural architecture of radiolarians is amazingly diverse (see, for example, the plate reproductions of some of Haeckel's drawings in the Dover Archive Series, Haeckel 1974, but see also the historical aside on Haeckel in Section 6.1). (**c**) Moth (*Hyalophora cecropia*). As well as the wing patterns note the stripe pattern on the body and the structure of the antennae. (**d**) California king snake. Sometimes the pattern consists of crossbands rather than a backstripe. (Photograph courtesy of Lloyd Lemke)

A phenomenological concept of pattern formation and differentiation called *positional information* was proposed by Wolpert (1969, see the reviews in 1971, 1981). He suggested that cells are preprogrammed to react to a chemical (or morphogen) concentration and differentiate accordingly, into different kinds of cells such as cartilage cells. The general introductory paper by Wolpert (1977) gives a very clear and nontechnical description of development of pattern and form in animals and the concepts and application of his positional information scenario. Although it is a phenomenological approach, with no actual mechanism involved it has given rise to an immense number of illuminating experimental studies, many associated with the development of the limb cartilage patterning in chick embryos and feather patterns on other bird embryos, such as the quail and guinea fowl (see, for example, Richardson et al. 1991 and references there). A literature search of positional information in development will produce an enormous number of references. Although it is a simple and attractive concept, which has resulted in significant advances in our knowledge of certain aspects of development, it is not a mechanism.

The chemical prepattern viewpoint of embryogenesis separates the process of development into several steps; the essential first step is the creation of a morphogen concentration spatial pattern. The name 'morphogen' is used for such a chemical because it effects morphogenesis. The notion of positional information relies on a chemical pre-specification so that the cell can read out its position in the coordinates of chemical concentration, and differentiate, undergo appropriate cell shape change, or migrate accordingly. So, once the prepattern is established, morphogenesis is a slave process. Positional information is not dependent on the specific mechanism which sets up the spatial prepattern of morphogen concentration. This chapter is concerned with reaction diffusion models as the possible mechanisms for generating biological pattern. The basic chemical theory or reaction diffusion theory of morphogenesis was put forward in the classical paper by Turing (1952). Reaction diffusion theory, which now has a vast literature, is a field of research in its own right.

With the complexity of animal forms the concept of positional information necessarily implies a very sophisticated interpretation of the 'morphogen map' by the cell. This need not pose any problem when we recall how immensely complex a cell is whether or not it is positional information or simply a cell responding in some way to small differences in chemical concentration. The scale of pattern that can be formed by reaction diffusion can be very small as seen in the experimental patterns shown in Figure 2.11. A very rough idea of cell complexity is given by comparing the weight per bit of information of the cell's DNA molecule (deoxyribonucleic acid) of around 10^{-22}, to that of, say, imaging by an electron beam of around 10^{-10} or of a magnetic tape of about 10^{-5}. The most sophisticated and compact computer chip is simply not in the same class as a cell.

An important point arising from theoretical models is that any pattern contains its own history. Consider the following simple engineering analogy (Murray et al. 1998) of our role in trying to understand a biological process. It is one thing to suggest that a bridge requires a thousand tons of steel, that any less will result in too weak a structure, and any more will result in excessive rigidity. It is quite another matter to instruct the workers on how best to put the pieces together. In morphogenesis, for example, it is conceivable that the cells involved in tissue formation and deformation have enough

expertise that given the right set of ingredients and initial instructions they could be persuaded to construct whatever element one wants. This is the hope of many who are searching for a full and predictive understanding. However, it seems very likely that the global effect of all this sophisticated cellular activity would be critically sensitive to the sequence of events occurring during development. As scientists we should concern ourselves with how to take advantage of the limited opportunities we have for communicating with the workforce so as to direct experiment towards an acceptable end-product.

None of the individual models that have been suggested for any biological patterning process, and not even all of them put together, could be considered a complete model. In the case of some of the widely studied problems (such as patterning in the developing limb bud), each model has shed light on different aspects of the process and we can now say what the important conceptual elements have to be in a complete model. These studies have served to highlight where our knowledge is deficient and to suggest directions in which fruitful experimentation might lead us. Indeed, a critical test of these theoretical constructs is in their impact on the experimental community.[2]

To conclude this section it must be stressed again that mathematical descriptions, including phenomenological descriptions, of patterning scenarios are *not* explanations. This is generally accepted, but often forgotten.

2.2 Reaction Diffusion (Turing) Mechanisms

Turing (1952) suggested that, under certain conditions, chemicals can react and diffuse in such a way as to produce steady state heterogeneous spatial patterns of chemical or morphogen concentration. In Chapter 11, Volume I we derived the governing equations for reaction diffusion mechanisms, namely, (11.16), which we consider here in the form:

$$\frac{\partial \mathbf{c}}{\partial t} = \mathbf{f}(\mathbf{c}) + D\nabla^2\mathbf{c}, \tag{2.1}$$

where $\mathbf{c}$ is the vector of morphogen concentrations, $\mathbf{f}$ represents the reaction kinetics and D is the diagonal matrix of positive constant diffusion coefficients. This chapter is mainly concerned with models for two chemical species, $A(\mathbf{r}, t)$ and $B(\mathbf{r}, t)$ say. The equation system is then of the form

$$\begin{aligned} \frac{\partial A}{\partial t} &= F(A, B) + D_A\nabla^2 A, \\ \frac{\partial B}{\partial t} &= G(A, B) + D_B\nabla^2 B, \end{aligned} \tag{2.2}$$

where F and G are the kinetics, which will always be nonlinear.

[2] In the case of the mechanical theory of pattern formation discussed later, after some discussion, Lewis Wolpert (a friend and colleague of many years) who did not believe in the mechanical theory of pattern formation, designed some experiments specifically to disprove the theory. Although the experiments did not in fact do so, he discovered something else about the biological process he was studying—patterning in the chick limb bud. The impact of the theory was biologically illuminating even if the motivation was not verification. As he freely admits, he would not have done these specific experiments had he not been stimulated (or rather provoked) to do so by the theory.

Turing's (1952) idea is a simple but profound one. He said that, if in the absence of diffusion (effectively $D_A = D_B = 0$), A and B tend to a linearly stable uniform steady state then, under certain conditions, which we shall derive, spatially inhomogeneous patterns can evolve by *diffusion driven instability* if $D_A \neq D_B$. Diffusion is usually considered a *stabilising* process which is why this was such a novel concept. To see intuitively how diffusion can be destablising consider the following, albeit unrealistic, but informative analogy.

Consider a field of dry grass in which there is a large number of grasshoppers which can generate a lot of moisture by sweating if they get warm. Now suppose the grass is set alight at some point and a flame front starts to propagate. We can think of the grasshopper as an inhibitor and the fire as an activator. If there were no moisture to quench the flames the fire would simply spread over the whole field which would result in a uniform charred area. Suppose, however, that when the grasshoppers get warm enough they can generate enough moisture to dampen the grass so that when the flames reach such a pre-moistened area the grass will not burn. The scenario for spatial pattern is then as follows. The fire starts to spread—it is one of the 'reactants,' the activator, with a 'diffusion' coefficient D_F say. When the grasshoppers, the inhibitor 'reactant,' ahead of the flame front feel it coming they move quickly well ahead of it; that is, they have a 'diffusion' coefficient, D_G say, which is much larger than D_F. The grasshoppers then sweat profusely and generate enough moisture to prevent the fire spreading into the moistened area. In this way the charred area is restricted to a finite domain which depends on the 'diffusion' coefficients of the reactants—fire and grasshoppers—and various 'reaction' parameters. If, instead of a single initial fire, there were a random scattering of them we can see how this process would result in a final spatially heterogeneous steady state distribution of charred and uncharred regions in the field and a spatial distribution of grasshoppers, since around each fire the above scenario would take place. If the grasshoppers and flame front 'diffused' at the same speed no such spatial pattern could evolve. It is clear how to construct other analogies; other examples are given below in Section 2.3 and another in the *Scientific American* article by Murray (1988).

In the following section we describe the process in terms of reacting and diffusing morphogens and derive the necessary conditions on the reaction kinetics and diffusion coefficients. We also derive the type of spatial patterns we might expect. Here we briefly record for subsequent use two particularly simple hypothetical systems and one experimentally realised example, which are capable of satisfying Turing's conditions for a pattern formation system. There are now many other systems which have been used in studies of spatial patterning. These have varying degrees of experimental plausibility. With the extensive discussion of the Belousov–Zhabotinskii reaction in Chapter 8, Volume I and the last chapter we should particularly note it. Even though many other real reaction systems have been found it is still the major experimental system.

The simplest system is the Schnakenberg (1979) reaction discussed in Chapter 7, Volume I which, with reference to the system form (2.2), has kinetics

$$\begin{aligned} F(A, B) &= k_1 - k_2 A + k_3 A^2 B, \\ G(A, B) &= k_4 - k_3 A^2 B, \end{aligned} \tag{2.3}$$

where the k's are the positive rate constants. Here A is created autocatalytically by the k_3A^2B term in $F(A, B)$. This is one of the prototype reaction diffusion systems. Another is the influential activator–inhibitor mechanism suggested by Gierer and Meinhardt (1972) and widely studied and used since then. Their system was discussed in Chapter 6, Volume I and is

$$F(A, B) = k_1 - k_2A + \frac{k_3A^2}{B}, \quad G(A, B) = k_4A^2 - k_5B, \tag{2.4}$$

where here A is the activator and B the inhibitor. The k_3A^2/B term is again autocatalytic. Koch and Meinhardt (1994) review the applications of the Gierer–Meinhardt reaction diffusion system to biological pattern formation of complex structures. They give an extensive bibliography of applications of this specific model and its variations.

The real empirical substrate-inhibition system studied experimentally by Thomas (1975) and also described in detail in Chapter 6, Volume I, has

$$\begin{aligned} &F(A, B) = k_1 - k_2A - H(A, B), \quad G(A, B) = k_3 - k_4B - H(A, B), \\ &H(A, B) = \frac{k_5AB}{k_6 + k_7A + k_8A^2}. \end{aligned} \tag{2.5}$$

Here A and B are respectively the concentrations of the substrate oxygen and the enzyme uricase. The substrate inhibition is evident in the H-term via k_8A^2. Since the H-terms are negative they contribute to reducing A and B; the rate of reduction is inhibited for large enough A. Reaction diffusion systems based on the Field–Körös–Noyes (FKN) model kinetics (cf. Chapter 8, Volume I) is a particularly important example because of its potential for experimental verification of the theory; references are given at the appropriate places below.

Before commenting on the types of reaction kinetics capable of generating pattern we must nondimensionalise the systems given by (2.2) with reaction kinetics from such as (2.3) to (2.5). By way of example we carry out the details here for (2.2) with F and G given by (2.3) because of its algebraic simplicity and our detailed analysis of it in Chapter 7, Volume I. Introduce L as a typical length scale and set

$$\begin{aligned} &u = A\left(\frac{k_3}{k_2}\right)^{1/2}, \quad v = B\left(\frac{k_3}{k_2}\right)^{1/2}, \quad t^* = \frac{D_At}{L^2}, \quad \mathbf{x}^* = \frac{\mathbf{x}}{L}, \\ &d = \frac{D_B}{D_A}, \quad a = \frac{k_1}{k_2}\left(\frac{k_3}{k_2}\right)^{1/2}, \quad b = \frac{k_4}{k_2}\left(\frac{k_3}{k_2}\right)^{1/2}, \quad \gamma = \frac{L^2k_2}{D_A}. \end{aligned} \tag{2.6}$$

The dimensionless reaction diffusion system becomes, on dropping the asterisks for algebraic convenience,

$$\begin{aligned} u_t &= \gamma(a - u + u^2v) + \nabla^2u = \gamma f(u, v) + \nabla^2u, \\ v_t &= \gamma(b - u^2v) + d\nabla^2v = \gamma g(u, v) + d\nabla^2v, \end{aligned} \tag{2.7}$$

where f and g are defined by these equations. We could incorporate γ into new length and timescales by setting $\gamma^{1/2}\mathbf{r}$ and γt for $\mathbf{r}$ and t respectively. This is equivalent to defining the length scale L such that $\gamma = 1$; that is, $L = (D_A/k_2)^{1/2}$. We retain the specific form (2.7) for reasons which become clear shortly as well as for the analysis in the next section and for the applications in the following chapters.

An appropriate nondimensionalisation of the reaction kinetics (2.4) and (2.5) give (see Exercise 1)

$$\begin{aligned} &f(u,v) = a - bu + \frac{u^2}{v}, \quad g(u,v) = u^2 - v, \\ &f(u,v) = a - u - h(u,v), \quad g(u,v) = \alpha(b - v) - h(u,v), \\ &h(u,v) = \frac{\rho u v}{1 + u + Ku^2}, \end{aligned} \tag{2.8}$$

where a, b, α, ρ and K are positive parameters. If we include activator inhibition in the activator–inhibitor system in the first of these we have, for f and g,

$$f(u,v) = a - bu + \frac{u^2}{v(1 + ku^2)}, \quad g(u,v) = u^2 - v, \tag{2.9}$$

where k is a measure of the inhibition; see also Section 6.7 in Chapter 6 in Volume I. Murray (1982) discussed each of these systems in detail and drew conclusions as to their relative merits as pattern generators; he presented a systematic analytical method for studying any two-species reaction diffusion system. For most pattern formation (analytical) illustrations with reaction diffusion mechanisms the simplest, namely, (2.7), turned out to be the most robust of those considered and, fortunately, the easiest to study.

All such reaction diffusion systems can be nondimensionalised and scaled to take the general form

$$u_t = \gamma f(u,v) + \nabla^2 u, \quad v_t = \gamma g(u,v) + d\nabla^2 v, \tag{2.10}$$

where d is the ratio of diffusion coefficients and γ can have any of the following interpretations.

- **(i)** $\gamma^{1/2}$ is proportional to the *linear* size of the spatial domain in one dimension. In two dimensions γ is proportional to the area. This meaning is particularly important as we shall see later in Section 2.5 and in Chapter 3.
- **(ii)** γ represents the relative strength of the reaction terms. This means, for example, that an increase in γ may represent an increase in activity of some rate-limiting step in the reaction sequence.
- **(iii)** An increase in γ can also be thought of as equivalent to a decrease in the diffusion coefficient ratio d.

Particular advantages of this general form are: (a) the dimensionless parameters γ and d admit a wider biological interpretation than do the dimensional parameters and (b) when we consider the domains in parameter space where particular spatial patterns appear, the results can be conveniently displayed in (γ, d) space. This aspect was exploited by Arcuri and Murray (1986).

Whether or not the systems (2.2) are capable of generating Turing-type spatial patterns crucially depends on the reaction kinetics f and g, and the values of γ and d. The detailed form of the null clines provides essential initial information. Figure 2.2 illustrates typical null clines for f and g defined by (2.7)–(2.9).

In spite of their different chemical motivation and derivation all of these kinetics are equivalent to some activation–inhibition interpretation and when coupled with unequal diffusion of the reactants, are capable of generating spatial patterns. The spatial activation–inhibition concept was discussed in detail in Section 11.5 in Chapter 11 in Volume I, and arose from an integral equation formulation: refer to equation (11.41) there. As we shall see in the next section the crucial aspect of the kinetics regarding pattern generation is incorporated in the form of the null clines and how they intersect in the vicinity of the steady state. There are two broad types illustrated in the last fig-

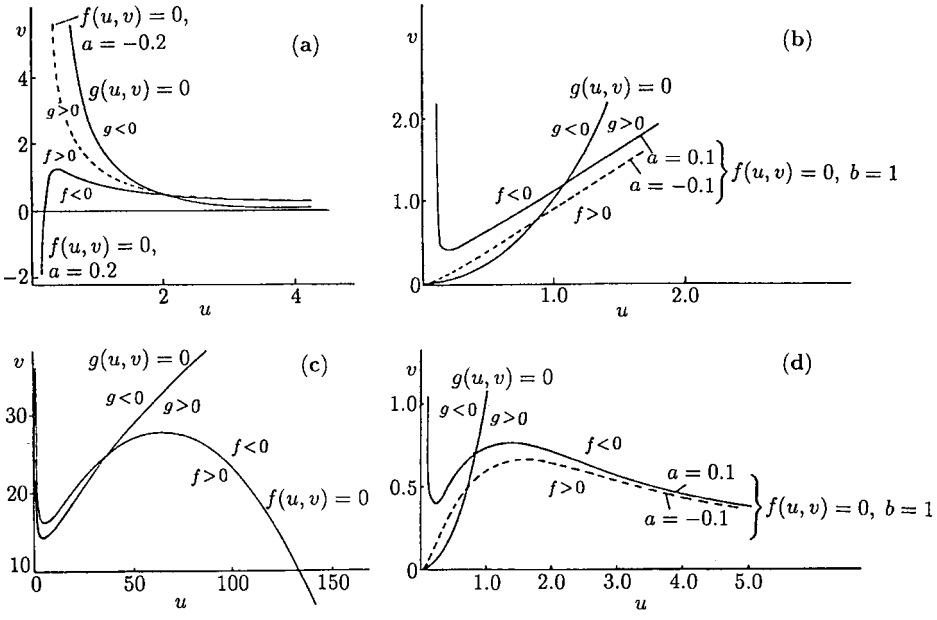

Figure 2.2. Null clines $f(u, v) = 0$, $g(u, v) = 0$: (**a**) The dimensionless Schnakenberg (1979) kinetics (2.7) with $a = 0.2$ and $b = 2.0$ with the dashed curve, where $a = -0.2$ and which is typical of the situation when $a < 0$. (**b**) The dimensionless Gierer and Meinhardt (1972) system with $a = \pm 0.1$, $b = 1$ and no activator inhibition. (**c**) The empirical Thomas (1975) system defined by (2.8) with parameter values $a = 150$, $b = 100$, $\alpha = 1.5$, $\rho = 13$, $K = 0.05$. (**d**) The kinetics in (2.9) with $a > 0$, $b > 0$ and $k > 0$, which implies activator inhibition; the dashed curve has $a < 0$.

ure. The steady state neighbourhood of the null clines in Figures 2.2(b), (c) and (d) are similar and represent one class, while that in Figure 2.2(a) is the other.

We should note here that there are other important classes of null clines which we do not consider, such as those in which there is more than one positive steady state; we discussed such kinetics in Chapter 7, Volume I for example. Reaction diffusion systems with such kinetics can generate even more complex spatial patterns: initial conditions here are particularly important. We also do not discuss here systems in which the diffusion coefficients are space-dependent and concentration- or population-dependent; these are important in ecological contexts (recall the discussion in Chapter 1 on the spread of genetically engineered organisms). We briefly considered density-dependent diffusion cases in Chapter 11, Volume I. Later in the book we discuss an important application in which the diffusion coefficient is space-dependent when we model the spread of brain tumours in anatomically realistic brains.

It is often useful and intuitively helpful in model building to express the mechanism's kinetics in schematic terms with some convention to indicate autocatalysis, activation, inhibition, degradation and unequal diffusion. If we do this, by way of illustration, with the activator–inhibitor kinetics given by the first of (2.8) in (2.10) we can adopt the convention shown in Figure 2.3(a).

The effect of different diffusion coefficients, here with $d > 1$, is to illustrate the prototype spatial concept of local activation and lateral inhibition illustrated in Figures 2.3(b) and 2.4(b). The general concept was introduced before in Chapter 11, Volume I. It is this generic spatial behaviour which is necessary for spatial patterning: the grasshoppers and the fire analogy is an obvious example with the fire the local activation and the grasshoppers providing the long range inhibition. It is intuitively clear that the diffusion coefficient of the inhibitor must be larger than that of the activator.

The concept of local activation and lateral inhibition is quite old going back at least to Ernst Mach in 1885 with his Mach bands. This is a visual illusion which occurs when dark and light bands are juxtaposed. Figure 2.4 is a schematic illustration of what happens together with an example of the Hermann illusion which is based on it.

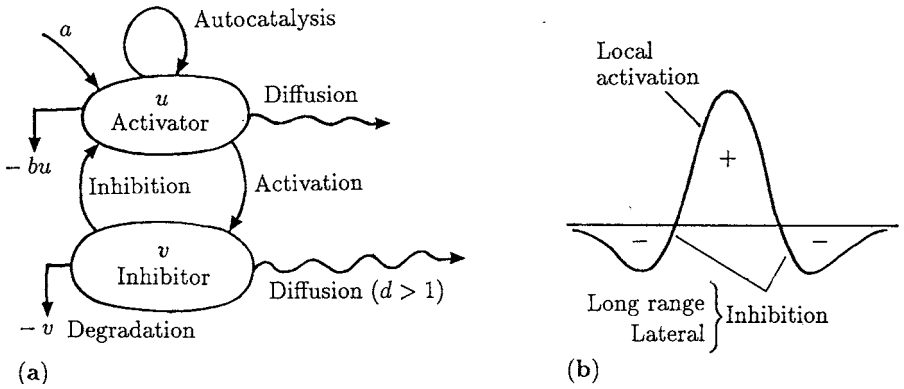

Figure 2.3. (**a**) Schematic representation of the activator–inhibitor system $u_t = a - bu + (u^2/v) + \nabla^2 u$, $v_t = u^2 - v + d\nabla^2 v$. (**b**) Spatial representation of local activation and long range inhibition.

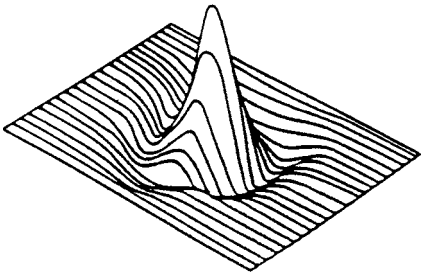

(a)

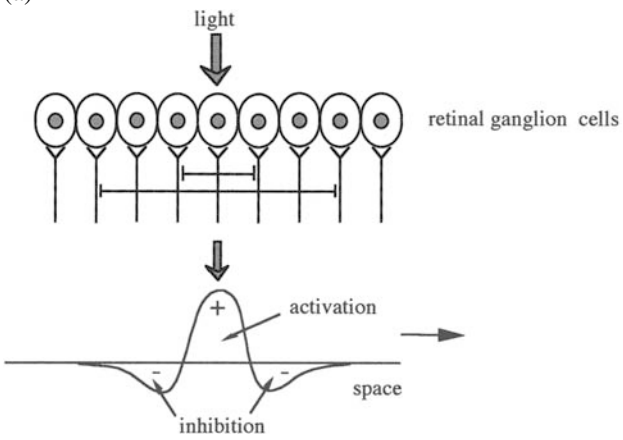

(b)

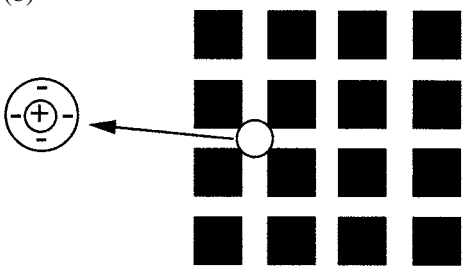

(c)

Figure 2.4. (**a**) If a light is shone on an array of retinal ganglion cells there is local activation of the cells in the immediate neighbourhood of the light with lateral inhibition of the cells farther away from the light source. The result is a landscape of local activation and lateral inhibition as illustrated in (**b**). (**c**) This illustrates the Hermann illusion. Here cells have more illumination in their inhibitory surrounding regions than cells in other white regions and so are more strongly inhibited and appear darker.

2.3 General Conditions for Diffusion-Driven Instability: Linear Stability Analysis and Evolution of Spatial Pattern

A reaction diffusion system exhibits diffusion-driven instability, sometimes called Turing instability, if the homogeneous steady state is stable to small perturbations in the absence of diffusion but unstable to small *spatial* perturbations when diffusion is present. The concept of instability in biology is often in the context of ecology, where a uniform steady state becomes unstable to small perturbations and the populations typically exhibit some temporal oscillatory behaviour. The instability we are concerned with here is of a quite different kind. The main process driving the spatially inhomogeneous instability is diffusion: the mechanism determines the spatial pattern that evolves. How the pattern or mode is selected is an important aspect of the analysis, a topic we discuss in this (and later) chapters.

We derive here the necessary and sufficient conditions for diffusion-driven instability of the steady state and the initiation of spatial pattern for the general system (2.10). To formulate the problem mathematically we require boundary and initial conditions. These we take to be zero flux boundary conditions and given initial conditions. The mathematical problem is then defined by

$$\begin{aligned} &u_t = \gamma f(u,v) + \nabla^2 u, \quad v_t = \gamma g(u,v) + d\nabla^2 v, \\ &(\mathbf{n}\cdot\nabla)\begin{pmatrix} u \\ v \end{pmatrix} = 0, \quad \mathbf{r} \text{ on } \partial B; \quad u(\mathbf{r},0),\ v(\mathbf{r},0) \text{ given}, \end{aligned} \tag{2.11}$$

where ∂B is the closed boundary of the reaction diffusion domain B and $\mathbf{n}$ is the unit outward normal to ∂B. There are several reasons for choosing zero flux boundary conditions. The major one is that we are interested in self-organisation of pattern; zero flux conditions imply no external input. If we imposed fixed boundary conditions on u and v the spatial patterning could be a direct consequence of the boundary conditions as we shall see in the ecological problem below in Section 2.7. In Section 2.4 we carry out the analysis for a specific one- and two-dimensional situation with the kinetics given by (2.7).

The relevant homogeneous steady state (u_0, v_0) of (2.11) is the positive solution of

$$f(u,v) = 0, \quad g(u,v) = 0. \tag{2.12}$$

Since we are concerned with *diffusion-driven* instability we are interested in linear instability of this steady state that is solely *spatially* dependent. So, in the absence of any spatial variation the homogeneous steady state must be linearly stable: we first determine the conditions for this to hold. These were derived in Chapter 3, Volume I but as a reminder and for notational completeness we briefly rederive them here.

With no spatial variation u and v satisfy

$$u_t = \gamma f(u,v), \quad v_t = \gamma g(u,v). \tag{2.13}$$

Linearising about the steady state (u_0, v_0) in exactly the same way as we did in Chapter 3, Volume I, we set

$$\mathbf{w} = \begin{pmatrix} u - u_0 \\ v - v_0 \end{pmatrix} \tag{2.14}$$

and (2.13) becomes, for $|\,\mathbf{w}\,|$ small,

$$\mathbf{w}_t = \gamma A\mathbf{w}, \quad A = \begin{pmatrix} f_u & f_v \\ g_u & g_v \end{pmatrix}_{u_0, v_0}, \tag{2.15}$$

where A is the stability matrix. From now on we take the partial derivatives of f and g to be evaluated at the steady state unless stated otherwise. We now look for solutions in the form

$$\mathbf{w} \propto e^{\lambda t}, \tag{2.16}$$

where λ is the eigenvalue. The steady state $\mathbf{w} = 0$ is linearly stable if $\mathrm{Re}\,\lambda < 0$ since in this case the perturbation $\mathbf{w} \to 0$ as $t \to \infty$. Substitution of (2.16) into (2.15) determines the eigenvalues λ as the solutions of

$$\begin{aligned} |\,\gamma A - \lambda I\,| &= \begin{vmatrix} \gamma f_u - \lambda & \gamma f_v \\ \gamma g_u & \gamma g_v - \lambda \end{vmatrix} = 0 \\ \Rightarrow \quad \lambda^2 - \gamma(f_u + g_v)\lambda + \gamma^2(f_u g_v - f_v g_u) &= 0, \end{aligned} \tag{2.17}$$

so

$$\lambda_1, \lambda_2 = \frac{1}{2}\gamma\left[(f_u + g_v) \pm \left\{(f_u + g_v)^2 - 4(f_u g_v - f_v g_u)\right\}^{1/2}\right]. \tag{2.18}$$

Linear stability, that is, $\mathrm{Re}\,\lambda < 0$, is guaranteed if

$$\mathrm{tr}\,A = f_u + g_v < 0, \quad |\,A\,| = f_u g_v - f_v g_u > 0. \tag{2.19}$$

Since (u_0, v_0) are functions of the parameters of the kinetics, these inequalities thus impose certain constraints on the parameters. Note that for all cases in Figure 2.2 in the neighbourhood of the steady state, $f_u > 0$, $g_v < 0$, and for Figure 2.2(a) $f_v > 0$, $g_u < 0$ while for Figure 2.2(b) to (d) $f_v < 0$, $g_u > 0$. So tr A and $|\,A\,|$ could be positive or negative: here we are only concerned with the conditions and parameter ranges which satisfy (2.19).

Now consider the full reaction diffusion system (2.11) and again linearise about the steady state, which with (2.14) is $\mathbf{w} = 0$, to get

$$\mathbf{w}_t = \gamma A\mathbf{w} + D\nabla^2\mathbf{w}, \quad D = \begin{pmatrix} 1 & 0 \\ 0 & d \end{pmatrix}. \tag{2.20}$$

To solve this system of equations subject to the boundary conditions (2.11) we first define $\mathbf{W}(\mathbf{r})$ to be the time-independent solution of the spatial eigenvalue problem defined by

$$\nabla^2\mathbf{W} + k^2\mathbf{W} = 0, \quad (\mathbf{n}\cdot\nabla)\mathbf{W} = 0 \quad \text{for} \quad \mathbf{r} \text{ on } \partial B, \tag{2.21}$$

where k is the eigenvalue. For example, if the domain is one-dimensional, say, $0 \le x \le a$, $\mathbf{W} \propto \cos(n\pi x/a)$ where n is an integer; this satisfies zero flux conditions at $x = 0$ and $x = a$. The eigenvalue in this case is $k = n\pi/a$. So, $1/k = a/n\pi$ is a measure of the wavelike pattern: the eigenvalue k is called the *wavenumber* and $1/k$ is proportional to the wavelength ω; $\omega = 2\pi/k = 2a/n$ in this example. From now on we shall refer to k in this context as the wavenumber. With finite domains there is a discrete set of possible wavenumbers since n is an integer.

Let $\mathbf{W}_k(\mathbf{r})$ be the eigenfunction corresponding to the wavenumber k. Each eigenfunction $\mathbf{W}_k$ satisfies zero flux boundary conditions. Because the problem is linear we now look for solutions $\mathbf{w}(\mathbf{r}, t)$ of (2.20) in the form

$$\mathbf{w}(\mathbf{r}, t) = \sum_k c_k e^{\lambda t}\mathbf{W}_k(\mathbf{r}), \tag{2.22}$$

where the constants c_k are determined by a Fourier expansion of the initial conditions in terms of $\mathbf{W}_k(\mathbf{r})$. λ is the eigenvalue which determines temporal growth. Substituting this form into (2.20) with (2.21) and cancelling $e^{\lambda t}$, we get, for each k,

$$\begin{aligned}\lambda\mathbf{W}_k &= \gamma A\mathbf{W}_k + D\nabla^2\mathbf{W}_k \\ &= \gamma A\mathbf{W}_k - Dk^2\mathbf{W}_k.\end{aligned}$$

We require nontrivial solutions for $\mathbf{W}_k$ so the λ are determined by the roots of the characteristic polynomial

$$|\,\lambda I - \gamma A + Dk^2\,| = 0.$$

Evaluating the determinant with A and D from (2.15) and (2.20) we get the eigenvalues $\lambda(k)$ as functions of the wavenumber k as the roots of

$$\begin{aligned}&\lambda^2 + \lambda[k^2(1+d) - \gamma(f_u + g_v)] + h(k^2) = 0, \\ &h(k^2) = dk^4 - \gamma(df_u + g_v)k^2 + \gamma^2|\,A\,|.\end{aligned} \tag{2.23}$$

The steady state (u_0, v_0) is linearly stable if both solutions of (2.23) have $\mathrm{Re}\,\lambda < 0$. We have already imposed the constraints that the steady state is stable in the absence of any spatial effects; that is, $\mathrm{Re}\,\lambda(k^2 = 0) < 0$. The quadratic (2.23) in this case is (2.17) and the requirement that $\mathrm{Re}\,\lambda < 0$ gave conditions (2.19). For the steady state to be unstable to *spatial* disturbances we require $\mathrm{Re}\,\lambda(k) > 0$ for some $k \neq 0$. This can happen if either the coefficient of λ in (2.23) is negative, or if $h(k^2) < 0$ for some $k \neq 0$. Since $(f_u + g_v) < 0$ from conditions (2.19) and $k^2(1+d) > 0$ for all $k \neq 0$ the

coefficient of λ, namely,

$$[k^2(1+d) - \gamma(f_u + g_v)] > 0,$$

so the only way $\mathrm{Re}\,\lambda(k^2)$ can be positive is if $h(k^2) < 0$ for some k. This is immediately clear from the solutions of (2.23), namely,

$$2\lambda = -[k^2(1+d) - \gamma(f_u + g_v)] \pm \{[k^2(1+d) - \gamma(f_u + g_v)]^2 - 4h(k^2)\}^{1/2}.$$

Since we required the determinant $|A| > 0$ from (2.19) the only possibility for $h(k^2)$ in (2.23) to be negative is if $(df_u + g_v) > 0$. Since $(f_u + g_v) < 0$ from (2.19) this implies that $d \neq 1$ and f_u and g_v must have opposite signs. So, a further requirement to those in (2.19) is

$$df_u + g_v > 0 \quad \Rightarrow \quad d \neq 1. \tag{2.24}$$

With the reaction kinetics giving the null clines in Figure 2.2 we noted that $f_u > 0$ and $g_v < 0$, so the first condition in (2.19) and the last inequality (2.24) require that the diffusion coefficient ratio $d > 1$. For example, in terms of the activator–inhibitor mechanism (2.8) this means that the inhibitor must diffuse faster than the activator as we noted above.

The inequality (2.24) is necessary but not sufficient for $\mathrm{Re}\,\lambda > 0$. For $h(k^2)$ to be negative for some nonzero k, the minimum $h_{\min}$ must be negative. From (2.23), elementary differentiation with respect to k^2 shows that

$$h_{\min} = \gamma^2 \left[|A| - \frac{(df_u + g_v)^2}{4d} \right], \quad k^2 = k_m^2 = \gamma \frac{df_u + g_v}{2d}. \tag{2.25}$$

Thus the condition that $h(k^2) < 0$ for some $k^2 \neq 0$ is

$$\frac{(df_u + g_v)^2}{4d} > |A|. \tag{2.26}$$

At bifurcation, when $h_{\min} = 0$, we require $|A| = (df_u + g_v)^2/4d$ and so for fixed kinetics parameters this defines a critical diffusion coefficient ratio $d_c(> 1)$ as the appropriate root of

$$d_c^2 f_u^2 + 2(2f_v g_u - f_u g_v) d_c + g_v^2 = 0. \tag{2.27}$$

The critical wavenumber k_c is then given (using (2.26)) by

$$k_c^2 = \gamma \frac{d_c f_u + g_v}{2d_c} = \gamma \left[\frac{|A|}{d_c} \right]^{1/2} = \gamma \left[\frac{f_u g_v - f_v g_u}{d_c} \right]^{1/2}. \tag{2.28}$$

Figure 2.5(a) shows how $h(k^2)$ varies as a function of k^2 for various d.

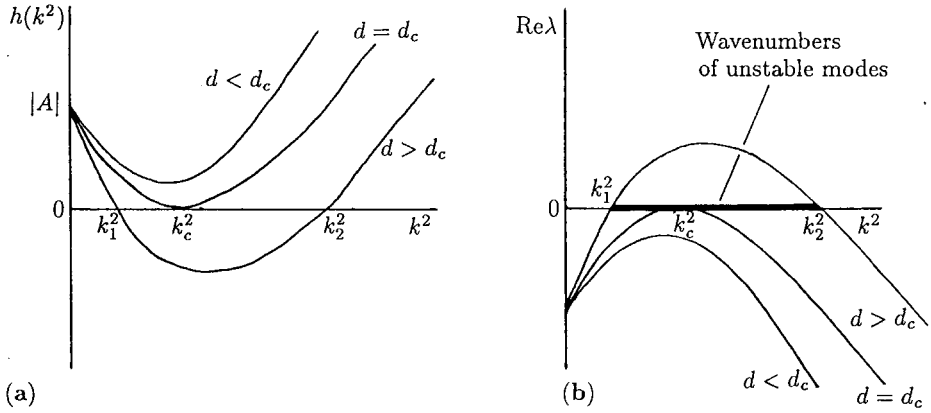

Figure 2.5. (**a**) Plot of $h(k^2)$ defined by (2.23) for typical kinetics illustrated in Figure 2.2. When the diffusion coefficient ratio d increases beyond the critical value d_c, $h(k^2)$ becomes negative for a finite range of $k^2 > 0$. (**b**) Plot of the largest of the eigenvalues $\lambda(k^2)$ from (2.23) as a function of k^2. When $d > d_c$ there is a range of wavenumbers $k_1^2 < k^2 < k_2^2$ which are linearly unstable.

Whenever $h(k^2) < 0$, (2.23) has a solution λ which is positive for the same range of wavenumbers that make $h < 0$. From (2.23) with $d > d_c$ the range of unstable wavenumbers $k_1^2 < k^2 < k_2^2$ is obtained from the zeros k_1^2 and k_2^2 of $h(k^2) = 0$ as

$$\begin{aligned} k_1^2 &= \frac{\gamma}{2d}\left[(df_u + g_v) - \{(df_u + g_v)^2 - 4d|\,A\,|\}^{1/2}\right] < k^2 \\ &< \frac{\gamma}{2d}\left[(df_u + g_v) + \{(df_u + g_v)^2 - 4d|\,A\,|\}^{1/2}\right] = k_2^2. \end{aligned} \tag{2.29}$$

Figure 2.5(b) plots a typical $\lambda(k^2)$ against k^2. The expression $\lambda = \lambda(k^2)$ is called a *dispersion relation*. We discuss the importance and use of dispersion relations in more detail in the next two sections. Note that, within the unstable range, $\mathrm{Re}\,\lambda(k^2) > 0$ has a maximum for the wavenumber k_m obtained from (2.25) with $d > d_c$. This implies that there is a fastest growing mode in the summation (2.22) for $\mathbf{w}$; this is an attribute we now exploit.

If we consider the solution $\mathbf{w}$ given by (2.22), the dominant contributions as t increases are those modes for which $\mathrm{Re}\,\lambda(k^2) > 0$ since all other modes tend to zero exponentially. From Figure 2.5, or analytically from (2.29), we determine the range, $k_1^2 < k^2 < k_2^2$, where $h(k^2) < 0$, and hence $\mathrm{Re}\,\lambda(k^2) > 0$, and so from (2.22)

$$\mathbf{w}(\mathbf{r}, t) \sim \sum_{k_1}^{k_2} c_k e^{\lambda(k^2)t}\mathbf{W}_k(\mathbf{r}) \quad \text{for large } t. \tag{2.30}$$

An analysis and graph of the dispersion relation are thus extremely informative in that they immediately say which eigenfunctions, that is, which spatial patterns, are linearly unstable and grow exponentially with time. We must keep in mind that, with finite domain eigenvalue problems, the wavenumbers are discrete and so only certain k in the range (2.29) are of relevance; we discuss the implications of this later.

The key assumption, and what in fact happens, is that these linearly unstable eigenfunctions in (2.30) which are growing exponentially with time will eventually be bounded by the nonlinear terms in the reaction diffusion equations and an ultimate steady state spatially inhomogeneous solution will emerge. A key element in this assumption is the existence of a confined set (or bounding domain) for the kinetics (see Chapter 3, Volume I). We would intuitively expect that if a confined set exists for the kinetics, the same set would also contain the solutions when diffusion is included. This is indeed the case and can be rigorously proved; see Smoller (1983). So, part of the analysis of a specific mechanism involves the demonstration of a confined set within the *positive* quadrant. A general nonlinear analysis for the evolution to the finite amplitude steady state spatial patterns is still lacking but singular perturbation analyses for d near the bifurcation value d_c have been carried out and a nonuniform spatially heterogeneous solution is indeed obtained (see, for example, Lara-Ochoa and Murray 1983, Zhu and Murray 1995). Singular perturbation analyses can be done near any of the critical parameters near bifurcation. There have now been many spatially inhomogeneous solutions evaluated numerically using a variety of specific reaction diffusion mechanisms; the numerical methods are now quite standard. The results presented in the next chapter illustrate some of the richness of pattern which can be generated.

To recap, we have now obtained conditions for the generation of spatial patterns by *two*-species reaction diffusion mechanisms of the form (2.11). For convenience we reproduce them here. Remembering that all derivatives are evaluated at the steady state (u_0, v_0), they are, from (2.19), (2.24) and (2.26),

$$\begin{aligned} &f_u + g_v < 0, \quad f_u g_v - f_v g_u > 0, \\ &df_u + g_v > 0, \quad (df_u + g_v)^2 - 4d(f_u g_v - f_v g_u) > 0. \end{aligned} \tag{2.31}$$

The derivatives f_u and g_v must be of opposite sign: with the reaction kinetics exhibited in Figure 2.2, $f_u > 0$, $g_v < 0$ so the first and third of (2.31) imply that the ratio of diffusion coefficients $d > 1$.

There are two possibilities for the cross-terms f_v and g_u since the only restriction is that $f_v g_u < 0$. So, we must have $f_v < 0$ and $g_u > 0$ or the other way round. These correspond to qualitatively different reactions. The two cases are illustrated schematically in Figure 2.6. Recall that the reactant which promotes growth in one is the activator and the other the inhibitor. In the case illustrated in Figure 2.6(a), u is the activator, which is also self-activating, while the inhibitor, v, inhibits not only u, but also itself. For pattern formation to take place the inhibitor must diffuse more quickly than the activator. In the case illustrated in Figure 2.6(b), v is the activator but is still self-inhibiting and diffuses more quickly. There is another difference between the two cases. The pattern grows along the unstable manifold associated with the positive eigenvalue. In Figure 2.6(a) this means that the two species are at high or low density in the same region as the pattern grows as in Figure 2.6(c); in case Figure 2.6(b) u is at a high density where v is low, and vice versa as in Figure 2.6(d). The qualitative features of the phase plane (just for the reaction terms) in the vicinity of the steady state are shown in Figure 2.6(e) and (f) for the two cases. The fact that the patterns are either in or out of phase has fundamental implications for biological applications.

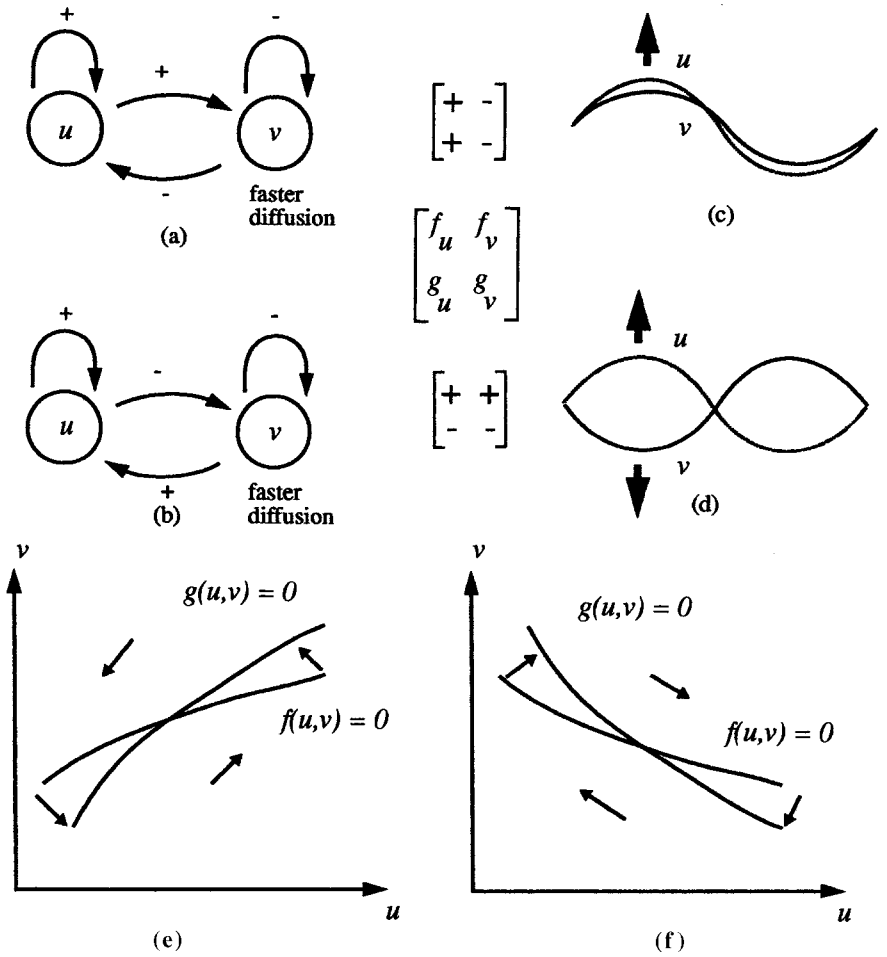

Figure 2.6. Schematic illustration of the two qualitatively different cases of diffusion driven instability. (**a**) self-activating u also activates v, which inhibits both reactants. The resulting initially growing pattern is shown in (**c**). (**b**) Here the self-activating u inhibits v but is itself activated by v with the resulting pattern illustrated in (**d**). The matrices give the signs of f_u, f_v, g_u, g_v evaluated at the steady state. (**e**) and (**f**) The reaction phase planes near the steady state. The arrows indicate the direction of change due to reaction (in the absence of diffusion). Case (**e**) corresponds to the interactions illustrated in (**a**) and (**c**) while that in (**f**) corresponds to the interactions illustrated in (**b**) and (**d**).

To get an intuitive feel for these two cases let us consider two different ecological predator–prey scenarios. In the first, that is, Figure 2.6(e), let u and v represent the prey and predator respectively. At high predator density prey numbers are reduced but at low densities their number is increased. Near the steady state the prey benefit from each other in that an increase in number is temporarily amplified. Predators decrease in numbers if the predator-to-prey ratio is high, but otherwise increase. Another example, from parasitology, is if v is a parasite dispersing via a motile host while u is a more sedentary host that is severely affected by the parasite. In these the interaction near the

steady state is as in Figure 2.6(a) with the local null clines and qualitative growth as in Figure 2.6(e).

A necessary condition for diffusion-driven instability in this predator–prey situation is that the predators disperse faster than the prey. In this case the patterns form as in Figure 2.6(c). Let us suppose there is a region of increased prey density. Without diffusion this would be damped out since the predators would temporarily increase and then drop back towards the steady state. However, with the predators diffusing it is possible that the local increase in predators (due to an increase in the prey) partially disperses and so is not strong enough to push the prey population back towards equilibrium. When predators disperse they lower the prey density in the neighbourhood. It is therefore possible to end up with clumps of high prey and predator populations interspersed with areas in which both densities are low. In the parasite analogy clumping of the sedentary prey (the host) coincides with areas of high parasite density. Hosts can also exist at high levels because the parasites continue to disperse into the nearby 'dead zone' in which there are few of this type of host. The scale on which patterning takes place depends on the ratio of the diffusion coefficients d.

Now consider the second type of interaction illustrated in Figures 2.6(b), (d) and (f). Again with a predator–prey situation let u now be the predator and v the prey. In this case the predators are 'autocatalytic' since when densities are close to the steady state, an increase in predator density is temporarily amplified, a not uncommon situation. For example, increased predator densities could improve hunting or reproductive efficiency. Another difference between this case and the first one is that it is now the prey that disperse at a faster rate.

Suppose again that there is a high prey density area. Without diffusion the predator numbers would increase and eventually make both populations return to the steady state. However, it could happen that the predators grow and reduce the prey population to a level below the steady state value (the temporary increase in prey is enough to prompt the autocatalytic growth of predators to kick in). This would result in a net flux of prey from neighbouring regions which in turn would cause the predator density to drop in those regions (as autocatalysis works in the other direction) thereby letting the prey populations grow above their steady state value. A pattern could become established in which areas of low predator/high prey supply with extra prey in those areas in which there are few prey and large numbers of predators. In effect, autocatalytic predators benefit both from being at a high density locally and also because nearby there are regions containing few predators which thus supply them with a constant extra flux of prey. Prey continue to flow towards regions of high predation because of the random nature of diffusion.

If the conditions (2.31) are satisfied there is a scale (γ)-dependent range of patterns, with wavenumbers defined by (2.29), which are linearly unstable. The spatial patterns which initially grow (exponentially) are those eigenfunctions $\mathbf{W}_k(\mathbf{r})$ with wavenumbers between k_1 and k_2 determined by (2.29), namely, those in (2.30). Note that the scale parameter γ plays a crucial role in these expressions, a point we consider further in the next section. Generally we would expect the kinetics and diffusion coefficients to be fixed. In the case of embryogenesis the natural variable parameter is then γ which reflects the size of the embryo or rather the embryonic domain (such as a developing limb bud) we are considering.

Diffusion-Driven Instability in Infinite Domains: Continuous Spectrum of Eigenvalues

In a finite domain the possible wavenumbers k and corresponding spatial wavelengths of allowable patterns are discrete and depend in part on the boundary conditions. In developmental biology the size of the embryo during the period of spatial patterning is often sufficiently large, relative to the pattern to be formed, that the 'boundaries' cannot play a major role in isolating specific wavelengths, as, for example, in the generation of patterns of hair, scale and feather primordia discussed in later chapters. Thus, for practical purposes the pattern formation domain is effectively infinite. Here we describe how to determine the spectrum of unstable eigenvalues for an infinite domain—it is easier than for a finite domain.

We start with the linearised system (2.20) and look for solutions in the form

$$\mathbf{w}(\mathbf{r}, t) \propto \exp[\lambda t + i\mathbf{k} \cdot \mathbf{r}],$$

where $\mathbf{k}$ is the wave vector with magnitude $k = |\,\mathbf{k}\,|$. Substitution into (2.20) again gives

$$|\,\lambda I - \gamma A + Dk^2\,| = 0$$

and so the dispersion relation giving λ in terms of the wavenumbers k is again given by (2.23). The range of eigenvalues for which $\mathrm{Re}\,\lambda(k^2) > 0$ is again given by (2.29). The crucial difference between the situation here and that for a finite domain is that there is always a spatial pattern if, in (2.29), $0 < k_1^2 < k_2^2$ since we are not restricted to a discrete class of k^2 defined by the eigenvalue problem (2.21). So, at bifurcation when k_c^2, given by (2.28), is linearly unstable the mechanism will evolve to a spatial pattern with the critical wavelength $\omega_c = 2\pi/k_c$. Thus the wavelength with the maximum exponential growth in Figure 2.5(b) will be the pattern which generally emerges at least in one dimension: it is not always the case and depends on the number of unstable modes and initial conditions. In the next chapter on biological applications we shall see that the difference between a finite domain and an effectively infinite one has important biological implications: finite domains put considerable restrictions on the allowable patterns.

2.4 Detailed Analysis of Pattern Initiation in a Reaction Diffusion Mechanism

Here we consider, by way of example, a specific two-species reaction diffusion system and carry out the detailed analysis. We lay the groundwork in this section for the subsequent applications to real biological pattern formation problems. We calculate the eigenfunctions, obtain the specific conditions on the parameters necessary to initiate spatial patterns and determine the wavenumbers and wavelengths of the spatial disturbances which initially grow exponentially.

We study the simplest reaction diffusion mechanism (2.7), first in one space dimension; namely,

$$\begin{aligned} u_t &= \gamma f(u,v) + u_{xx} = \gamma(a - u + u^2 v) + u_{xx}, \\ v_t &= \gamma g(u,v) + d v_{xx} = \gamma(b - u^2 v) + d v_{xx}. \end{aligned} \tag{2.32}$$

The kinetics null clines $f = 0$ and $g = 0$ are illustrated in Figure 2.2(a). The uniform positive steady state (u_0, v_0) is

$$u_0 = a + b, \quad v_0 = \frac{b}{(a+b)^2}, \quad b > 0, \quad a + b > 0 \tag{2.33}$$

and, at the steady state,

$$\begin{aligned} &f_u = \frac{b-a}{a+b}, \quad f_v = (a+b)^2 > 0, \quad g_u = \frac{-2b}{a+b} < 0, \\ &g_v = -(a+b)^2 < 0, \quad f_u g_v - f_v g_u = (a+b)^2 > 0. \end{aligned} \tag{2.34}$$

Since f_u and g_v must have opposite signs we must have $b > a$. With these expressions, conditions (2.31) require

$$\begin{aligned} &f_u + g_v < 0 \quad \Rightarrow \quad 0 < b - a < (a+b)^3, \\ &f_u g_v - f_v g_u > 0 \quad \Rightarrow \quad (a+b)^2 > 0, \\ &d f_u + g_v > 0 \quad \Rightarrow \quad d(b-a) > (a+b)^3, \\ &(d f_u + g_v)^2 - 4d(f_u g_v - f_v g_u) > 0 \\ &\Rightarrow \quad [d(b-a) - (a+b)^3]^2 > 4d(a+b)^4. \end{aligned} \tag{2.35}$$

These inequalities define a domain in (a, b, d) parameter space, called the pattern formation space (or Turing space), within which the mechanism is unstable to certain spatial disturbances of given wavenumbers k, which we now determine.

Consider the related eigenvalue problem (2.21) and let us choose the domain to be $x \in (0, p)$ with $p > 0$. We then have

$$\mathbf{W}_{xx} + k^2 \mathbf{W} = 0, \quad \mathbf{W}_x = 0 \text{ for } x = 0, p \tag{2.36}$$

the solutions of which are

$$\mathbf{W}_n(x) = \mathbf{A}_n \cos(n\pi x/p), \quad n = \pm 1, \pm 2, \ldots, \tag{2.37}$$

where the $\mathbf{A}_n$ are arbitrary constants. The eigenvalues are the *discrete* wavenumbers $k = n\pi/p$. Whenever (2.34) are satisfied and there is a range of wavenumbers $k = n\pi/p$ lying within the bounds defined by (2.29), then the corresponding eigenfunctions $\mathbf{W}_n$ are linearly unstable. Thus the eigenfunctions (2.37) with wavelengths $\omega = 2\pi/k = 2p/n$ are the ones which initially grow with time like $\exp\{\lambda([n\pi/p]^2)t\}$. The band of wavenumbers from (2.29), with (2.34), is given by

$$\gamma L(a,b,d) = k_1^2 < k^2 = \left(\frac{n\pi}{p}\right)^2 < k_2^2 = \gamma M(a,b,d)$$

$$L = \frac{[d(b-a)-(a+b)^3] - \{[d(b-a)-(a+b)^3]^2 - 4d(a+b)^4\}^{1/2}}{2d(a+b)}, \quad (2.38)$$

$$M = \frac{[d(b-a)-(a+b)^3] + \{[d(b-a)-(a+b)^3]^2 - 4d(a+b)^4\}^{1/2}}{2d(a+b)}.$$

In terms of the wavelength $\omega = 2\pi/k$, the range of unstable modes $\mathbf{W}_n$ have wavelengths bounded by ω_1 and ω_2, where

$$\frac{4\pi^2}{\gamma L(a,b,d)} = \omega_1^2 > \omega^2 = \left(\frac{2p}{n}\right)^2 > \omega_2^2 = \frac{4\pi^2}{\gamma M(a,b,d)}. \quad (2.39)$$

Note in (2.38) the importance of scale, quantified by γ. The smallest wavenumber is π/p; that is, $n = 1$. For fixed parameters a, b and d, if γ is sufficiently small (2.38) says that there is *no allowable* k in the range, and hence no mode $\mathbf{W}_n$ in (2.37), which can be driven unstable. This means that all modes in the solution $\mathbf{w}$ in (2.30) tend to zero exponentially and the steady state is stable. We discuss this important role of scale in more detail below.

From (2.30) the spatially heterogeneous solution which emerges is the sum of the unstable modes, namely,

$$\mathbf{w}(x,t) \sim \sum_{n_1}^{n_2} \mathbf{C}_n \exp\left[\lambda\left(\frac{n^2\pi^2}{p^2}\right)t\right] \cos\frac{n\pi x}{p}, \quad (2.40)$$

where λ is given by the positive solution of the quadratic (2.23) with the derivatives from (2.34), n_1 is the smallest integer greater than or equal to pk_1/π, n_2 the largest integer less than or equal to pk_2/π and $\mathbf{C}_n$ are constants which are determined by a Fourier series analysis of the initial conditions for $\mathbf{w}$. Initial conditions in any biological context involve a certain stochasticity and so it is inevitable that the Fourier spectrum will contain the whole range of Fourier modes; that is, the $\mathbf{C}_n$ are nonzero. We can therefore assume at this stage that γ is sufficiently large to ensure that allowable wavenumbers exist in the unstable range of k. Before discussing the possible patterns which emerge let us first obtain the corresponding two-dimensional result.

Consider the two-dimensional domain defined by $0 < x < p$, $0 < y < q$ whose rectangular boundary we denote by ∂B. The spatial eigenvalue problem in place of that in (2.36) is now

$$\nabla^2\mathbf{W} + k^2\mathbf{W} = 0, \quad (\mathbf{n}\cdot\nabla)\mathbf{W} = 0 \quad \text{for} \quad (x,y) \text{ on } \partial B \quad (2.41)$$

the eigenfunctions of which are

$$\mathbf{W}_{p,q}(x,y) = \mathbf{C}_{n,m} \cos\frac{n\pi x}{p} \cos\frac{m\pi y}{q}, \quad k^2 = \pi^2\left(\frac{n^2}{p^2} + \frac{m^2}{q^2}\right), \quad (2.42)$$

where n and m are integers. The two-dimensional modes $\mathbf{W}_k(x, y)$ which are linearly unstable are those with wavenumbers k, defined by the last equation, lying within the unstable band of wavenumbers defined in terms of a, b and d by (2.38). We again assume that γ is sufficiently large so that the range of unstable wavenumbers contains at least one possible mode. Now the unstable spatially patterned solution is given by (2.30) with (2.42) as

$$\begin{aligned} \mathbf{w}(x, y, t) &\sim \sum_{n,m} \mathbf{C}_{n,m} e^{\lambda(k^2)t} \cos\frac{n\pi x}{p} \cos\frac{m\pi y}{q}, \\ \gamma L(a, b, d) = k_1^2 < k^2 &= \pi^2 \left(\frac{n^2}{p^2} + \frac{m^2}{q^2}\right) < k_2^2 = \gamma M(a, b, d), \end{aligned} \tag{2.43}$$

where the summation is over all pairs (n, m) which satisfy the inequality, L and M are defined by (2.38) as before and $\lambda(k^2)$ is again the positive solution of (2.23) with the expressions for the derivatives of f and g given by (2.34). As t increases a spatial pattern evolves which is initially made up of the modes in (2.43).

Now consider the type of spatial patterns we might expect from the unstable solutions in (2.40) and (2.43). Suppose first that the domain size, as measured by γ, is such that the range of unstable wavenumbers in (2.38) admits only the wavenumber $n = 1$: the corresponding dispersion relation for λ in terms of the wavelengths $\omega = 2p/n$ is illustrated in Figure 2.7(a). The only unstable mode, from (2.37) is then $\cos(\pi x/p)$ and the growing instability is given by (2.40) as

$$\mathbf{w}(x, t) \sim \mathbf{C}_1 \exp\left[\lambda\left(\frac{\pi^2}{p^2}\right)t\right] \cos\frac{\pi x}{p},$$

where λ is the positive root of the quadratic (2.23) with f_u, f_v, g_u and g_v from (2.34) and with $k^2 = (\pi/p)^2$. Here all other modes decay exponentially with time. We can only determine the $\mathbf{C}_1$ from initial conditions. To get an intuitive understanding for what is going on, let us simply take $\mathbf{C}_1$ as $(\varepsilon, \varepsilon)$ for some small positive ε and consider the morphogen u; that is, from the last equation and the definition of $\mathbf{w}$ from (2.14),

$$u(x, t) \sim u_0 + \varepsilon \exp\left[\lambda\left(\frac{\pi^2}{p^2}\right)t\right] \cos\frac{\pi x}{p}. \tag{2.44}$$

This unstable mode, which is the dominant solution which emerges as t increases, is illustrated in Figure 2.7(b). In other words, this is the pattern predicted by the dispersion relation in Figure 2.7(a).

Clearly if the exponentially growing solution were valid for all time it would imply $u \to \infty$ as $t \to \infty$. For the mechanism (2.32), the kinetics has a confined set, within the positive quadrant, which bounds the solution. So the solution in the last equation must be bounded and lie in the positive quadrant. We hypothesise that this growing solution eventually settles down to a spatial pattern which is similar to the single cosine mode shown in Figure 2.7(b). As mentioned before, singular perturbation analyses in the

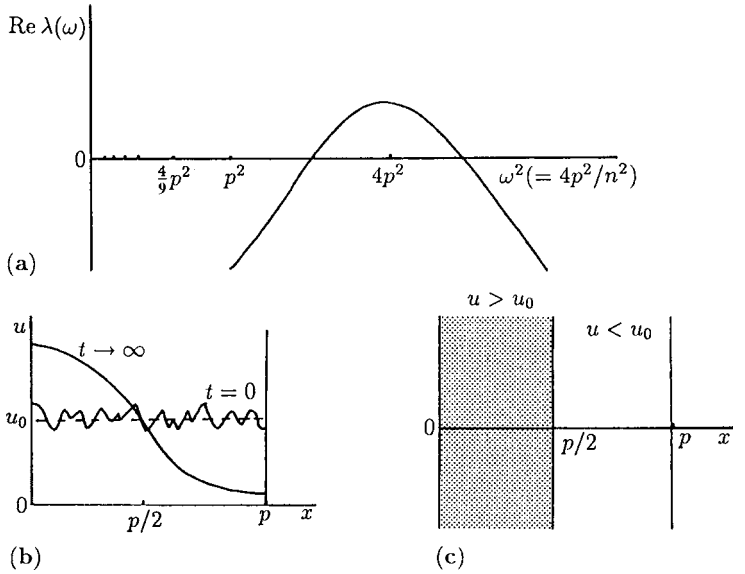

Figure 2.7. (**a**) Typical dispersion relation for the growth factor $\mathrm{Re}\,\lambda$ as a function of the wavelength ω obtained from a linearization about the steady state. The only mode which is linearly unstable has $n = 1$; all other modes have $\mathrm{Re}\,\lambda < 0$. (**b**) The temporally growing linear mode which eventually evolves from random initial conditions into a finite amplitude spatial pattern such as shown in (**c**), where the shaded area corresponds to a concentration higher than the steady state u_0 and the unshaded area to a concentration lower than the steady state value.

vicinity of the bifurcation in one of the parameters, for example, near the critical domain size for γ, such that a single wavenumber is just unstable, or when the critical diffusion coefficient ratio is near d_c, bear this out as do the many numerical simulations of the full nonlinear equations. Figure 2.7(c) is a useful way of presenting spatial patterned results for reaction diffusion mechanisms—the shaded region represents a concentration above the steady state value while the unshaded region represents concentrations below the steady state value. As we shall see, this simple way of presenting the results is very useful in the application of chemical prepattern theory to patterning problems in developmental biology, where it is postulated that cells differentiate when one of the morphogen concentrations is above (or below) some threshold level.

Let us now suppose that the domain size is doubled, say. With the definition of γ chosen to represent scale this is equivalent to multiplying the original γ by 4 since in the one-dimensional situation $\sqrt{\gamma}$ is proportional to size, that is, the length here, of the domain. This means that the dispersion relation and the unstable range are simply moved along the k^2-axis or along the ω^2-axis. Suppose the original $\gamma = \gamma_1$. The inequalities (2.38) determine the unstable modes as those with wavelengths $\omega(= 2\pi/k)$ determined by (2.39); namely,

$$\frac{4\pi^2}{\gamma_1 L(a,b,d)} > \omega^2 > \frac{4\pi^2}{\gamma_1 M(a,b,d)}. \tag{2.45}$$

Let this be the case illustrated in Figure 2.7(a) and which gives rise to the pattern in Figure 2.7(c). Now let the domain double in size. We consider exactly the same domain as in Figure 2.7 but with an increased γ to $4\gamma_1$. This is equivalent to having the same γ_1 but with a domain 4 times that in Figure 2.7. We choose the former means of representing a change in scale. The equivalent dispersion relation is now illustrated in Figure 2.8(a)—it is just the original one of Figure 2.7(a) moved along so that the wavelength of the excited or unstable mode now has $\omega = p$; that is, $n = 2$. The equivalent spatial pattern is then as in Figure 2.8(b). As we shall see in the applications chapters which follow, it is a

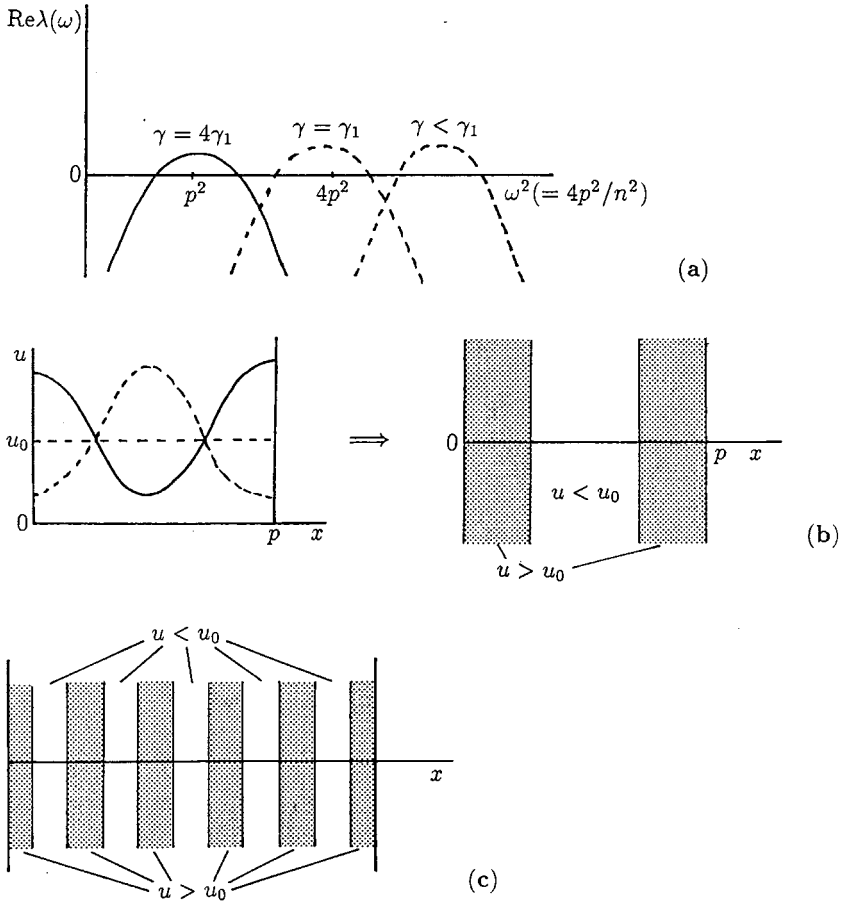

Figure 2.8. (**a**) Dispersion relation Re λ as a function of the wavelength ω when the single mode with $n = 2$ is unstable for a domain size $4\gamma_1$; the dashed curves are those with $\gamma = \gamma_1$ and $\gamma < \gamma_c < \gamma_1$, where γ_c is the critical bifurcation scale value of the domain that will not admit any heterogeneous pattern. (**b**) The spatial pattern in the morphogen u predicted by the dispersion relation in (**a**). The dashed line, the mirror image about $u = u_0$, is also an allowable form of this solution. The initial conditions determine which pattern is obtained. (**c**) The spatial pattern obtained when the domain is sufficiently large to fit in the number of unstable modes equivalent to $n = 10$: the shaded regions represent morphogen levels $u > u_0$, the uniform steady state.

particularly convenient way, when presenting spatial patterned solutions, to incorporate scale solely via a change in γ.

We can thus see with this example how the patterning process works as regards domain size. There is a basic wavelength picked out by the analysis for a given $\gamma = \gamma_1$, in this example that with $n = 1$. As the domain grows it eventually can incorporate the pattern with $n = 2$ and progressively higher modes the larger the domain, as shown in Figure 2.8(c). In the same way if the domain is sufficiently small there is clearly a $\gamma = \gamma_c$ such that the dispersion relation, now moved to the right in Figure 2.8(a), will not even admit the wavelength with $n = 1$. In this case no mode is unstable and so no spatial pattern can be generated. The concept of a critical domain size for the existence of spatial pattern is an important one both in developmental biology, and in spatially dependent ecological models as we show later.

Note in Figure 2.8(b) the two possible solutions for the same parameters and zero flux boundary conditions. Which of these is obtained depends on the bias in the initial conditions. Their existence poses certain conceptual difficulties from a developmental biology point of view within the context of positional information. If cells differentiate when the morphogen concentration is larger than some threshold then the differentiated cell pattern is obviously different for each of the two possible solutions. Development, however, is a sequential process and carries with it its own history so, a previous stage generally cues the next. In the context of reaction diffusion models this implies a bias in the initial conditions towards one of the patterns.

Now consider the two-dimensional problem with a dispersion relation such that the unstable modes are given by (2.43). Here the situation is not so straightforward since for a given γ, representing the *scale*, the actual modes which are unstable now depend on the domain *geometry* as measured by the length p and the width q. Referring to (2.43), first note that if the width is sufficiently small, that is, q is small enough, even the first mode with $m = 1$ lies outside the unstable range. The problem is then equivalent to the above one-dimensional situation. As the width increases, that is, q increases, genuine two-dimensional modes with $n \neq 0$ and $m \neq 0$ become unstable since

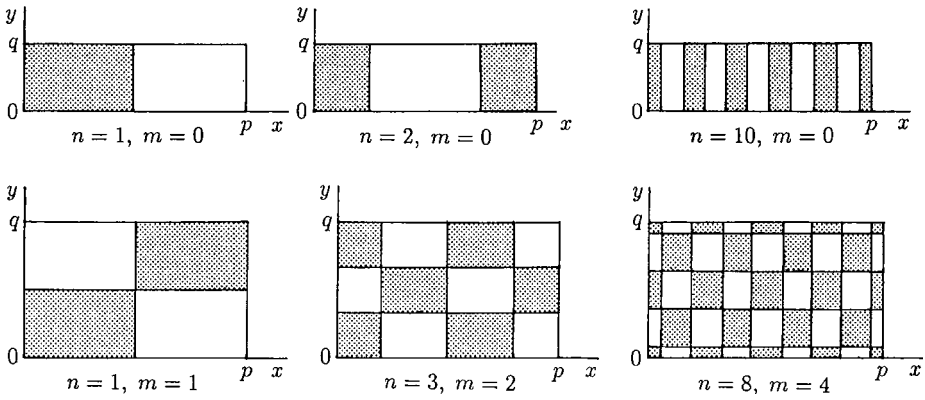

Figure 2.9. Typical two-dimensional spatial patterns indicated by the linearly unstable solution (2.43) when various wavenumbers are in the unstable range. The shaded regions are where $u > u_0$, the uniform steady state.

$\pi^2(n^2/p^2 + m^2/q^2)$ lies in the range of unstable wavenumbers. Figure 2.9 illustrates typical temporally growing spatial patterns indicated by (2.43) with various nonzero n and m.

Regular Planar Tesselation Patterns

The linear patterns illustrated in the last figure arise from the simplest two-dimensional eigenfunctions of (2.41). Less simple domains require the solutions of

$$\nabla^2\psi + k^2\psi = 0, \quad (\mathbf{n}\cdot\nabla)\psi = 0 \quad \text{for} \quad \mathbf{r} \text{ on } \partial B. \tag{2.46}$$

Except for simple geometries the analysis quickly becomes quite complicated. Even for circular domains the eigenvalues have to be determined numerically. There are, however, some elementary solutions for symmetric domains which tesselate the plane, namely, squares, hexagons, rhombi and, by subdivision, triangles; these were found by Christopherson (1940). In other words we can cover the complete plane with, for example, regular hexagonal tiles. (The basic symmetry group of regular polygons are hexagons, squares and rhombi, with, of course, triangles, which are subunits of these.) Hexagonal patterns, as we shall see, are common in many real developmental situations—feather distribution on the skin of birds is just one example (just look at the skin of a plucked chicken). Refer also to Figure 2.11 below where a variety of experimentally obtained patterns is shown. Thus we want solutions ψ where the unit cell, with zero flux conditions on its boundary, is one of the regular tesselations which can cover the plane. That is, we want solutions which are *cell* periodic; here the word 'cell' is, of course, meant as the unit of tesselation.

The solution of (2.46) for a hexagon is

$$\begin{aligned}\psi(x,y) &= \frac{\cos k\left(\frac{\sqrt{3}y}{2} + \frac{x}{2}\right) + \cos k\left(\frac{\sqrt{3}y}{2} - \frac{x}{2}\right) + \cos kx}{3} \\ &= \frac{\cos\left\{kr\sin\left(\theta + \frac{\pi}{6}\right)\right\} + \cos\left\{kr\sin\left(\theta - \frac{\pi}{6}\right)\right\} + \cos\left\{kr\sin\left(\theta - \frac{\pi}{2}\right)\right\}}{3}.\end{aligned} \tag{2.47}$$

From (2.46), a linear equation, ψ is independent to the extent of multiplication by an arbitrary constant: the form chosen here makes $\psi = 1$ at the origin. This solution satisfies zero flux boundary conditions on the hexagonal symmetry boundaries if $k = n\pi, n = \pm1, \pm2, \ldots$. Figure 2.10(a) shows the type of pattern the solution can generate.

The polar coordinate form shows the invariance to hexagonal rotation, that is, invariance to rotation by $\pi/3$, as it must. That is,

$$\psi(r,\theta) = \psi\left(r, \theta + \frac{\pi}{3}\right) = H\psi(r,\theta) = \psi(r,\theta),$$

where H is the hexagonal rotation operator.

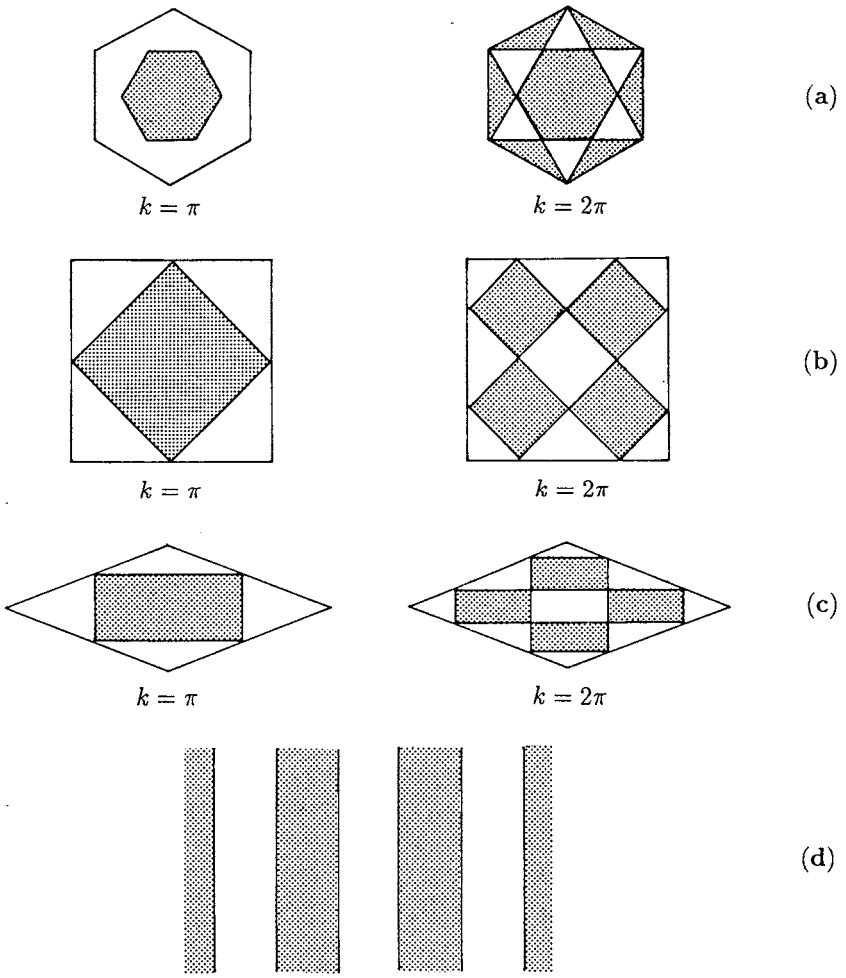

Figure 2.10. (**a**) Patterns which are obtained with the solution (2.47) with $k = \pi$ and $k = 2\pi$. The shaded region is where $\psi > 0$ and the unshaded region where $\psi < 0$. (**b**) Patterns generated by the solution (2.48) for a square tesselation with $k = \pi$ and $k = 2\pi$. (**c**) Rhombic patterns from (2.49) with $k = \pi$ and $k = 2\pi$. (**d**) One-dimensional roll patterns from (2.50).

The solution for the square is

$$\begin{aligned} \psi(x, y) &= \frac{\cos kx + \cos ky}{2} \\ &= \frac{\cos(kr\cos\theta) + \cos(kr\sin\theta)}{2}, \end{aligned} \tag{2.48}$$

where $k = \pm 1, \pm 2 \ldots$ and $\psi(0, 0) = 1$. This solution is square rotationally invariant since

$$\psi(r,\theta) = \psi\left(r, \theta + \frac{\pi}{2}\right) = S\psi(r,\theta) = \psi(r,\theta),$$

where S is the square rotational operator. Typical patterns are illustrated in Figure 2.10(b).

The solution for the rhombus is

$$\begin{aligned}\psi(x,y) &= \frac{\cos kx + \cos\{k(x\cos\phi + y\sin\phi)\}}{2} \\ &= \frac{\cos\{kr\cos\theta\} + \cos\{kr\cos(\theta-\phi)\}}{2},\end{aligned} \tag{2.49}$$

where ϕ is the rhombus angle and again $k = \pm 1, \pm 2, \ldots$. This solution is invariant under a rhombic rotation; that is,

$$\psi(r,\theta;\phi) = \psi(r,\theta+\pi;\phi) = R\psi(r,\theta;\phi),$$

where R is the rhombic rotation operator. Illustrative patterns are shown in Figure 2.10(c).

A further cell periodic solution is the one-dimensional version of the square; that is, there is only variation in x. The solutions here are of the form

$$\psi(x,y) = \cos kx, \quad k = n\pi, \quad n = \pm 1, \pm 2, \ldots \tag{2.50}$$

and represent rolls with patterns as in Figure 2.10(d). These, of course, are simply the one-dimensional solutions (2.37).

When the full nonlinear equations are solved numerically with initial conditions taken to be small random perturbations about the steady state, linear theory turns out to be a good predictor of the ultimate steady state in the one-dimensional situation, particularly if the unstable modes have large wavelengths, that is, small wavenumbers. With larger wavenumbers the predictions are less reliable—and even more so with two-dimensional structures. Since the equations we have studied are linear and invariant when multiplied by a constant, we can have equivalent solutions which are simply mirror images in the line $u = u_0$; refer to Figure 2.8(b). Thus the pattern that evolves depends on the initial conditions and the final pattern tends to be the one closest to the initial conditions. There is, in a sense, a basin of attraction for the spatial patterns as regards the initial conditions. Once again near bifurcation situations singular perturbation analysis indicates nonlinear patterns closely related to the linear predictions. In general, however, away from the bifurcation boundaries linear predictions are much less reliable; see the computed patterns exhibited in the next chapter. Except for the simplest patterns, we should really use linear theory for two and three dimensions only as a guide to the wealth of patterns which can be generated by pattern formation mechanisms. Linear theory does, however, determine parameter ranges for pattern generation.

Figure 2.10 shows a selection of regular patterns that can be formed by reaction diffusion equations based on linear theory. Mathematically (and experimentally of course) a key question is which of these will be formed from given initial conditions. If one pattern is formed, variation of which parameters will effect changing to another? To de-

termine which of the various possible patterns—hexagons, rhombi, squares or rolls—will be stable we have to go beyond linear theory and carry out a weakly nonlinear analysis; that is, the parameters are such that they are close to the bifurcation boundary from homogeneity to heterogeneity. When we do such a nonlinear analysis we can determine the conditions on the parameters for stability of these steady state spatially heterogeneous solutions. This has been done for reaction diffusion equations by Ermentrout (1991) and Nagorcka and Mooney (1992) using a multi-scale singular perturbation analysis. Other pattern formation mechanisms, namely, cell-chemotaxis and mechanical mechanisms for pattern formation were studied by Zhu and Murray (1995). The latter compare chemotaxis systems and their patterning potential with reaction diffusion systems. Zhu and Murray (1995) were particularly interested in determining the parameter spaces which give rise to stable stripes, spots, squares and hexagons and their spatial characteristics such as wavelength and so on.

In the case of spots they could also determine which of the tessalation spot arrangement patterns would be stable. They compared the robustness and sensitivity of different models and confirmed the results with extensive numerical simulations of the equations. The analytical technique is well established but the details are fairly complex. Zhu and Murray (1995) show from their numerical study of the equations how the transition takes place from stripes to spots and then to hexagonal patterns and the converse pathway how hexagons become unstable and eventually end up in stripes. The hexagons in effect become elongated and rhombic in character with the spots lining up in lines and eventually fusing; it makes intuitive sense. The analytical procedure near bifurcation is referred to as weakly nonlinear stability analysis, an extensive review of which is given by Wollkind et al. (1994). Generally the form of the interaction kinetics plays a major role in what patterns are obtained. Cubic interactions tend to favour stripes while quadratic interactions tend to produce spots. When different boundary conditions (other than zero flux ones) are used the patterns obtained can be very different and less predictable. Barrio et al. (1999) investigated the effect of these and the role of the nonlinearities in the patterns obtained. From extensive numerical simulations they sugggest that such reaction diffusion mechanisms could play a role in some of the complex patterns observed on fish.

The patterns we have discussed up to now have mainly been regular in the sense that they are stripes, spots, hexagonal patterns and so on. Reaction diffusion systems can generate an enormous range of irregular patterns as we shall see in the following chapter where we discuss a few practical examples. The recent article by Meinhardt (2000: see also other references there) discusses complex patterns and in particular the application of reaction diffusion mechanisms to patterns of gene activation, a subject not treated in this book. He also reviews other important applications not treated here such as branching structures in plant morphology.

In the analyses of the pattern formation potential of reaction diffusion systems here the reactants, or morphogens, must have different diffusion coefficients. In many developmental situations there are often preferred directions in which the diffusion of the same morphogen may have different values in different directions; that is, the diffusion is anisotropic. Although we do not discuss it here, this can have, as we would expect, a marked affect on the patterns formed in a Turing instability of the uniform state (see Exercise 10).

It has been known for a long time, from the 1970's in fact, from many numerical studies that reaction diffusion systems can produce steady state finite amplitude spatial patterns. It is only in the last 10 years, however, that such steady state patterns, sometimes called Turing structures or Turing patterns, have been found experimentally. The experimental breakthrough started in 1989; see Ouyang et al. (1990, 1993), Castets et al. (1990), Ouyang and Swinney (1991), Gunaratne et al. (1994), De Kepper et al. (1994) and other references in these articles. The last two are good reviews to get an overall picture of some of these developments. The latter also describe the complex structures which are obtained when the Turing structures interact with travelling waves; they can be highly complex with such phenomena as spatiotemporal intermittency and spot splitting to form more complex patterns and so on. Ouyang and Swinney (1991) experimentally demonstrate the transition from a uniform state to hexagonal and eventually striped patterns; the transition is similar to that found by Zhu and Murray (1995) for both reaction diffusion and cell-chemotaxis pattern formation mechanisms. Since these early experimental studies, Turing patterns have been found with several quite different reaction systems; the details of the chemistry and experimental arrangements are given in detail in the papers. Figure 2.11 shows chemical Turing patterns obtained experimentally with a chlorite-iodide-malonic acid reaction diffusion system from Gunaratne et al. (1994). Note the small size of the domain and the accurately defined wavelength of the patterns which vary from 0.11 mm to 0.18 mm; these are certainly in the range we would expect of many morphogenetic situations and clearly demonstrate the potential for fine-scale delineation of pattern with reaction diffusion mechanisms and, from the theoretical studies of Zhu and Murray (1994) with other pattern generators. That they are of morphogenetic scale, in the case of the developing chick limb, at the time of the patterning associated with cartilage formation the width of the limb bud is of the order of 2 mm (see the discussion on a limb bud patterning scenario in Chapter 6). Wollkind and Stephenson (2000a,b) give a thorough and comprehensive discussion of the various transitions between patterns, including the black eye pattern shown in Figure 2.11. They specifically study the chlorite-iodide-malonic acid reaction system which was used in the experiments and importantly compare their results with experiment. They also relate these transitions between symmetry breaking structures in the chemical system to similar ones in quite different scientific contexts.

The application of reaction diffusion pattern generation to specific developmental biology problems is often within the context of a prepattern theory whereby cells differentiate according to the level of the morphogen concentration in which they find themselves. If the spatial patterns is quite distinct, as described above or with relatively large gradients, less sensitive tuning is required of the cells in order to carry out their assigned roles than if the pattern variation or the concentration gradients are small. It is perhaps useful therefore to try to get a quantitative measure of spatial heterogeneity, which is meaningful biologically, so as to compare different mechanisms. Another biologically relevant method will be discussed in the next section.

Berding (1987) introduced a 'heterogeneity' function for the spatial patterns generated by reaction diffusion systems with zero flux boundary conditions. Suppose the general mechanism (2.10), in one space variable, is diffusionally unstable and the solutions evolve to spatially inhomogeneous steady state solutions $U(x)$ and $V(x)$ as $t \to \infty$. With the definition of γ in (2.6) proportional to the square of the domain length we can

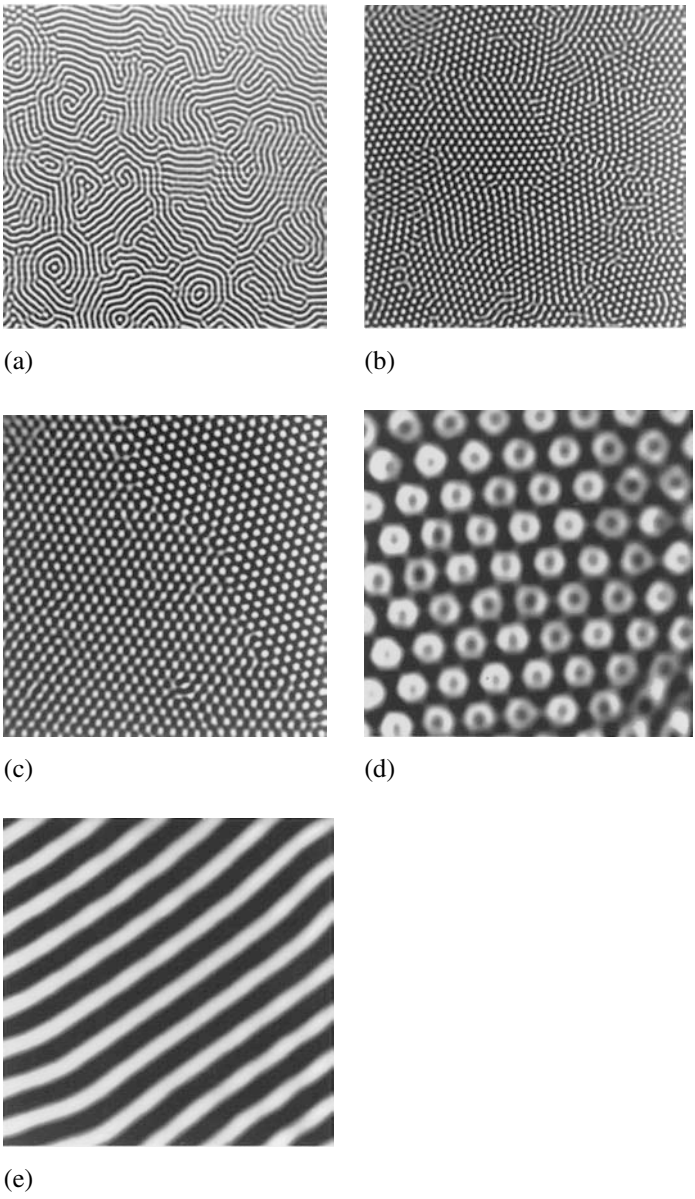

Figure 2.11. Chemical patterns obtained with the reaction diffusion system with the chlorite-iodide-malonic reaction from Gunaratne et al. (1994). The domain size is 6 mm × 6 mm. (**a**) Multiple domains with stripes with wavelength 0.11 mm. (**b**) This shows multiple domains of hexagonal patterns with different orientations. Here the wavelength is 0.12 mm. (**c**) This again shows hexagonal patterns with a single boundary separating the hexagonal lattices with different orientations: the wavelength here is 0.18 mm. (**d**) This shows a fully developed complex black eye pattern: the domain size is 1.6 mm × 1.6 mm. (**e**) When the hexagonal pattern in (**d**) becomes unstable it deforms into rhombic structures and the spots line up eventually becoming the striped pattern (in a similar way to the transition patterns in Zhu and Murray 1995): the domain is again 1.6 mm × 1.6 mm. The experimental details are given in Gunaratne et al. (1994). (Photographs reproduced courtesy of Harry Swinney)

measure domain size by γ and hence take x to be in $(0, 1)$. Then (U, V) satisfy the dimensionless equations

$$\begin{aligned} &U'' + \gamma f(U, V) = 0, \quad dV'' + \gamma g(U, V) = 0, \\ &U'(0) = U'(1) = V'(0) = V'(1) = 0. \end{aligned} \tag{2.51}$$

The non-negative heterogeneity function is defined by

$$H = \int_0^1 (U'^2 + V'^2)\, dx \geq 0, \tag{2.52}$$

which depends only on the parameters of the system and the domain scale γ. H is an 'energy function.' If we now integrate by parts, using the zero flux boundary conditions in (2.51),

$$H = -\int_0^1 (UU'' + VV'')\, dx$$

which, on using (2.51) for U'' and V'', becomes

$$H = \frac{\gamma}{d} \int_0^1 [dUf(U, V) + Vg(U, V)]\, dx. \tag{2.53}$$

If there is no spatial patterning, U and V are simply the uniform steady state solutions of $f(U, V) = g(U, V) = 0$ and so $H = 0$, as also follows, of course, from the definition (2.52).

From (2.53) we see how the scale parameter and diffusion coefficient ratio appear in the definition of heterogeneity. For example, suppose the domain is such that it sustains a single wave for $\gamma = \gamma_1$, in dimensional terms a domain length $L = L_1$ say. If we then double the domain size to $2L_1$ we can fit in two waves and so, intuitively from (2.52), H must increase as there is more heterogeneity. Since $\gamma \propto L^2$, H from (2.53) is simply quadrupled. From an embryological point of view, for example, this means that as the embryo grows we expect more and more structure. An example of this increase in structure in a growing domain is illustrated in Figure 2.18 below. Berding (1987) discusses particular applications and compares specific reaction diffusion mechanisms as regards their potential for heterogeneity.

2.5 Dispersion Relation, Turing Space, Scale and Geometry Effects in Pattern Formation Models

We first note some general properties about the dispersion relation and then exploit it further with the specific case we analysed in the last section. The formation of spatial patterns by any morphogenetic model is principally a nonlinear phenomenon. However, as we noted, a good indication of the patterns in one dimension can be obtained by a simple linear analysis. For spatial patterns to form, we saw that two conditions must

hold simultaneously. First, the spatially uniform state must be stable to small perturbations, that is, all $\lambda(k^2)$ in (2.22) have $\mathrm{Re}\,\lambda(k^2 = 0) < 0$, and second, only patterns of a certain spatial extent, that is, patterns within a definite range of wavelengths k, can begin to grow, with $\mathrm{Re}\,\lambda(k^2 \neq 0) > 0$. These conditions are encapsulated in the dispersion relation in either the (λ, k^2) or (λ, ω^2) forms such as in Figure 2.5(b) and Figure 2.7(a). The latter, for example, also says that if the spatial pattern of the disturbances has k^2 large, that is, very small wavelength disturbances, the steady state is again linearly stable. A dispersion relation therefore immediately gives the initial rate of growth or decay of patterns of various sizes. Dispersion relations are obtained from the general evolution equations of the pattern formation mechanism. A general and nontechnical biologically oriented discussion of pattern formation models is given by Oster and Murray (1989).

Since the solutions to the linear eigenfunction equations such as (2.36) are simply sines and cosines, the 'size' of various spatial patterns is measured by the wavelength of the trigonometric functions; for example, $\cos(n\pi x/p)$ has a wavelength $\omega = 2p/n$. So, the search for growing spatial patterns comes down to seeing how many sine or cosine waves can 'fit' into a domain of a given size. The two-dimensional situation is similar, but with more flexibility as to how they fit together.

A very important use of the dispersion relation is that it shows immediately whether patterns can grow, and if so, what the sizes of the patterns are. The curves in Figure 2.5(b) and Figure 2.7(a) are the prototype—no frills—dispersion relation for generating spatial patterns. We show later that other forms are possible and imply different pattern formation scenarios. However, these are less common and much is still not known as to which patterns will evolve from them. The mechanochemical models discussed in detail in Chapter 6 can in fact generate a surprisingly rich spectrum of dispersion relations (see Murray and Oster 1984) most of which cannot be generated by two- or three-species reaction diffusion models.

The prototype dispersion relation has the two essential characteristics mentioned above: (i) the spatially featureless state ($k = 0, \omega = \infty$) is stable; that is, the growth rate of very large wavelength waves is negative, and (ii) there is a small band, or window, of wavelengths which can grow (that is, a finite band of unstable 'modes,' $\cos(n\pi x/L)$, for a finite number of integers n in the case of a finite domain). Of these growing modes, one grows fastest, the one closest to the peak of the dispersion curve. This mode, k_m say, is the solution of

$$\frac{\partial \lambda}{\partial k^2} = 0 \quad \Rightarrow \quad \max[\mathrm{Re}\,\lambda] = \mathrm{Re}\,\lambda(k_m^2).$$

Strictly k_m may not be an allowable mode in a finite domain situation. In this case it is the possible mode closest to the analytically determined k_m.

Thus the dispersion curve shows that while the spatially homogeneous state is stable, the system will amplify patterns of a particular spatial extent, should they be excited by random fluctuations, which are always present in a biological system, or by cues from earlier patterns in development. Generally, one of the model parameters is 'tuned' until the dispersion curve achieves the qualitative shape shown. For example, in Figure 2.5(b) if the diffusion ratio d is less than the critical d_c, $\mathrm{Re}\,\lambda < 0$ for all k^2. As d increases, the

curve rises until $d = d_c$ after which it pushes its head above the axis at some wavenumber k_c, that is, wavelength $\omega_c = 2\pi/k_c$, whereupon a cosine wave of that wavelength can start to grow, assuming it is an allowable eigenfunction. This critical wavenumber is given by (2.28) and, with $d = d_c$ from (2.27), we thus have the critical wavelength

$$\omega_c = \frac{2\pi}{k_c} = 2\pi \left\{ \frac{d_c}{\gamma^2(f_u g_v - f_v g_u)} \right\}^{1/4}. \tag{2.54}$$

With the illustrative example (2.32) there are 4 dimensionless parameters: a and b, the kinetics parameters, d, the ratio of diffusion coefficients and γ, the scale parameter. We concentrated on how the dispersion relation varied with d and showed how a bifurcation value d_c existed when the homogeneous steady state became unstable, with the pattern 'size' determined by k_c or ω_c given by the last equation. It is very useful to know the parameter space, involving all the parameters, wherein pattern forms and how we move into this pattern forming domain by varying whatever parameter we choose, or indeed when we vary more than one parameter. Clearly the more parameters there are the more complicated is this corresponding parameter or Turing space. We now determine (analytically) the parameter space for the model (2.32) by extending the parametric method we described in Chapter 3, Volume I, for determining the space in which oscillatory solutions were possible. The technique was developed and applied to several reaction diffusion models by Murray (1982); it is a general procedure applicable to other pattern formation mechanisms. Numerical procedures can also be used such as those developed by Zhu and Murray (1995)

The conditions on the parameters a, b and d for the mechanism (2.32) to generate spatial patterns, if the domain is sufficiently large, are given by (2.35) with γ coming into the picture via the possible unstable modes determined by (2.38). Even though the inequalities (2.35) are probably the simplest realistic set we could have in any reaction diffusion mechanism they are still algebraically quite messy to deal with. With other than extremely simple kinetics it is not possible to carry out a similar analysis analytically. So let us start with the representation of the steady state used in Section 7.4, Volume I, namely, (7.24), with u_0 as the nonnegative parametric variable; that is, v_0 and b are given in terms of a and u_0 from (7.24) (Volume I), or (2.33) above, as

$$v_0 = \frac{u_0 - a}{u_0^2}, \quad b = u_0 - a. \tag{2.55}$$

The inequalities (2.35), which define the conditions on the parameters for spatial patterns to grow, involve, on using the last expressions,

$$\begin{aligned} f_u &= -1 + 2u_0 v_0 = 1 - \frac{2a}{u_0}, \quad f_v = u_0^2, \\ g_u &= -2u_0 v_0 = -\frac{2(u_0 - a)}{u_0}, \quad g_v = -u_0^2. \end{aligned} \tag{2.56}$$

We now express the conditions for diffusion-driven instability given by (2.31) as inequalities in terms of the parameter u_0; these define boundary curves for domains in

parameter space. With the first,

$$\begin{aligned} f_u + g_v < 0 \quad &\Rightarrow \quad 1 - \frac{2a}{u_0} - u_0^2 < 0 \\ &\Rightarrow \quad a > \frac{u_0(1-u_0^2)}{2}, \quad b = u_0 - a > \frac{u_0(1+u_0^2)}{2}, \\ &\Rightarrow \quad b = \frac{u_0(1+u_0^2)}{2} \end{aligned} \tag{2.57}$$

as the boundary where, since we are interested in the boundary curve, the $b = u_0 - a$ comes from the steady state definition (2.55) and where we replace a by its expression from the inequality involving only u_0 and a. These define a domain parametrically in (a, b) space as we let u_0 take all positive values; if the inequality is replaced by an equality sign, (2.57) define the boundary curve parametrically. We now do this with each of the conditions in (2.31).

The second condition of (2.31), using (2.56), requires

$$f_u g_v - f_v g_u > 0 \quad \Rightarrow \quad u_0^2 > 0, \tag{2.58}$$

which is automatically satisfied. The third condition requires

$$\begin{aligned} df_u + g_v > 0 \Rightarrow \quad &a < \frac{u_0(d-u_0^2)}{2d}, \quad b = u_0 - a > \frac{u_0(d+u_0^2)}{2d}, \\ &\Rightarrow \quad b = \frac{u_0(d+u_0^2)}{2d} \end{aligned} \tag{2.59}$$

as the boundary curve.

The fourth condition in (2.31) is a little more complicated. Here

$$\begin{aligned} &(df_u + g_v)^2 - 4d(f_u g_v - f_v g_u) > 0 \\ &\Rightarrow \quad [u_0(d-u_0^2) - 2da]^2 - 4du_0^4 > 0 \\ &\Rightarrow \quad 4a^2d^2 - 4adu_0(d-u_0^2) + [u_0^2(d-u_0^2)^2 - 4u_0^4 d] > 0 \end{aligned}$$

which, on factorising the left-hand side, implies

$$a < \frac{u_0}{2}\left(1 - \frac{2u_0}{\sqrt{d}} - \frac{u_0^2}{d}\right) \quad \text{or} \quad a > \frac{u_0}{2}\left(1 + \frac{2u_0}{\sqrt{d}} - \frac{u_0^2}{d}\right).$$

Thus this inequality results in *two* boundary curves, namely,

$$\begin{aligned} a &= \frac{1}{2}u_0\left(1 - \frac{2u_0}{\sqrt{d}} - \frac{u_0^2}{d}\right), \quad b = u_0 - a = \frac{1}{2}u_0\left(1 + \frac{2u_0}{\sqrt{d}} + \frac{u_0^2}{d}\right), \\ a &= \frac{1}{2}u_0\left(1 + \frac{2u_0}{\sqrt{d}} - \frac{u_0^2}{d}\right), \quad b = u_0 - a = \frac{1}{2}u_0\left(1 - \frac{2u_0}{\sqrt{d}} + \frac{u_0^2}{d}\right). \end{aligned} \tag{2.60}$$

The curves, and the enclosed domains, defined parametrically by (2.57)–(2.60), define the parameter space or *Turing space* (see Murray 1982), where the steady state can be diffusionally driven unstable and hence create spatial patterns. As we noted in Section 2.4 the first and third conditions in (2.35) require f_u and g_v to have opposite signs which require $b > a$ and hence $d > 1$.

It is now a straightforward plotting exercise to obtain the curves defined by (2.57)–(2.60); we simply let u_0 take on a range of positive values and calculate the corresponding a and b for a given d. In general, with inequalities (2.57)–(2.60), five curves are involved in defining the boundaries. Here, as is often the case, several are redundant in that they are covered by one of the others. For example, in the first of (2.60),

$$a < \frac{1}{2}u_0\left(1 - \frac{2u_0}{\sqrt{d}} - \frac{u_0^2}{d}\right) < \frac{1}{2}u_0\left(1 - \frac{u_0^2}{d}\right)$$

since we are considering $u_0 > 0$, so (2.59) is automatically satisfied if we satisfy the first condition in (2.60). Also, since $d > 1$,

$$\frac{1}{2}u_0\left(1 - \frac{u_0^2}{d}\right) > \frac{1}{2}u_0\left(1 - u_0^2\right)$$

so the curve defined by (2.57) lies below the curve defined by (2.59); the former is a lower limiting boundary curve, so a suitable domain is defined if we use the first of (2.60). Furthermore, since

$$\frac{1}{2}u_0\left(1 - \frac{u_0^2}{d}\right) < \frac{1}{2}u_0\left(1 + \frac{2u_0}{\sqrt{d}} - \frac{u_0^2}{d}\right)$$

there can be no domain satisfying (2.59) and the second curve in (2.60).

Finally, therefore, for this mechanism we need only two parametric curves, namely, those defined by (2.57) and the first of (2.60), and the Turing space is determined by

$$\begin{aligned} &a > \frac{1}{2}u_0(1 - u_0^2), \quad b = \frac{1}{2}u_0(1 + u_0^2), \\ &a < \frac{1}{2}u_0\left(1 - \frac{2u_0}{\sqrt{d}} - \frac{u_0^2}{d}\right), \quad b = \frac{1}{2}u_0\left(1 + \frac{2u_0}{\sqrt{d}} + \frac{u_0^2}{d}\right). \end{aligned} \tag{2.61}$$

We know that when $d = 1$ there is no Turing space; that, is there is no domain where spatial patterns can be generated. The curves defined by (2.61) with $d = 1$ contradict each other and hence no Turing space exists. Now let d take on values greater than 1. For a critical d, d_c say, a Turing space starts to grow for $d > d_c$. Specifically $d = d_c = 3 + 2\sqrt{2}$, calculated from (2.61) by determining the d such that both curves give $a = 0$ at $b = 1$ and at this value the two inequalities are no longer contradictory. The space is defined, in fact, by two surfaces in (a, b, d) space. Figure 2.12 shows the cross-

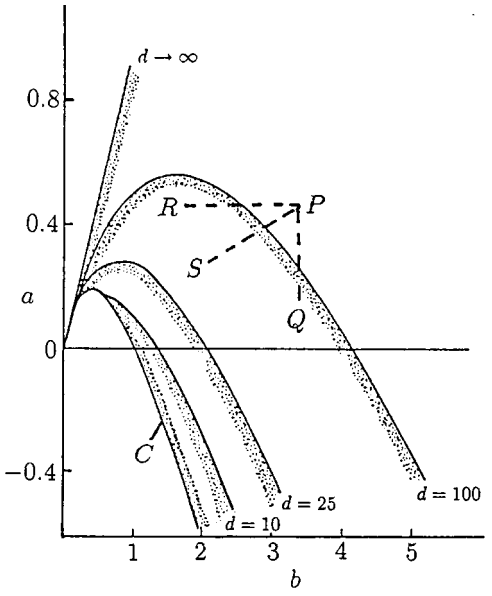

Figure 2.12. Turing space for (2.32), that is, the parameter space where spatial patterns can be generated by the reaction diffusion mechanism (2.32). For example, if $d = 25$ any values for a and b lying within the domain bounded by the curves marked C (that is, $d = 1$) and $d = 25$ will result in diffusion-driven instability. Spatial pattern will evolve if the domain (quantified by γ) is sufficiently large for allowable k^2, defined by (2.38) and (2.43).

sectional regions in (a, b) parameter space where the mechanism (2.32) can generate spatial patterns.

Even if a and b, for a given $d > 1$, lie within the Turing space this does not guarantee that the mechanism will generate spatial patterns, because scale and geometry play a major role. Depending on the size of γ and the actual spatial domain in which the mechanism operates, the unstable eigenfunctions, or modes, may not be allowable solutions. It is here that the detailed form of the dispersion relation comes in again. To be specific consider the one-dimensional finite domain problem defined by (2.36). The eigenvalues, that is, the wavenumbers, $k = n\pi/p,\ n = \pm 1, \pm 2 \ldots$ are *discrete*. So, referring to Figure 2.5(b), unless the dispersion relation includes in its range of unstable modes at least one of these discrete values no structure can develop. We must therefore superimpose on the Turing space in Figure 2.12 another axis representing the scale parameter γ. If γ is included in the parameters of the Turing space it is not necessarily simply connected since, if the dispersion relation, as γ varies, does not include an allowable eigenfunction in its unstable modes, no pattern evolves. Let us consider this aspect and examine the dispersion relation in more detail.

The Turing space involves only dimensionless parameters which are appropriate groupings of the dimensional parameters of the model. The parameters a, b and d in the last figure are, from (2.6),

$$a = \frac{k_1}{k_2}\left(\frac{k_3}{k_2}\right)^{1/2}, \quad b = \frac{k_4}{k_2}\left(\frac{k_3}{k_2}\right)^{1/2}, \quad d = \frac{D_B}{D_A}.$$

Suppose, for example, $d = 100$ and a and b have values associated with P in Figure 2.12; that is, the mechanism is not in a pattern formation mode. There is no unique

way to move into the pattern formation domain; we could decrease either a or b so that we arrive at Q or R respectively. In dimensional terms we can reduce a, for example, by appropriately changing k_1, k_2 or k_3—or all of them. Varying other than k_1 will also affect b, so we have to keep track of b as well. If we only varied k_2 the path in the Turing space is qualitatively like that from P to S. If d can vary, which means either of D_A or D_B can vary, we can envelope P in the pattern formation region by simply increasing d. Interpreting the results from a biological point of view, therefore, we see that it is the *orchestration of several effects which produce pattern*, not just one, since we can move into the pattern formation regime by varying one of several parameters. Clearly we can arrive at a specific point in the space by one of several paths. The concept of equivalent effects, via parameter variation, producing the same pattern is an important one in the interpretation and design of relevant experiments associated with any model. It is not a widely appreciated concept in biology. We shall discuss some important biological applications of the practical use of dimensionless groupings in subsequent chapters.

To recap briefly, the dispersion relation for the general reaction diffusion system (2.10) is given by the root $\lambda(k^2)$ of (2.23) with the larger real part. The key to the existence of unstable spatial modes is whether or not the function

$$h(k^2) = dk^4 - \gamma(df_u + g_v)k^2 + \gamma^2(f_u g_v - f_v g_u) \tag{2.62}$$

is negative for a range of $k^2 \neq 0$; see Figure 2.5(a). Remember that the f and g derivatives are evaluated at the steady state (u_0, v_0) where $f(u_0, v_0) = g(u_0, v_0) = 0$, so $h(k^2)$ is a quadratic in k^2 whose coefficients are functions only of the parameters of the kinetics, d the diffusion coefficient ratio and the scale parameter γ. The minimum, $h_{\min}$, at $k = k_m$ corresponds to the λ with the maximum $\mathrm{Re}\,\lambda$ and hence the mode with the largest growth factor $\exp[\lambda(k_m^2)t]$. From (2.25), or simply from the last equation, $h_{\min}$ is given by

$$\begin{aligned} h_{\min} = h(k_m^2) &= -\frac{1}{4}\gamma^2\left[df_u^2 + \frac{g_v^2}{d} - 2(f_u g_v - 2f_v g_u)\right], \\ k_m^2 &= \gamma\frac{df_u + g_v}{2d}. \end{aligned} \tag{2.63}$$

The bifurcation between spatially stable and unstable modes is when $h_{\min} = 0$. When this holds there is a critical wavenumber k_c which, from (2.28) or again simply derived from (2.62), is when the parameters are such that

$$(df_u + g_v)^2 = 4d(f_u g_v - f_v g_u) \quad \Rightarrow \quad k_c^2 = \gamma\frac{df_u + g_v}{2d}. \tag{2.64}$$

As the parameters move around the Turing space we can achieve the required equality, the first of the equations in (2.64), by letting one or other of the parameters pass through its bifurcation values, all other parameters being kept fixed. In the last section, and in Figure 2.5(b), for example, we chose d as the parameter to vary and for given a and b we evaluated the bifurcation value d_c. In this situation, just at bifurcation, that is, when $h_{\min}(k_c^2) = 0$, a single spatial pattern with wavenumber k_c is driven unstable, or

excited, for $d = d_c + \varepsilon$, where $0 < \varepsilon \ll 1$. This critical wavenumber from (2.64) is proportional to $\sqrt{\gamma}$ and so we can vary which spatial pattern is initiated by varying γ. This is called *mode selection* and is important in applications as we shall see later.

In the case of finite domains we can isolate a specific mode to be excited, or driven unstable, by choosing the width of the band of unstable wavenumbers to be narrow and centred round the desired mode. Let us take the parameters in the kinetics to be fixed and let $d = d_c + \varepsilon$, $0 < \varepsilon \ll 1$. We then get from (2.64) the appropriate γ for a specified k as

$$\gamma \approx \frac{2d_c k^2}{d_c f_u + g_v}, \tag{2.65}$$

where the kinetics parameters at bifurcation, sometimes called the *marginal kinetics state*, satisfy the first of (2.64). So, by varying γ we can isolate whatever mode we wish to be excited. Figure 2.13(a) shows a typical situation. Arcuri and Murray (1986) have carried out an extensive Turing space analysis for the much more complex Thomas (1975) mechanism in such a case. Note in Figure 2.13(a) that as γ increases $h_{\min}$ becomes more negative, as is indicated by (2.63).

Suppose now we keep γ and the kinetics parameters fixed, and let d increase from its bifurcation value d_c. From (2.63) $h_{\min} \sim -(d/4)(\gamma f_u)^2$ for d large and so $\lambda \to \infty$ with d. The width of the band of unstable modes has wavenumbers bounded by the zeros k_1 and k_2 of $h(k^2)$ in (2.62). These are given by (2.29), or immediately from (2.62) as

$$\begin{aligned} k_1^2 &= \frac{\gamma}{4d}\left[(df_u + g_v) - \{(df_u + g_v)^2 - 4d(f_u g_v - f_v g_u)\}^{1/2}\right], \\ k_2^2 &= \frac{\gamma}{4d}\left[(df_u + g_v) + \{(df_u + g_v)^2 - 4d(f_u g_v - f_v g_u)\}^{1/2}\right], \end{aligned} \tag{2.66}$$

from which we get

$$k_1^2 \sim 0, \quad k_2^2 \sim \gamma f_u \quad \text{as} \quad d \to \infty. \tag{2.67}$$

So, for a fixed scale there is an upper limit for the unstable mode wavenumber and hence a lower limit for the possible wavelengths of the spatial patterns. Figure 2.13(b) illustrates a typical case for the Thomas (1975) system given by (2.8).

With all kinetics parameters fixed, each parameter pair (d, γ) defines a unique parabola $h(k^2)$ in (2.62), which in turn specifies a set of unstable modes. We can thus consider the (d, γ) plane to be divided into regions where specific modes or a group of modes are diffusively unstable. When there are several unstable modes, because of the form of the dispersion relation, such as in Figure 2.5(b), there is clearly a mode with the largest growth rate since there is a maximum Re λ for some k_m^2 say. From (2.23), the positive eigenvalue $\lambda_+(k^2)$ is given by

$$2\lambda_+(k^2) = \gamma(f_u + g_v) - k^2(1 + d) + \{[\gamma(f_u + g_v) - k^2(1 + d)]^2 - 4h(k^2)\}^{1/2}$$

which has a maximum for the wavenumber k_m given by

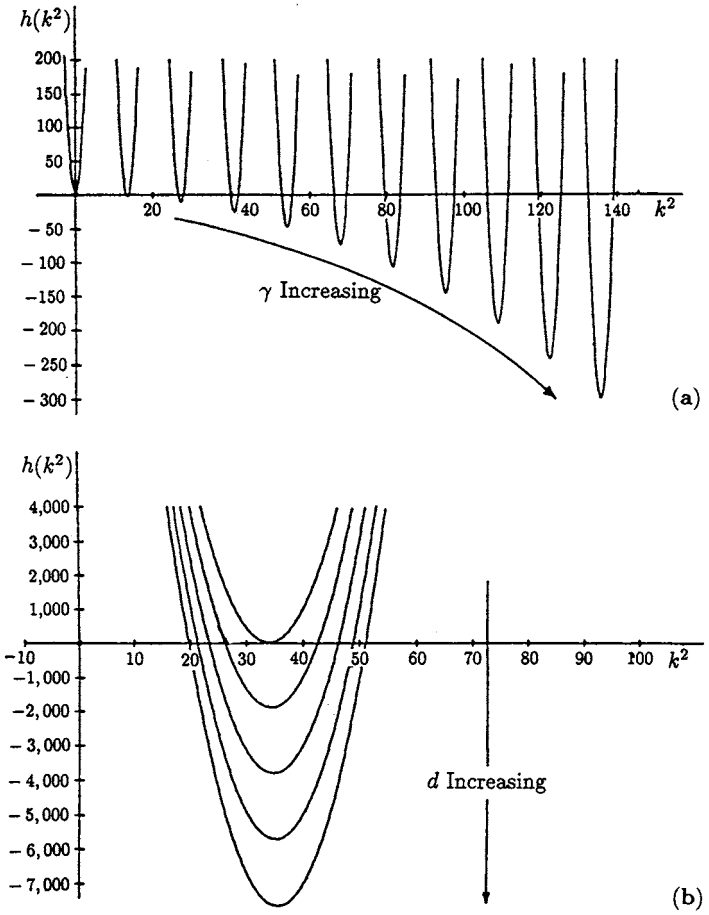

Figure 2.13. (**a**) Isolation of unstable modes (that is, $h(k^2) < 0$ in (2.23)) by setting the diffusion ratio $d = d_c + \varepsilon, 0 < \varepsilon \ll 1$ and varying the scale γ for the Thomas (1975) kinetics (2.8) with $a = 150$, $b = 100$, $\alpha = 1.5$, $\rho = 13$, $K = 0.05$, $d = 27.03$: the critical $d_c = 27.02$. (**b**) The effect of increasing d with all other parameters fixed as in (**a**). As $d \to \infty$ the range of unstable modes is bounded by $k^2 = 0$ and $k^2 = \gamma f_u$.

$$k^2 = k_m^2 = \frac{\gamma}{d-1}\left\{(d+1)\left[-\frac{f_v g_u}{d}\right]^{1/2} - f_u + g_v\right\}. \tag{2.68}$$

As we have noted the prediction is that the fastest growing k_m-mode will be that which dominates and hence will be the mode which evolves into the steady state nonlinear pattern. This is only a reasonable prediction for the lower modes. The reason is that with the higher modes the interaction caused by the nonlinearities is more complex than when only the simpler modes are linearly unstable. Thus using (2.68) we can map the regions in (d, γ) space where a specific mode, and hence pattern, will evolve; see Arcuri and Murray (1986). Figures 2.14(a) and (b) show the mappings for the Thomas (1975)

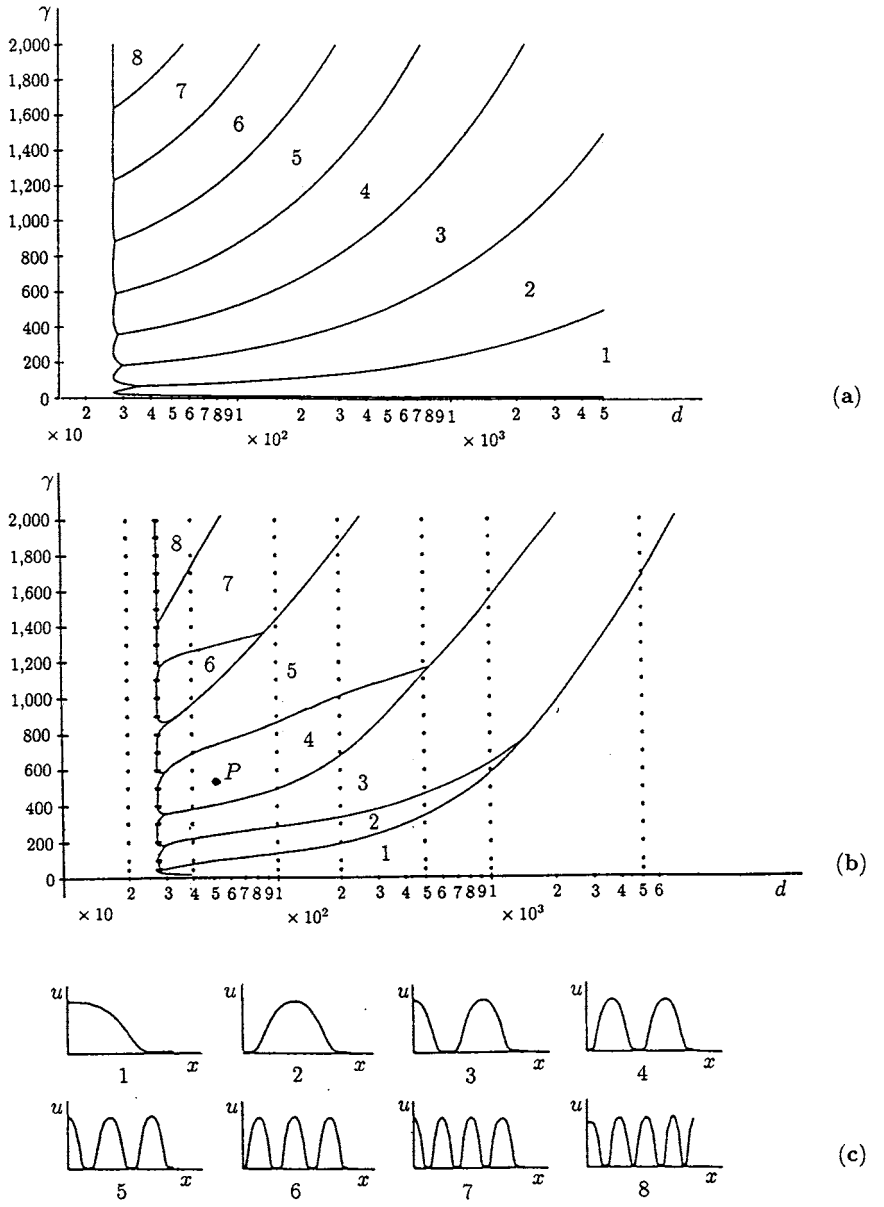

Figure 2.14. (**a**) Predicted solution space, based on linear theory, showing the regions with the fastest growing modes for the Thomas (1975) system (2.8) with parameter values as in Figure 2.13 and zero flux boundary conditions. (**b**) A typical space as evaluated from the numerical simulation of the full nonlinear Thomas system (2.8) with the same parameter values and zero flux boundary conditions as in (**a**). Each (γ, d) point marked with a period represents a specific simulation of the full nonlinear system. (**c**) The corresponding spatial concentration patterns obtained with parameters d and γ in the regions indicated in (**b**). Spatial patterns can be visualised by setting a threshold u^* and shading for $u > u^*$. The first two morphogen distributions, for example, correspond to the first two patterns in Figure 2.9. (From Arcuri and Murray 1986)

system in one space dimension calculated from the linear theory and the full nonlinear system, while Figure 2.14(c) shows the corresponding spatial morphogen patterns indicated by Figure 2.14(b).

An important use of such parameter spaces is the measure of the robustness of the mechanism to random parameter variation. With Figure 2.14(b), for example, suppose the biological conditions result in a (d, γ) parameter pair giving P, say, in the region which evolves to the 4-mode. A key property of any model is how sensitive it is to the inevitable random perturbations which exist in the real world. From Figure 2.14(b) we see what leeway there is if a 4-mode pattern is required in the developmental sequence. This (d, γ) space is but one of the relevant spaces to consider, of course, since any mechanism involves other parameters. So, in assessing robustness, or model sensitivity, we must also take into account the size and shape of the Turing space which involves all of the kinetics parameters. Probably (d, γ) spaces will not be too different qualitatively from one reaction diffusion system to another. What certainly is different, however, is the size and shape of the Turing space, and it is this space which provides another useful criterion for comparing relevant robustness of models. Murray (1982) studied this specific problem and compared various specific reaction diffusion mechanisms with this in mind. He came to certain conclusions as to the more robust mechanisms: both the Thomas (1975) and Schnakenberg (1979) systems, given respectively by (2.7) and (2.8), have relatively large Turing spaces, whereas that of the activator–inhibitor model of Gierer and Meinhardt (1972), given by (2.9) is quite small and implies a considerable sensitivity of pattern to small parameter variation. In the next chapter on specific pattern formation problems in biology we touch on other important aspects of model relevance which are implied by the form of the dispersion relation and the nondimensionalisation used.

The parameter spaces designating areas for specific patterns were all obtained with initial conditions taken to be random perturbations about the uniform steady state. Even in the low modes the polarity can be definitively influenced by biased initial conditions. We can, for example, create a single hump pattern with a single maximum in the centre of the domain or with a single minimum in the centre; see Figure 2.8(b). So even though specific modes can be isolated, initial conditions can strongly influence the polarity. When several of the modes are excitable, and one is naturally dominant from the dispersion relation, we can still influence the ultimate pattern by appropriate initial conditions. If the initial conditions include a mode within the unstable band and whose amplitude is sufficiently large, then this mode can persist through the nonlinear region to dominate the other unstable modes and the final pattern qualitatively often has roughly that wavelength. We discuss this in more detail in the next section. These facts also have highly relevant implications for biological applications.

2.6 Mode Selection and the Dispersion Relation

Consider a typical no frills or simplest dispersion relation giving the growth factor λ as a function of the wavenumber or wavelength ω such as shown in Figure 2.5(b) where a band of wavenumbers is linearly unstable. Let us also suppose the domain is finite so that the spectrum of eigenvalues is discrete. In the last section we saw how geometry

and scale played key roles in determining the particular pattern predicted from linear theory, and this was borne out by numerical simulation of the nonlinear system; see also the results presented in the next chapter. We pointed out that initial conditions can play a role in determining, for example, the polarity of a pattern or whether a specific pattern will emerge. If the initial conditions consist of small random perturbations about the uniform steady state then the likely pattern to evolve is that with the largest linear growth. In many developmental problems, however, the trigger for pattern initiation is scale; there are several examples in the following chapter, Chapter 4 in particular, but also in later chapters. In other developmental situations a perturbation from the uniform steady state is initiated at one end of the spatial domain and the spatial pattern develops from there, eventually spreading throughout the whole domain. The specific pattern that evolves for a given mechanism therefore can depend critically on how the instability is initiated. In this section we investigate this further so as to suggest what patterns will evolve from which initial conditions, for given dispersion relations, as key parameters pass through bifurcation values. The problem of which pattern will evolve, namely, mode selection, is a constantly recurring one. The following discussion, although motivated by reaction diffusion pattern generators, is quite general and applies to any pattern formation model which produces a similar type of dispersion relation.

Consider a basic dispersion relation $\lambda(\omega^2)$ where the wavelength $\omega = 2\pi/k$ with k the wavenumber, such as in Figure 2.15(a). Now take a one-dimensional domain and consider in turn the three possible ways of initiating pattern as shown in Figures 2.15(b), (c) and (d).

Consider first the case in Figure 2.15(b). Here the initial perturbation has all modes present in its expansion in terms of the eigenfunctions and so all modes in the unstable band of wavelengths in Figure 2.15(a) are stimulated. The mode with the maximum λ, ω_2, is the one with the fastest growth and it ultimately dominates. The steady state inhomogeneous pattern that persists is then that with wavelength ω_2.

In Figure 2.15(c) we envisage the domain to be growing at a rate that is slow compared with the time to generate spatial pattern. Later in this section we describe a caricature system where growth is not small. In Chapter 4 we go into the important effect of growth on pattern in more detail; the interaction is crucial there. For small $L(t)$ the domain is such that it cannot contain any wave with wavelengths in the unstable band. When it reaches L_c, the critical domain size for pattern, it can sustain the smallest wavelength pattern, namely, that with wavelength ω_1. In the time it takes $L(t)$ to grow sufficiently to allow growth of the next wavenumber, that with wavelength ω_1 is sufficiently established to dominate the nonlinear stage. So the final pattern that emerges is that with the base wavelength ω_1.

Travelling Wave Initiation of Pattern

Consider the situation, as in Figure 2.15(d), where the pattern is initiated at one end of the domain; what happens here is more subtle. We expect the final pattern to have a wavelength somewhere within the unstable band predicted by the dispersion relation. To see how to calculate the wavenumber in general let us start with an infinite one-dimensional domain and a general linear system

$$\mathcal{J}\mathbf{w} = 0, \quad \mathbf{w}(x,t) \propto \exp(ikx + \lambda t) \quad \Rightarrow \quad \lambda = \lambda(k), \tag{2.69}$$

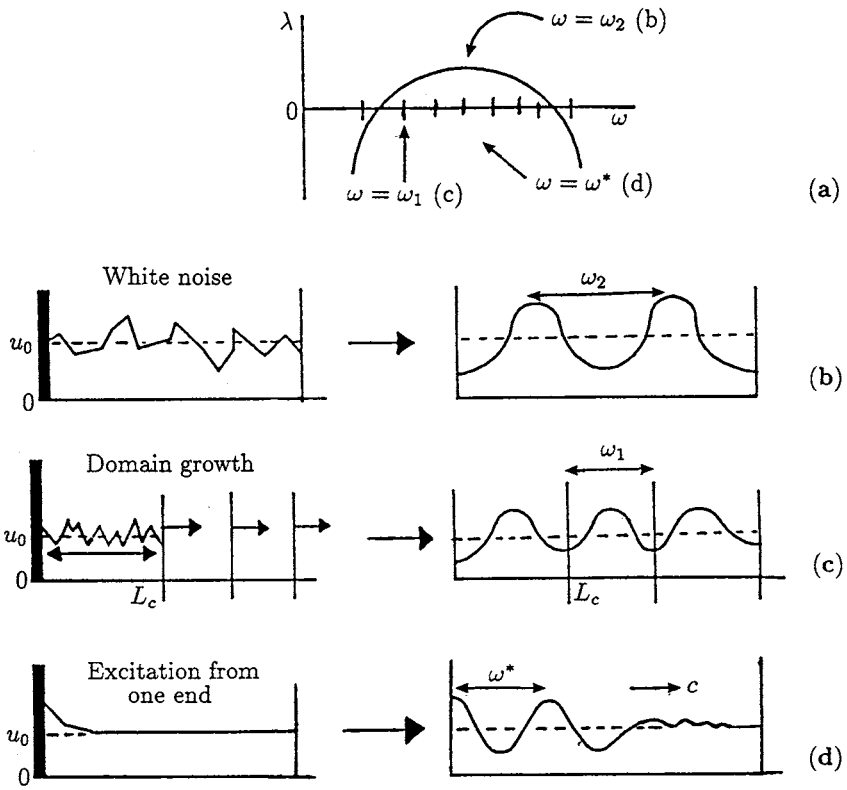

Figure 2.15. (**a**) Typical basic dispersion relation giving the growth coefficient λ as a function of the wavelength ω of the spatial pattern. (**b**) Here the initial disturbance is a random perturbation (white noise) about the uniform steady state u_0. The pattern which evolves corresponds to ω_2 in (**a**), the mode with the largest growth rate. (**c**) Pattern evolution in a growing domain. The first unstable mode to be excited, ω_1, remains dominant. (**d**) Here the initial disturbance is at one end and it lays down a pattern as the disturbance moves through the domain. The pattern which evolves has a wavelength ω^* somewhere within the band of unstable wavelengths.

where $\mathcal{J}$ is a linear operator such as that associated with the linear form of reaction diffusion equations. For (2.20), for example, $\mathcal{J} = (\partial/\partial t) - \gamma A - D\nabla^2)$ and the dispersion relation $\lambda(k)$ is like that in Figure 2.5(b) or in the last figure, Figure 2.16(a), with ω replaced by k; in other words the classic form. The general solution $\mathbf{w}$ of the linear system in (2.69) is

$$\mathbf{w}(x,t) = \int \mathbf{A}(k) \exp[ikx + \lambda(k)t]\, dk, \tag{2.70}$$

where the $\mathbf{A}(k)$ are determined by a Fourier transform of the initial conditions $\mathbf{w}(x, 0)$. Since we are concerned with the final structure and not the transients we do not need to evaluate $\mathbf{A}(k)$ here.

Suppose the initial conditions $\mathbf{w}(x, 0)$ are confined to a small finite domain around $x = 0$ and the pattern propagates out from this region. We are interested in the wavelike

generation of pattern as shown in the second figure in Figure 2.15(d). This means that we should look at the form of the solution well away from the origin. In other words, we should focus our attention on the asymptotic form of the solution for x and t large but such that x/t is $O(1)$, which means we move with a velocity $c = x/t$ and so are in the vicinity of the 'front,' roughly where the arrow (with c at the end) is in the second figure in Figure 2.15(d). We write (2.70) in the form

$$\mathbf{w}(x,t) = \int \mathbf{A}(k) \exp[\sigma(k)t]\, dk, \quad \sigma(k) = ikc + \lambda(k), \quad c = \frac{x}{t}. \tag{2.71}$$

The asymptotic evaluation of this integral for $t \to \infty$ is given by analytically continuing the integrand into the complex k-plane and using the method of steepest descents (see Murray's 1984 book, Chapter 3) which gives

$$\mathbf{w}(x,t) \sim \mathbf{J}(k_0) \left[\frac{2\pi}{t\,|\,\sigma''(k_0)\,|} \right]^{1/2} \exp\{t[ik_0c + \lambda(k_0)]\},$$

where $\mathbf{J}$ is a constant and k_0 (now complex) is given by

$$\sigma'(k_0) = ic + \lambda'(k_0) = 0. \tag{2.72}$$

The asymptotic form of the solution is thus

$$\mathbf{w}(x,t) \sim \frac{\mathbf{K}}{t^{1/2}} \exp\{t[ick_0 + \lambda(k_0)]\}, \tag{2.73}$$

where $\mathbf{K}$ is a constant.

For large t the wave 'front' is roughly the point between the pattern forming tail and the leading edge which initiates the disturbances, that is, where $\mathbf{w}$ neither grows nor decays. This is thus the point where

$$\text{Re}\,[ick_0 + \lambda(k_0)] \approx 0. \tag{2.74}$$

At the 'front' the wavenumber is Re k_0 and the solution frequency of oscillation ω is

$$\omega = \text{Im}\,[ick_0 + \lambda(k_0)].$$

Denote by k^* the wavenumber of the pattern laid down behind the 'front.' We now assume there is conservation of nodes across the 'front' which implies

$$k^*c = \omega = \text{Im}\,[ick_0 + \lambda(k_0)]. \tag{2.75}$$

The three equations (2.72), (2.74) and (2.75) now determine k_0 and the quantities we are interested in, namely, c and k^*, which are respectively the speed at which the pattern is laid down and the steady state pattern wavenumber. Because of the complex variables this is not as simple as it might appear. Myerscough and Murray (1992), for the case of a cell-chemotaxis system (see also Chapter 4), used the technique and developed a

caricature dispersion relation to solve the three equations analytically. They compared their analytical results with the exact numerical simulations; the comparison was good and, of course, qualitatively useful since analytical results were obtained. This technique has also been used (numerically) by Dee and Langer (1983) for a reaction diffusion mechanism.

Dynamics of Pattern Formation in Growing Domains

The time evolution of patterns in growing domains can be quite complex, particularly if the domain growth is comparable with the generation time of the spatial pattern and there are two or more space dimensions. The form of the dispersion relation as the scale γ increases can have highly pertinent biological implications as we shall see in Chapter 6 when we consider, as one example, cartilage formation in the developing limb. Here we introduce the phenomenon and discuss some of the implications of two specific classes of dispersion relation behaviour as γ increases with time.

The form of reaction diffusion equations in growing domains has to be derived carefully and this is done in Chapter 4 which is mainly concerned with patterning problems and the effect of growth on the patterns formed. Here we consider only a caricature form to demonstrate certain time-dependent effects of growing domains. With a simplified caricature we should not expect to capture all of the possible sequential spatial patterns and this is indeed the case. Crampin et al. (1999), in a comprehensive analytical and numerical examination of reaction diffusion systems in growing one-dimensional domains, categorise the sequential patterns which evolve. They consider different growth forms. They use a self-similarity argument to predict frequency doubling in the case of exponential growth and show how growth may be a mechanism for increasing pattern robustness. Kulesa et al. (1996a,b) (see also Chapter 4) show that the sequential positioning of teeth primordia (precursors of teeth) is intimately related to jaw growth, which is experimentally determined. The correct sequence of primordial appearance depends crucially on the interaction of the pattern formation process and domain growth dynamics. A somewhat different approach to including domain change was used by Murray and Myerscough (1992) in their study of snake patterns which we discuss in some detail in Chapter 4: they looked at bifurcations from solutions of the steady state equations (cell-chemotaxis equations in this case).

In Figure 2.8(a) we saw that as the scale γ increased the dispersion curve was moved along the axis where it successively excited modes with smaller wavelengths. Figure 2.16(a) is a repeat example of this behaviour. Figure 2.16(b) is another possible behaviour of a dispersion relation as the scale γ increases. They imply different pattern generation scenarios for growing domains.

Consider first the situation in Figure 2.16(a). Here for $\gamma = \gamma_1$ the mode with wavelength ω_1 is excited and starts to grow. As the domain increases we see that for $\gamma = \gamma_2$ no mode lies within the unstable band and so the pattern decays to the spatially uniform steady state. With further increase in scale, to $\gamma = \gamma_3$ say, we see that a pattern with wavelength ω_2 is created. So the pattern formation is effectively a discrete process with successively more structure created as γ increases but with each increase in structure interspersed with a regime of spatial homogeneity. Figure 2.17(a) illustrates the sequence of events as γ increases in the way we have just described.

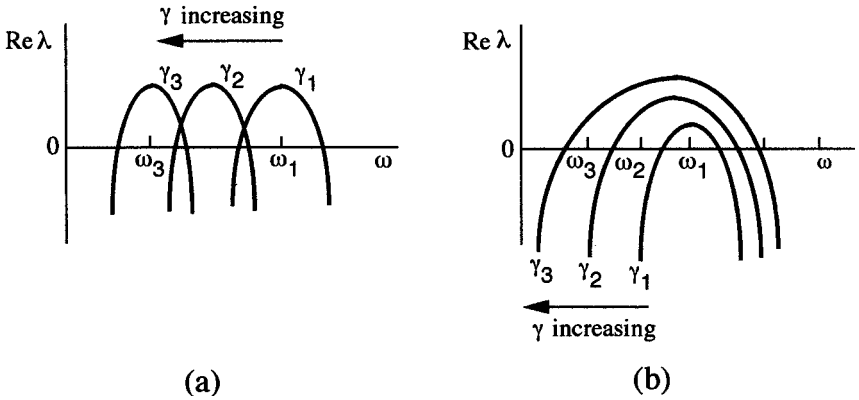

Figure 2.16. (**a**) As the scale γ increases from γ_1 to γ_3 the dispersion relation isolates specific modes interspersed with gaps during which no pattern can form. (**b**) Here as γ increases the number of unstable modes increases: the mode with maximum growth varies with γ. Unstable modes exist for all $\gamma \geq \gamma_1$.

Consider now the behaviour implied by the dispersion relation dependence on scale implied by Figure 2.16(b). Here the effect of scale is simply to increase the band of unstable modes. The dominant mode changes with γ so there is a continuous evolution from one mode, dominant for $\gamma = \gamma_1$ say, to another mode as it becomes dominant for $\gamma = \gamma_3$ say. This dynamic development of pattern is illustrated in Figure 2.17(b). We shall see later in Section 6.6 how the implications of Figures 2.16 and 2.17 have a direct bearing on how cartilage patterns form in the developing limb.

When comparing different models with experiments it is not always possible to choose a given time as regards pattern generation to carry out the experiments since it is not generally known exactly when the pattern formation takes place in embryogenesis.

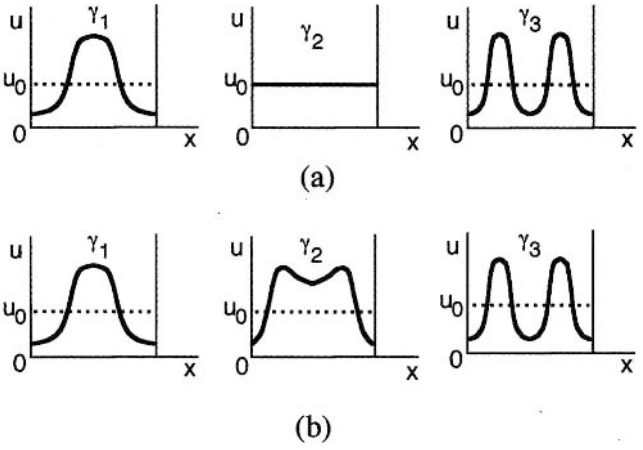

Figure 2.17. (**a**) Development of spatial patterns with a dispersion relation dependence on scale, via γ, as shown in Figure 2.16(a). (**b**) Sequential development of pattern as γ varies according to the dispersion relation in Figure 2.16(b).

When it is possible, then similarity of pattern is a necessary first step in comparison with theory. When it is not possible, the dynamic form of the pattern can be important and can be the key step in deciding which mechanism is the more appropriate. We shall recall these comments later in Chapters 4 and 6.

A computed example of dynamic pattern formation as the scale γ is increased is shown in Figure 2.18.

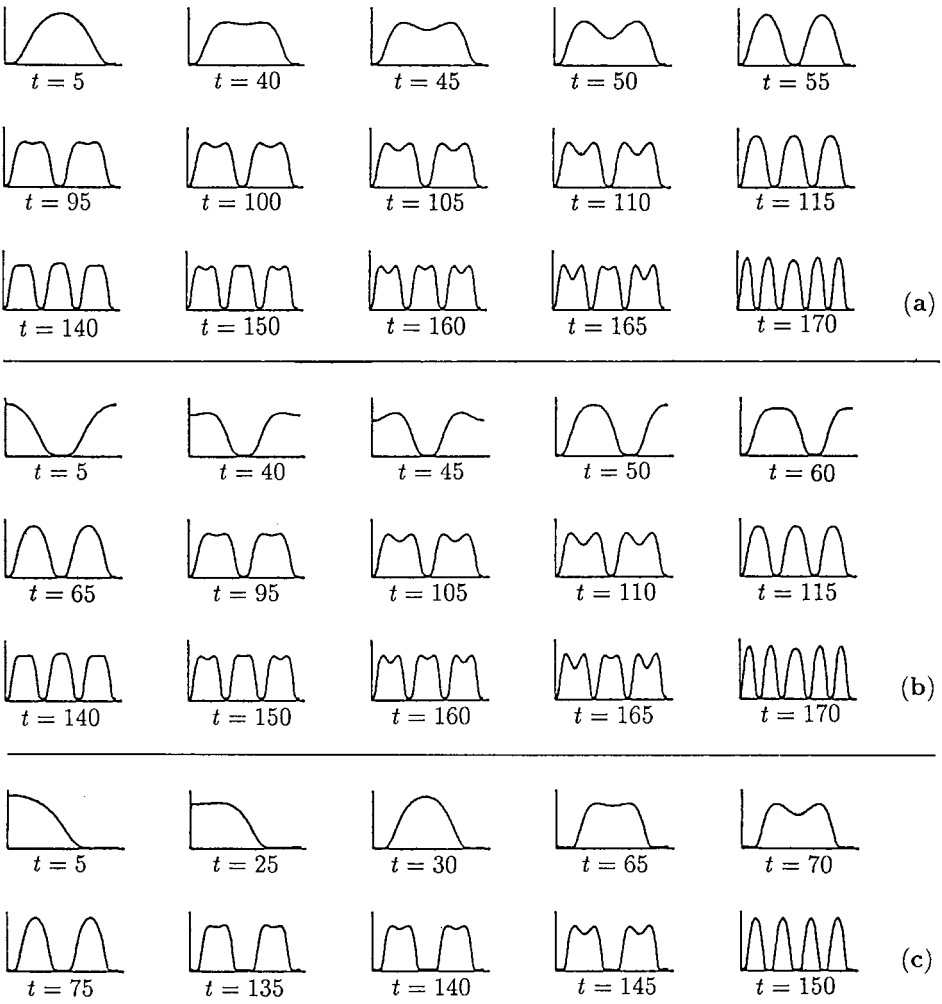

Figure 2.18. Sequence of one-dimensional spatial patterns obtained numerically with the mechanism (2.10) and kinetics given by the second of (2.8). Zero flux boundary conditions were used and the domain growth is incorporated in the scale parameter $\gamma(t) = s + 0.1t^2$ with s fixed. This gives a caricature for the reaction diffusion system for a linear rate of domain growth since $\gamma \propto (length)^2$. Parameter values for the kinetics are as in Figure 2.13(a) except for d. (**a**) and (**b**) have $d = 30$ ($d_c \approx 27$), $s = 100$ and two different sets of initial random perturbations. Note how the two sets of patterns converge as time t increases. (**c**) has $d = 60$, $s = 50$. As d increases more modes are missed in the pattern sequence and there is a distinct tendency towards frequency doubling. (After Arcuri and Murray 1986)

In these simulations the mechanism's pattern generation time is smaller than a representative growth time since the sequence of patterns clearly forms before breaking up to initiate the subsequent pattern. This is an example of a dispersion relation behaviour like that in Figure 2.16(b); that is, there is no regime of spatial homogeneity. The tendency to period doubling indicated by Figure 2.18(c) is interesting and as yet unexplained. Arcuri and Murray (1986) consider this and other aspects of pattern formation in growing domains. It must be kept in mind that the latter study is a caricature reaction diffusion system in a growing domain; refer to Chapter 4 for the exact formulation with exponential domain growth and Crampin et al. (1999) for a comprehensive discussion.

2.7 Pattern Generation with Single-Species Models: Spatial Heterogeneity with the Spruce Budworm Model

We saw above that if the domain size is not large enough, that is, γ is too small, reaction diffusion models with zero flux boundary conditions cannot generate spatial patterns. Zero flux conditions imply that the reaction diffusion domain is isolated from the external environment. We now consider different boundary conditions which take into account the influence of the region exterior to the reaction diffusion domain. To be specific, consider the single reaction diffusion equation in the form

$$u_t = f(u) + D\nabla^2 u, \tag{2.76}$$

and think of the model in an ecological setting; that is, u denotes the population density of a species. Here $f(u)$ is the species' dynamics and so we assume $f(0) = 0$, $f'(0) \neq 0$, $f(u_i) = 0$ for $i = 1$ if there is only one (positive) steady state or $i = 1, 2, 3$ if there are three. Later we shall consider the population dynamics $f(u)$ to be those of the spruce budworm, which we studied in detail in Chapter 1, Volume I, Section 1.2 and which has three steady states as in Figure 1.5(b) (Volume I). The diffusion coefficient D is a measure of the dispersal efficiency of the relevant species.

We consider in the first instance the one-dimensional problem for a domain $x \in (0, L)$, the exterior of which is completely hostile to the species. This means that on the domain boundaries $u = 0$. The mathematical problem we consider is then

$$\begin{aligned} &u_t = f(u) + Du_{xx}, \\ &u(0,t) = 0 = u(L,t), \quad u(x,0) = u_0(x), \\ &f(0) = 0, \quad f'(0) > 0, \quad f(u_2) = 0, \quad f'(u_2) > 0, \\ &f(u_i) = 0, \quad f'(u_i) < 0, \quad i = 1, 3, \end{aligned} \tag{2.77}$$

where u_0 is the initial population distribution. The question we want to answer is whether or not such a model can sustain spatial patterns.

In the spatially homogeneous situation $u = 0$ and $u = u_2$ are unstable and u_1 and u_3 are stable steady states. In the absence of diffusion the dynamics imply that u tends to one or other of the stable steady states and which it is depends on the initial

conditions. In the spatial situation, therefore, we would expect $u(x,t)$ to try to grow from $u = 0$ except at the boundaries. Because $u_x \neq 0$ at the boundaries the effect of diffusion implies that there is a flux of u out of the domain $(0, L)$. So, for u small there are two competing effects, the growth from the dynamics and the loss from the boundaries. As a first step we examine the linear problem obtained by linearising about $u = 0$. The relevant formulation is, from (2.77),

$$\begin{aligned} &u_t = f'(0)u + Du_{xx}, \\ &u(0,t) = u(L,t) = 0, \quad u(x,0) = u_0(x). \end{aligned} \tag{2.78}$$

We look for solutions in the form

$$u(x,t) = \sum_n a_n e^{\lambda t} \sin(n\pi x/L),$$

which by inspection satisfy the boundary conditions at $x = 0, L$. Substitution of this into (2.78) and equating coefficients of $\sin(n\pi x/L)$ determines λ as $\lambda = [f'(0) - D(n\pi/L)^2]$ and so the solution is given by

$$u(x,t) = \sum_n a_n \exp\left\{\left[f'(0) - D\left(\frac{n\pi}{L}\right)^2\right]t\right\} \sin\frac{n\pi x}{L}, \tag{2.79}$$

where the a_n are determined by a Fourier series expansion of the initial conditions $u_0(x)$. We do not need the a_n in this analysis. From (2.79) we see that the dominant mode in the expression for u is that with the largest λ, namely, that with $n = 1$, since

$$\exp\left[f'(0) - D\left(\frac{n\pi}{L}\right)^2\right]t < \exp\left[f'(0) - D\left(\frac{\pi}{L}\right)^2\right]t, \quad \text{for all} \quad n \geq 2.$$

So, if the dominant mode tends to zero as $t \to \infty$, so then do all the rest. We thus get as our condition for the linear stability of $u = 0$,

$$f'(0) - D\left(\frac{\pi}{L}\right)^2 < 0 \quad \Rightarrow \quad L < L_c = \pi\left[\frac{D}{f'(0)}\right]^{1/2}. \tag{2.80}$$

In dimensional terms D has units $\mathrm{cm}^2\mathrm{s}^{-1}$ (or $\mathrm{km}^2\mathrm{yr}^{-1}$ or whatever scale we are interested in) and $f'(0)$ has units s^{-1} since it is the linear birth rate (for u small $f(u) \approx f'(0)u$) which together give L_c in centimetres. Thus if the domain size L is less than the critical size L_c, $u \to 0$ as $t \to \infty$ and no spatial structure evolves. The larger the diffusion coefficient the larger is the critical domain size; this is in keeping with the observation that as D increases so also does the flux out of the region.

The scenario for spatial structure in a growing domain is that as the domain grows and L just passes the bifurcation length L_c, $u = 0$ becomes unstable and the first mode

$$a_1 \exp\left[f'(0) - D\left(\frac{\pi}{L}\right)^2 t\right] \sin\frac{\pi x}{L}$$

starts to grow with time. Eventually the nonlinear effects come into play and $u(x,t)$ tends to a steady state spatially inhomogeneous solution $U(x)$, which, from (2.77), is determined by

$$DU'' + f(U) = 0, \quad U(0) = U(L) = 0, \tag{2.81}$$

where the prime denotes differentiation with respect to x. Because $f(U)$ is nonlinear we cannot, in general, get an explicit solution for U.

From the spatial symmetry in (2.77) and (2.81) — setting $x \to -x$ leaves the equations unchanged — we expect the solutions to be symmetric in x about the midpoint $x = L/2$. Since $u = 0$ at the boundaries we assume the midpoint is the maximum, u_m say, where $U' = 0$; it is helpful now to refer to Figure 2.19(a). If we multiply (2.81) by U' and integrate with respect to x from 0 to L we get

$$\frac{1}{2}DU'^2 + F(U) = F(u_m), \quad F(U) = \int_0^U f(s)\,ds \tag{2.82}$$

since $U = u_m$ when $U' = 0$. It is convenient to change the origin to $L/2$ so that $U'(0) = 0$ and $U(0) = u_m$; that is, set $x \to x - L/2$. Then

$$\left(\frac{D}{2}\right)^{1/2} \frac{dU}{dx} = [F(u_m) - F(U)]^{1/2}$$

which integrates to give

$$|x| = \left(\frac{D}{2}\right)^{1/2} \int_{U(x)}^{u_m} [F(u_m) - F(w)]^{-1/2} dw, \tag{2.83}$$

which gives the solution $U(x)$ implicitly; typical solutions are illustrated schematically in Figure 2.19(b). The boundary conditions $u = 0$ at $x = \pm L/2$ and the last equation give

$$L = (2D)^{1/2} \int_0^{u_m} [F(u_m) - F(w)]^{-1/2} dw \quad \Rightarrow \quad u_m = u_m(L). \tag{2.84}$$

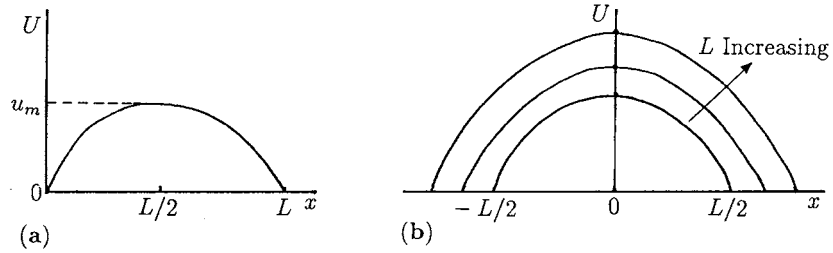

Figure 2.19. (**a**) Typical steady state pattern in the population u governed by (2.77) when the domain length $L > L_c$, the critical size for instability in the zero steady state. Note the symmetry about $L/2$. (**b**) Schematic steady state solution with the origin at the symmetry point where $u = u_m$ and $u_x = 0$.

We thus obtain, implicitly, u_m as a function of L. The actual determination of the dependence of u_m on L has to be carried out numerically. Note the singularity in the integrand when $w = u_m$, but because of the square root it is integrable. Typically u_m increases with L as illustrated in Figure 2.19(b).

Spatial Patterning of the Spruce Budworm

Now consider the model for the spruce budworm, the dynamics for which we derived in Chapter 1, Volume I. Here, using (1.8) for $f(u)$, (2.77) becomes

$$u_t = ru\left(1 - \frac{u}{q}\right) - \frac{u^2}{1+u^2} + Du_{xx} = f(u) + Du_{xx}, \tag{2.85}$$

where the positive parameters r and q relate to the dimensionless quantities associated with the dimensional parameters in the model defined by (1.7) in Chapter 1, Volume I; q is proportional to the carrying capacity and r is directly proportional to the linear birth rate and inversely proportional to the intensity of predation. The population dynamics $f(u)$ is sketched in Figure 2.20(a) when the parameters are in the parameter domain giving three positive steady states u_1, u_2 and u_3, the first and third being linearly stable and the second unstable. With $F(u)$ defined by (2.82) and substituted into (2.84) we have u_m as a function of the domain size L. This was evaluated numerically by Ludwig et al. (1979) the form of which is shown in Figure 2.20(b); there is another critical length, L_0 say, such that for $L > L_0$ more than one solution exists. We analyse this phenomenon below.

From an ecological viewpoint we would like to know the critical domain size L_0 when the maximum population can be in the outbreak regime; that is, $u_m > u_2$ in Figure 2.20(a). This is determined from numerical integration of (2.84) and is shown in Figure 2.20(b). When $L > L_0$ we see from Figure 2.20(b) that there are three possible solutions with different u_m. The ones with u in the refuge and outbreak regimes are

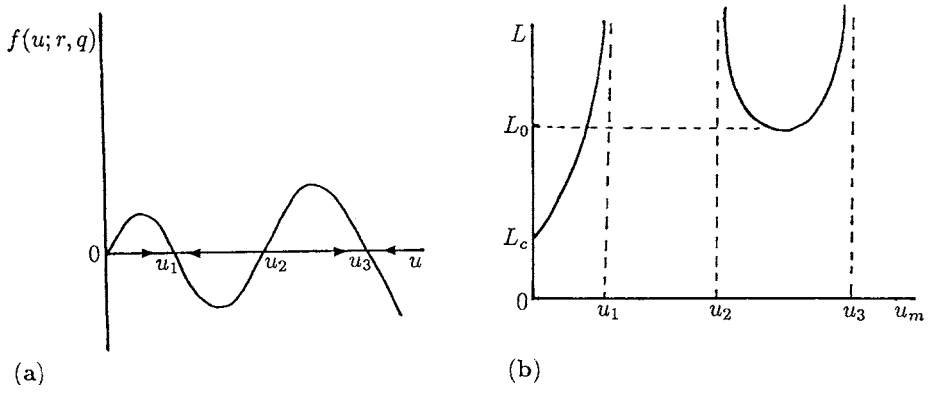

Figure 2.20. (**a**) Typical dynamics $f(u; r, q)$ for the spruce budworm as defined by (2.85). (**b**) The maximum population u_m as a function of the domain size L. For $u_m < u_1$ the population is in the refuge range, whereas $u_m > u_2$ for $L > L_0$, which is in the outbreak regime.

stable and the other, the middle one, is unstable. Which solution is obtained depends on the initial conditions. Later we shall consider possible ecological uses of this model in the control of the budworm. Before doing so we describe a useful technique for determining approximate values for L_0 analytically.

Analytical Method for Determining Critical Domain Sizes and Maximum Populations

The numerical evaluation of $u_m(L)$ when there are three possible u_m's for a given L is not completely trivial. Since the critical domain size L_0, which sustains an outbreak, is one of the important and useful quantities we require for practical applications, we now derive an ad hoc analytical method for obtaining it by exploiting an idea described by Lions (1982).

The steady state problem is defined by (2.81). Let us rescale the problem so that the domain is $x \in (0, 1)$ by setting $x \to x/L$ so that the equivalent $U(x)$ is now determined from

$$DU'' + L^2 f(U) = 0, \quad U(0) = U(1) = 0. \tag{2.86}$$

From Figure 2.19 the solution looks qualitatively like a sine. With the rescaling so that $x \in (0, 1)$ the solution is thus qualitatively like $\sin(\pi x)$. This means that $U'' \approx -\pi^2 U$ and so the last equation implies

$$-D\pi^2 U + L^2 f(U) \approx 0 \quad \Rightarrow \quad \frac{D\pi^2 U}{L^2} \approx f(U). \tag{2.87}$$

We are interested in the value of L such that the last equation has three roots for U: this corresponds to the situation in Figure 2.20(b) when $L > L_0$. Thus all we need do to determine an approximate L_0 is simply to plot the last equation as in Figure 2.21 and determine the value L such that three solutions exist.

For a fixed dispersal coefficient D we see how the solutions U vary with L. As L increases from $L \approx 0$ the first critical L, L_c, is given when the straight line $D\pi^2 U/L^2$ intersects $f(U)$, that is, when $D\pi^2/L^2 = f'(0)$, as given by (2.80). As L increases further we can determine the critical L_0 when $D\pi^2 U/L_0^2$ is tangent to the curve $f(U)$, at P in Figure 2.21. It is simply a matter of determining L which gives a double positive root of

$$\frac{D\pi^2 U}{L^2} = f(U).$$

It is left as an exercise (Exercise 7) to determine L_0 as a function of r, q and D when $f(U)$ is given by (2.85). For any given L the procedure also determines, approximately, the maximum U. From Figure 2.21 we clearly obtain by this procedure a figure similar to that in Figure 2.20(b). This simple procedure is quite general for determining critical domain sizes, both for structure bifurcating from the zero steady state and for domains which can sustain larger populations arising from population dynamics with multiple positive steady states.

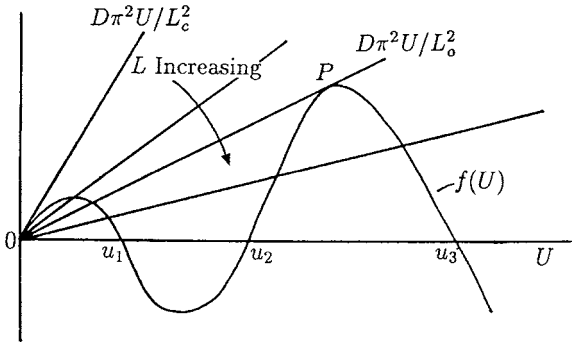

Figure 2.21. Approximate analytic procedure for determining the critical domain sizes L_c and L_0 which can sustain respectively a refuge and an outbreak in the species population where the dynamics is described by $f(U)$. L_c is the value of L when $D\pi^2U/L^2$ is tangent to $f(U)$ at $U = 0$. L_0 is given by the value of L when $D\pi U/L^2$ is just tangent to $F(U)$ at P.

2.8 Spatial Patterns in Scalar Population Interaction Diffusion Equations with Convection: Ecological Control Strategies

In practical applications of such models the domains of interest are usually two-dimensional and so we must consider (2.76). Also, with insect pests in mind, the exterior region is not generally completely hostile, so $u = 0$ on the boundaries is too restrictive a condition. Here we briefly consider a one- and two-dimensional problem in which the exterior domain is not completely hostile and there is a prevailing wind. This is common in many insect dispersal situations and can modify the spatial distribution of the population in a major way.

Suppose, for algebraic simplicity, that the two-dimensional domain is a rectangular region B defined by $0 \leq x \leq a$, $0 \leq y \leq b$ having area A. The completely hostile problem is then given by

$$\begin{aligned} u_t &= f(u) + D\left(\frac{\partial^2 u}{\partial x^2} + \frac{\partial^2 u}{\partial y^2}\right), \\ u &= 0 \quad \text{for} \quad (x, y) \text{ on } \partial B. \end{aligned} \tag{2.88}$$

Following the same procedure as in the last section for u small we get the solution of the linearised problem to be

$$u(x, y, t) = \sum_{n,m} a_{mn} \exp\left\{\left[f'(0) - D\pi^2\left(\frac{n^2}{a^2} + \frac{m^2}{b^2}\right)\right]t\right\} \sin\frac{n\pi x}{a} \sin\frac{m\pi y}{b}. \tag{2.89}$$

So the critical domain size, which involves both a and b, is given by any combination of a and b such that

$$\frac{a^2b^2}{a^2+b^2} = \frac{D\pi^2}{f'(0)}.$$

Since

$$a^2 + b^2 > 2ab = 2A \quad \Rightarrow \quad \frac{a^2b^2}{a^2+b^2} < \frac{A}{2}$$

we get an inequality estimate for spatial patterning to exist, namely,

$$A > \frac{2D\pi^2}{f'(0)}. \tag{2.90}$$

Estimates for general two-dimensional domains were obtained by Murray and Sperb (1983). Clearly the mathematical problem is that of finding the smallest eigenvalue for the spatial domain considered.

In all the scalar models considered above the spatial patterns obtained have only a single maximum. With completely hostile boundary conditions these are the only type of patterns that can be generated. With two-species reaction diffusion systems, however, we saw that more diverse patterns could be generated. It is natural to ask whether there are ways in which similar multi-peak patterns could be obtained with single-species models in a one-dimensional context. We now show how such patterns could occur.

Suppose there is a constant prevailing wind $\mathbf{w}$ which contributes a convective flux $(\mathbf{w}\cdot\nabla)u$ to the conservation equation for the population $u(\mathbf{r}, t)$. Also suppose that the exterior environment is not completely hostile in which case appropriate boundary conditions are

$$(\mathbf{n}\cdot\nabla)u + hu = 0, \quad \mathbf{r} \text{ on } \partial B, \tag{2.91}$$

where $\mathbf{n}$ is the unit normal to the domain boundary ∂B. The parameter h is a measure of the hostility: $h = \infty$ implies a completely hostile exterior, whereas $h = 0$ implies a closed environment, that is, zero flux boundaries. We briefly consider the latter case later. The mathematical problem is thus

$$u_t + (\mathbf{w}\cdot\nabla)u = f(u) + D\nabla^2 u, \tag{2.92}$$

with boundary conditions (2.91) and given initial distribution $u(\mathbf{r}, 0)$. Here we consider the one-dimensional problem and follow the analysis of Murray and Sperb (1983), who also deal with the two-dimensional analogue and more general aspects of such problems.

The problem we briefly consider is the one-dimensional system which defines the steady state spatially inhomogeneous solutions $U(x)$. From (2.91) and (2.92), since

$$(\mathbf{w}\cdot\nabla)u = w_1 u_x,$$

$$(\mathbf{n}\cdot\nabla)u + hu = 0 \quad \Rightarrow \quad u_x + hu = 0,\ x = L; \quad u_x - hu = 0,\ x = 0,$$

where w_1 is the x-component of the wind $\mathbf{w}$, the mathematical problem for $U(x)$ is

$$\begin{aligned} &DU'' - w_1 U' + f(U) = 0, \\ &U'(0) - hU(0) = 0, \quad U'(L) + hU(L) = 0. \end{aligned} \tag{2.93}$$

We study the problem using phase plane analysis by setting

$$U' = V, \quad DV' = w_1 V - f(U) \quad \Rightarrow \quad \frac{dV}{dU} = \frac{w_1 V - f(U)}{DV}, \tag{2.94}$$

and we look for phase plane trajectories which, from the boundary conditions in (2.93), join any point on one of the following lines to any point on the other line,

$$V = hU, \quad V = -hU. \tag{2.95}$$

The phase plane situation is illustrated in Figures 2.22(a) and (b) as we now show.

Refer first to Figure 2.22(a). From (2.94) we get the sign of dV/dU at any point (U, V). On the curve $V = f(U)/w_1$, $dV/dU = 0$ with dV/dU positive and negative when (U, V) lies respectively above (if $V > 0$) and below it. So, if we start on the boundary line $V = hU$ at say, P, the trajectory will qualitatively be like T_1

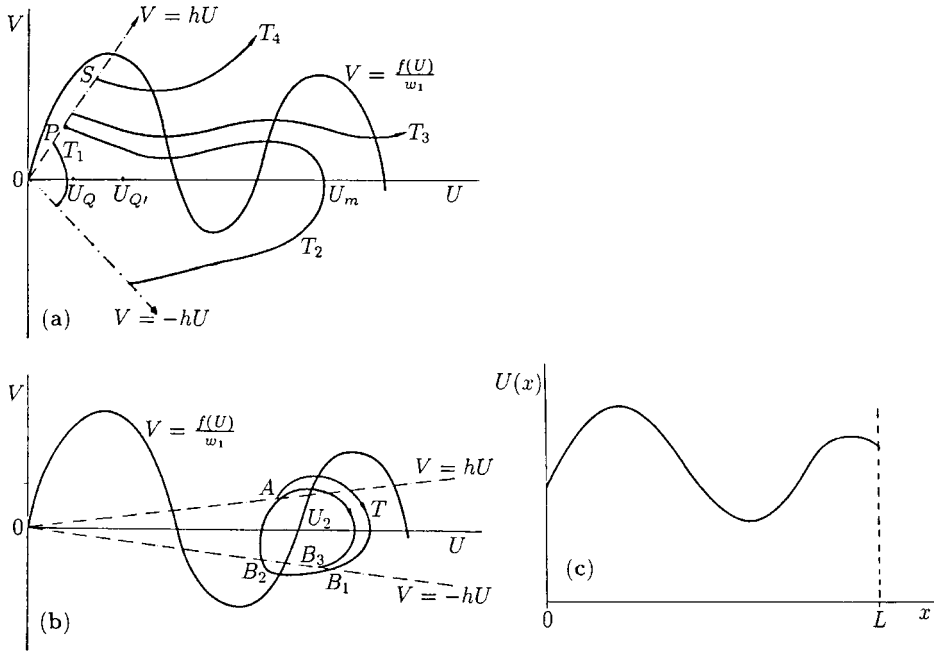

Figure 2.22. (**a**) With h sufficiently large the possible trajectories from $V = hU$ to $V = -hU$ admit solution trajectories like T_1 and T_2 with only a single maximum U_m. (**b**) For small enough h it is possible to have more complex patterns as indicated by the specimen trajectory T. (**c**) A typical solution $U(x)$ for a phase trajectory like T in (**b**).

since $dV/dU < 0$ everywhere on it. If we start at S, say, although the trajectory starts with $dV/dU < 0$, it intersects the $dV/dU = 0$ line and passes through to the region where $dV/dU > 0$ and so the trajectory turns up. The trajectories T_2, T_3 and T_4 are all possible scenarios depending on the parameters and where the solution trajectory starts. T_3 and T_4 are not solution trajectories satisfying (2.94) since they do not terminate on the boundary curve $V = -hU$. T_1 and T_2 are allowable solution paths and each has a single maximum U where the trajectory crosses the $V = 0$ axis.

We now have to relate the corresponding domain length L to these solution trajectories. To be specific let us focus on the trajectory T_2. Denote the part of the solution with $V > 0$ by $V^+(U)$ and that with $V < 0$ by $V^-(U)$. If we now integrate the first equation in (2.94) from U_Q to U'_Q, that is, the U-values at either end of the T_2 trajectory, we get the corresponding length of the domain for the solution represented by T_2 as

$$L = \int_{U_Q}^{U_m} [V^+(U)]^{-1}\, dU + \int_{U_m}^{U'_Q} [V^-(U)]^{-1}\, dU. \tag{2.96}$$

So, for each allowable solution trajectory we can obtain the corresponding size of the solution domain. The qualitative form of the solution $U(x)$ as a function of x can be deduced from the phase trajectory since we know U and U' everywhere on it and from the last equation we can calculate the domain size. With the situation represented by Figure 2.22(a) there can only be a single maximum in $U(x)$. Because of the wind convection term, however, there is no longer the solution symmetry of the solutions as in the last Section 2.7.

Now suppose the exterior hostility decreases, that is, h in (2.95) decreases, so that the boundary lines are now as illustrated in Figure 2.22(b). Proceeding in the same way as for the solution trajectories in Figure 2.22(a) we see that it is possible for a solution to exist corresponding to the trajectory T. On sketching the corresponding solution $U(x)$ we see that here there are two maxima in the domain: see Figure 2.22(c). In this situation, however, we are in fact patching several possible solutions together. Referring to Figure 2.22(b) we see that a possible solution is represented by that part of the trajectory T from A to B_1. It has a single maximum and a domain length L_1 given by the equivalent of (2.96). So if we restrict the domain size to be L_1 this is the relevant solution. However, if we allow a larger L the continuation from B_1 to B_2 is now possible and so the trajectory AB_1B_2 corresponds to a solution of (2.93). Increasing L further we can include the rest of the trajectory to B_3. It is thus possible to have multi-humped solutions if the domain is large enough. The length L corresponding to the solution path T is obtained in exactly the same way as above, using the equivalent of (2.96).

So, for small enough values of h it is possible to have more and more structure as the trajectory winds round the point u_2 in the (U, V) phase plane. For such solutions to exist, of course, it is essential that $w_1 \neq 0$. If $w_1 = 0$ the solutions are symmetric about the U-axis and so no spiral solutions are possible. Thus, a prevailing wind is essential for complex patterning. It also affects the critical domain size for patterns to exist. General results and further analysis are given by Murray and Sperb (1983).

An Insect Pest Control Strategy

Consider now the problem of insect pest control. The forest budworm problem is very much a two-dimensional spatial problem. As we pointed out in Chapter 1, Volume I, Section 1.2, a good control strategy would be to maintain the population at a refuge level. As we also showed in Section 1.2, Volume I it would be strategically advantageous if the dynamics parameters r and q in (2.85) could be changed so that only a single positive steady state exists. This is not really ecologically feasible. With the more realistic spatial problem, however, we have a further possible means of keeping the pest levels within the refuge range by ensuring that their spatial domains are of a size that does not permit populations in the outbreak regime. The arguments go through for two-dimensional domains, but for illustrative purposes let us consider first the one-dimensional situation.

Refer to Figure 2.20(b). If the spatial region were divided up into regions with size $L < L_0$, that is, so that the maximum u_m was always less than u_1, the refuge population level, we would have achieved our goal. So, a possible strategy is to spray the region in strips so that the non-sprayed regions impose an effective $L < L_0$ as in Figure 2.23(a): the solid vertical lines separating the sprayed regions are the boundaries to a completely hostile exterior.

Of course it is not practical to destroy all pests that stray out of the unsprayed region, so a more realistic model is that with boundary conditions (2.91) where some insects can survive outside the untreated domain. The key mathematical problem to be solved then is the determination of the critical width of the insect 'break' L_b. This must be such that the contributions from neighbouring untreated areas do not contribute a sufficient number of insects, which diffuse through the break, to initiate an outbreak in the neighbouring patches even though $L < L_0$, the critical size in isolation. A qualitative population distribution would typically be as shown by the dashed line in Figure 2.23(a).

The two-dimensional analogue is clear but the solution of the optimisation problem is more complicated. First the critical domain A_0 which can sustain an insect pest

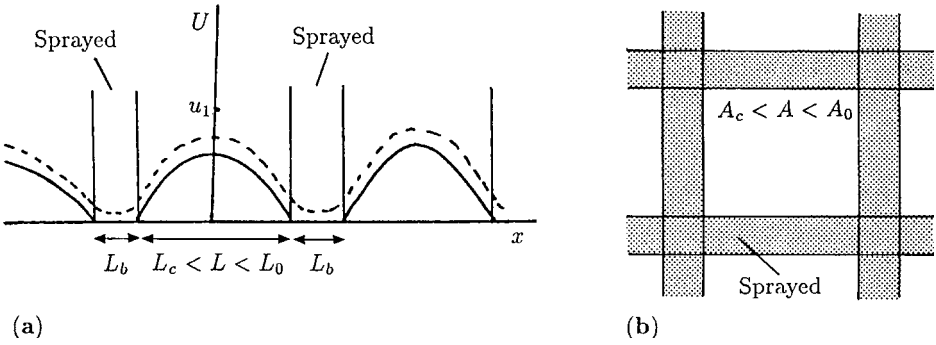

Figure 2.23. (**a**) A possible control strategy to contain the insect pest in a refuge rather than an outbreak environment. Strips—insect 'breaks'—are sprayed to maintain an effective domain size $L < L_0$, the critical size for an outbreak. The broken line is a more typical situation in practice. (**b**) Equivalent two-dimensional analogue where $A > A_c$ is a typical domain which can sustain a pest refuge population but which is not sufficient to sustain an outbreak; that is, $A < A_0$.

outbreak has to be determined for boundary conditions (2.91). Then the width of the sprayed strips has to be determined. It is not a trivial problem to solve, but certainly a possible one. A preliminary investigation of these problems was carried out by Ben-Yu et al. (1986).

Although we have concentrated on the budworm problem the techniques and control strategies are equally applicable to other insect pests. The field of insect dispersal presents some very important ecological problems, such as the control of killer bees now sweeping up through the western United States (see, for example, Taylor 1977) and locust plagues in Africa. Levin (see, for example, 1981a,b) has made realistic and practical studies of these and other problems associated with spatially heterogeneous ecological models. The concept of a break control strategy to prevent the spatial spread of a disease epidemic will be discussed in some detail later in Chapter 13 when we discuss the spatial spread of rabies; it is now in use.

In an interesting ecological application of diffusion-driven instability Hastings et al. (1997) investigated an outbreak of the western tussock moth which had been hypothesised to be the result of a predator–prey interaction between the moths and parasitoids. The model they analyse qualitatively is a two-species system in which the prey do not move. We saw in Chapter 13, Section 13.7, Volume I how the effect of having a percentage of the prey sessile gave rise to counterintuitive results. Hastings et al. (1997) also obtain counterintuitive results by considering a quite general system with typical predator–prey interactions in which the prey does not diffuse. Their new analysis is very simple but highly illuminating. Their approach is reminiscent of that in Section 1.6 on excitable waves for determining where the trajectory for the wave in the phase plane is closed, thereby determining the wavespeed among other things, and revolves around the existence of three possible steady states at each spatial position, two of which are stable, with the possibility of a jump, or rather a steep singular region joining them. They then show that, counterintuitively, the spatial distribution of the prey will have its highest density at the edge of the outbreak domain. This phenomenon has been observed in western tussock moth outbreaks. The role of theory in predicting counterintuitive behaviours and subsequent experimental or observational confirmation is particularly important when, as is frequently the case, the plethora of observational facts is bewildering rather than illuminating. The article by Kareiva (1990) is particularly relevant to this relation of theory to data.

2.9 Nonexistence of Spatial Patterns in Reaction Diffusion Systems: General and Particular Results

The scalar one-dimensional reaction diffusion system with zero flux is typically of the form

$$\begin{aligned} &u_t = f(u) + u_{xx}, \quad x \in (0,1), \quad t > 0 \\ &u_x(0,t) = u_x(1,t) = 0, \quad t > 0. \end{aligned} \tag{2.97}$$

Intuitively the only stable solution is the spatially homogeneous one $u = u_0$, the steady state solution of $f(u) = 0$: if there is more than one stable solution of $f(u) = 0$

which will obtain depends on the initial conditions. It can be proved that any spatially nonuniform steady state solution is unstable (the analysis is given in the first edition of this book: it involves estimating eigenvalues). This result does *not* carry over completely to scalar equations in more than one space dimension as has been shown by Matano (1979) in the case where $f(u)$ has two linearly stable steady states. The spatial patterns that can be obtained, however, depend on specific domain boundaries, non-convex to be specific. For example, a dumbbell shaped domain with a sufficiently narrow neck is an example. The pattern depends on the difficulty of diffusionally transporting enough flux of material through the neck to effect a change from one steady state to another so as to achieve homogeneity.

We saw in Sections 2.3 and 2.4 how reaction diffusion systems with zero flux boundary conditions could generate a rich spectrum of spatial patterns if the parameters and kinetics satisfied appropriate conditions: crucially the diffusion coefficients of the reactants had to be different. Here we show that for general multi-species systems patterning can be destroyed if the diffusion is sufficiently large. This is intuitively what we might expect, but it is not obvious if the diffusion coefficients are unequal. This we now prove. The analysis, as we show, gives another condition involving the kinetic relaxation time of the mechanism which is certainly not immediately obvious.

Before discussing the multi-species multi-dimensional theory it is pedagogically helpful to consider first the general one-dimensional two-species reaction diffusion system

$$\begin{aligned} u_t &= f(u, v) + D_1 u_{xx}, \\ v_t &= g(u, v) + D_2 v_{xx} \end{aligned} \tag{2.98}$$

with zero flux boundary conditions and initial conditions

$$\begin{aligned} u_x(0, t) = u_x(1, t) = v_x(0, t) = v_x(1, t) = 0 \\ u(x, 0) = u_0(x), \\ v(x, 0) = v_0(x), \end{aligned} \tag{2.99}$$

where $u_0'(x)$ and $v_0'(x)$ are zero on $x = 0, 1$. Define an energy integral E by

$$E(t) = \frac{1}{2} \int_0^1 (u_x^2 + v_x^2)\, dx. \tag{2.100}$$

This is, except for the $1/2$, the heterogeneity function introduced in (2.52). Differentiate E with respect to t to get

$$\frac{dE}{dt} = \int_0^1 (u_x u_{xt} + v_x v_{xt})\, dx$$

and substitute from (2.98), on differentiating with respect to x, to get, on integrating by parts,

$$\begin{aligned}\frac{dE}{dt} &= \int_0^1 [u_x(D_1u_{xx})_x + u_x(f_uu_x + f_vv_x) \\ &\quad + v_x(D_2v_{xx})_x + v_x(g_uu_x + g_vv_x)]\,dx, \\ &= [u_xD_1u_{xx} + v_xD_2v_{xx}]_0^1 - \int_0^1 (D_1u_{xx}^2 + D_2v_{xx}^2)\,dx \\ &\quad + \int_0^1 \left[f_uu_x^2 + g_vv_x^2 + (f_v + g_u)u_xv_x\right] dx.\end{aligned}$$

Because of the zero flux conditions the integrated terms are zero.

Now define the quantities d and m by

$$d = \min(D_1, D_2), \quad m = \max_{u,v}\left(f_u^2 + f_v^2 + g_u^2 + g_v^2\right)^{1/2}, \tag{2.101}$$

where $\max_{u,v}$ means the maximum for u and v taking all possible solution values. If we want we could define m by some norm involving the derivatives of f and g; it is not crucial for our result. From the equation for dE/dt, with these definitions, we then have

$$\begin{aligned}\frac{dE}{dt} &\le -d\int_0^1 (u_{xx}^2 + v_{xx}^2)\,dx + 4m\int_0^1 (u_x^2 + v_x^2)\,dx \\ &\le (4m - 2\pi^2 d)E,\end{aligned} \tag{2.102}$$

where we have used the result

$$\int_0^1 u_{xx}^2\,dx \ge \pi^2\int_0^1 u_x^2\,dx \tag{2.103}$$

with a similar inequality for v; see Appendix A for a derivation of (2.103).

From the inequality (2.102) we now see that if the minimum diffusion coefficient d, from (2.101), is large enough so that $(4m - 2\pi^2 d) < 0$ then $dE/dt < 0$, which implies that $E \to 0$ as $t \to \infty$ since $E(t) \ge 0$. This implies, with the definition of E from (2.100), that $u_x \to 0$ and $v_x \to 0$ which implies spatial homogeneity in the solutions u and v as $t \to \infty$. The result is not precise since there are many appropriate choices for m; (2.101) is just one example. The purpose of the result is simply to show that it is possible for diffusion to dampen *all* spatial heterogeneities. We comment briefly on the biological implication of this result below.

We now prove the analogous result for general reaction diffusion systems. Consider

$$\mathbf{u}_t = \mathbf{f}(\mathbf{u}) + D\nabla^2\mathbf{u}, \tag{2.104}$$

where $\mathbf{u}$, with components u_i, $i = 1, 2, \ldots, n$, is the vector of concentrations or populations, and D is a diagonal matrix of the positive diffusion coefficients D_i, $i = 1, 2, \ldots, n$ and $\mathbf{f}$ is the nonlinear kinetics. The results we prove are also valid for a diffusion matrix with certain cross-diffusion terms, but for simplicity here we only deal with (2.104). Zero flux boundary and initial conditions for $\mathbf{u}$ are

$$(\mathbf{n}\cdot\nabla)\mathbf{u}=0 \quad \mathbf{r}\text{ on }\partial B, \quad \mathbf{u}(\mathbf{r},0)=\mathbf{u}_0(\mathbf{r}), \tag{2.105}$$

where $\mathbf{n}$ is the unit outward normal to ∂B, the boundary of the domain B. As before we assume that all solutions $\mathbf{u}$ are bounded for all $t \geq 0$. Practically this is effectively assured if a confined set exists for the reaction kinetics.

We now generalise the previous analysis; it helps to refer to the equivalent steps in the above. Define the energy $E(t)$ by

$$E(t)=\frac{1}{2}\int_B ||\nabla\mathbf{u}||^2\,d\mathbf{r}, \tag{2.106}$$

where the norm

$$||\nabla\mathbf{u}||^2=\sum_{i=1}^{n}|\nabla u_i|^2.$$

Let d be the smallest eigenvalue of the matrix D, which in the case of a diagonal matrix is simply the smallest diffusion coefficient of all the species. Now define

$$m=\max_{\mathbf{u}}||\nabla_{\mathbf{u}}\mathbf{f}(\mathbf{u})||, \tag{2.107}$$

where $\mathbf{u}$ takes on all possible solution values and $\nabla_{\mathbf{u}}$ is the gradient operator with respect to $\mathbf{u}$.

Differentiating $E(t)$ in (2.106), using integration by parts, the boundary conditions (2.105) and the original system (2.104) we get, with $\langle\mathbf{a},\mathbf{b}\rangle$ denoting the inner product of $\mathbf{a}$ and $\mathbf{b}$,

$$\begin{aligned}\frac{dE}{dt}&=\int_B\langle\nabla\mathbf{u},\nabla\mathbf{u}_t\rangle\,d\mathbf{r}\\&=\int_B\langle\nabla\mathbf{u},\nabla D\nabla^2\mathbf{u}\rangle\,d\mathbf{r}+\int_B\langle\nabla\mathbf{u},\nabla\mathbf{f}\rangle\,d\mathbf{r}\\&=\int_{\partial B}\langle\nabla\mathbf{u},D\nabla^2\mathbf{u}\rangle\,d\mathbf{r}-\int_B\langle\nabla^2\mathbf{u},D\nabla^2\mathbf{u}\rangle\,d\mathbf{r}+\int_B\langle\nabla\mathbf{u},\nabla_{\mathbf{u}}\mathbf{f}\cdot\nabla\mathbf{u}\rangle\,d\mathbf{r}\\&\leq -d\int_B|\nabla^2\mathbf{u}|^2\,d\mathbf{r}+mE.\end{aligned} \tag{2.108}$$

In Appendix A we show that when $(\mathbf{n}\cdot\nabla)\mathbf{u}=0$ on ∂B,

$$\int_B|\nabla^2\mathbf{u}|^2\,d\mathbf{r}\geq\mu\int_B||\nabla\mathbf{u}||^2\,d\mathbf{r}, \tag{2.109}$$

where μ is the least positive eigenvalue of

$$\nabla^2\phi+\mu\phi=0, \quad (\mathbf{n}\cdot\nabla)\phi=0 \quad \mathbf{r}\text{ on }\partial B,$$

where ϕ is a scalar. Using the result (2.109) in (2.108) we get

$$\frac{dE}{dt} \leq (m - 2\mu d)E \quad \Rightarrow \quad \lim_{t\to\infty} E(t) = 0 \quad \text{if} \quad m < 2\mu d \tag{2.110}$$

and so, once again, if the smallest diffusion coefficient is large enough this implies that $\nabla \mathbf{u} \to 0$ and so all spatial patterns tend to zero as $t \to \infty$.

Othmer (1977) has pointed out that the parameter m defined by (2.101) and (2.107) is a measure of the sensitivity of the reaction rates to changes in $\mathbf{u}$ since $1/m$ is the shortest kinetic relaxation time of the mechanism. On the other hand $1/(2\mu d)$ is a measure of the longest diffusion time. So the result (2.110), which is $1/m > 1/(2\mu d)$, then implies that if the shortest relaxation time for the kinetics is greater than the longest diffusion time then all spatial patterning will die out as $t \to \infty$. The mechanism will then be governed solely by kinetics dynamics. Remember that the solution of the latter can include limit cycle oscillations.

Suppose we consider the one-dimensional situation with a typical embryological domain of interest, say, $L = O$ (1 mm). With $d = O(10^{-6}\text{cm}^2\text{s}^{-1})$ the result (2.110) then implies that homogeneity will result if the shortest relaxation time of the kinetics $1/m > L^2/(2\pi^2 d)$, that is, a time of $O(500\text{ s})$.

Consider the general system (2.104) rescaled so that the length scale is 1 and the diffusion coefficients are scaled relative to D_1 say. Now return to the formulation used earlier, in (2.10), for instance, in which the scale γ appears with the kinetics in the form $\gamma\mathbf{f}$. The effect of this on the condition (2.110) now produces $\gamma m - 2\mu < 0$ as the stability requirement. We immediately see from this form that there is a critical γ, proportional to the domain area, which in one dimension is (length)^2, below which no structure can exist. This is of course a similar result to the one we found in Sections 2.3 and 2.4.

We should reiterate that the results here give qualitative bounds and not estimates for the various parameters associated with the model mechanisms. The evaluation of an appropriate m is not easy. In Sections 2.3 and 2.4 we derived specific quantitative relations between the parameters, when the kinetics were of a particular class, to give spatially structured solutions. The general results in this section, however, apply to all types of kinetics, oscillatory or otherwise, as long as the solutions are bounded.

In this chapter we have dealt primarily with reaction or population interaction kinetics which, in the absence of diffusion, do not exhibit oscillatory behaviour in the restricted regions of parameter space which we have considered. We may ask what kind of spatial structure can be obtained when oscillatory kinetics is coupled with diffusion. We saw in Chapter 1 that such a combination could give rise to travelling wavetrains when the domain is infinite. If the domain is finite we could anticipate a kind of regular sloshing around within the domain which is a reflection of the existence of spatially and temporally unstable modes. This can in fact occur but it is not always so. One case to point is the classical Lotka–Volterra system with equal diffusion coefficients for the species. Murray (1975) showed that in a finite domain all spatial heterogeneities must die out (see Exercise 11).

There are now several pattern formation mechanisms, other than reaction-diffusion-chemotaxis systems. One of the best critical and thorough reviews on models for self-organisation in development is by Wittenberg (1993). He describes the models in detail and compares and critically reviews several of the diverse mechanisms includ-

ing reaction-diffusion-chemotaxis systems, mechanochemical mechanisms and cellular automaton models.

In the next chapter we shall discuss several specific practical biological pattern formation problems. In later chapters we shall describe other mechanisms which can generate spatial patterns. An important system which has been widely studied is the reaction-diffusion-chemotaxis mechanism for generating aggregation patterns in bacteria and also for slime mould amoebae, one model for which we derived in Chapter 11, Volume I, Section 11.4. Using exactly the same kind of analysis we discussed above for diffusion-driven instability we can show how spatial patterns can arise in these model equations and the conditions on the parameters under which this will happen (see Exercise 9). As mentioned above these chemotaxis systems are becoming increasingly important with the upsurge in interest in bacterial patterns and is the reason for including Chapter 5 below. We discuss other quite different applications of cell-chemotaxis mechanisms in Chapter 4 when we consider the effect of growing domains on patterning, such as the complex patterning observed on snakes.

Exercises

1. Determine the appropriate nondimensionalisation for the reaction kinetics in (2.4) and (2.5) which result in the forms (2.8).

2. An activator–inhibitor reaction diffusion system in dimensionless form is given by

$$u_t = \frac{u^2}{v} - bu + u_{xx}, \quad v_t = u^2 - v + dv_{xx},$$

where b and d are positive constants. Which is the activator and which the inhibitor? Determine the positive steady states and show, by an examination of the eigenvalues in a linear stability analysis of the diffusionless situation, that the reaction kinetics cannot exhibit oscillatory solutions if $b < 1$.

Determine the conditions for the steady state to be driven unstable by diffusion. Show that the parameter domain for diffusion-driven instability is given by $0 < b < 1$, $db > 3 + 2\sqrt{2}$ and sketch the (b, d) parameter space in which diffusion-driven instability occurs. Further show that at the bifurcation to such an instability the critical wavenumber k_c is given by $k_c^2 = (1 + \sqrt{2})/d$.

3. An activator–inhibitor reaction diffusion system with activator inhibition is modelled by

$$\begin{aligned} u_t &= a - bu + \frac{u^2}{v(1 + Ku^2)} + u_{xx}, \\ v_t &= u^2 - v + dv_{xx}, \end{aligned}$$

where K is a measure of the inhibition and a, b and d are constants. Sketch the null clines for positive b, various $K > 0$ and positive or negative a.

Show that the (a, b) Turing (parameter) space for diffusion-driven instability is defined parametrically by

$$a = bu_0 - (1 + Ku_0^2)^2$$

combined with

$$b > 2[u(1 + Ku_0^2)]^{-1} - 1, \quad b > 0, \quad b > 2[u(1 + Ku_0^2)]^{-2} - \frac{1}{d},$$
$$b < 2[u(1 + Ku_0^2)]^{-2} - 2\sqrt{2}[du(1 + Ku_0^2)]^{-1/2} + \frac{1}{d},$$

where the parameter u_0 takes on all values in the range $(0, \infty)$. Sketch the Turing space for (i) $K = 0$ and (ii) $K \neq 0$ for various d (Murray 1982).

4. Determine the relevant axisymmetric eigenfunctions $\mathbf{W}$ and eigenvalues k^2 for the circular domain bounded by R defined by

$$\nabla^2\mathbf{W} + k^2\mathbf{W} = 0, \quad \frac{d\mathbf{W}}{dr} = 0 \text{ on } r = R.$$

Given that the linearly unstable range of wavenumbers k^2 for the reaction diffusion mechanism (2.7) is given by

$$\gamma L(a, b, d) < k^2 < \gamma M(a, b, d),$$

where L and M are defined by (2.38), determine the critical radius R_c of the domain below which no spatial pattern can be generated. For R just greater than R_c sketch the spatial pattern you would expect to evolve.

5. Consider the reaction diffusion mechanism given by

$$u_t = \gamma\left(\frac{u^2}{v} - bu\right) + u_{xx}, \quad v_t = \gamma(u^2 - v) + dv_{xx},$$

where γ, b and d are positive constants. For the domain $0 \leq x \leq 1$ with zero flux conditions determine the dispersion relation $\lambda(k^2)$ as a function of the wavenumbers k of small spatial perturbations about the uniform steady state. Is it possible with this mechanism to isolate successive modes by judicious variation of the parameters? Is there a bound on the excitable modes as $d \to \infty$ with b and γ fixed?

6. Suppose fishing is regulated within a zone H km from a country's shore (taken to be a straight line) but outside of this zone overfishing is so excessive that the population is effectively zero. Assume that the fish reproduce logistically, disperse by diffusion and within the zone are harvested with an effort E. Justify the following model for the fish population $u(x, t)$.

$$u_t = ru\left(1 - \frac{u}{K}\right) - EU + Du_{xx},$$
$$u = 0 \text{ on } x = H, \quad u_x = 0 \text{ on } x = 0,$$

where r, K, $E(< r)$ and D are positive constants.

If the fish stock is not to collapse show that the fishing zone H must be greater than $\frac{\pi}{2}[D/(r-E)]^{1/2}$ km. Briefly discuss any ecological implications.

7. Use the approximation method described in Section 2.7 to determine analytically the critical length L_0 as function of r, q and D such that an outbreak can exist in the spruce budworm population model

$$u_t = ru\left(1 - \frac{u}{q}\right) - \frac{u^2}{1+u^2} + Du_{xx}, \quad u = 0 \text{ on } x = 0, 1.$$

Determine the maximum population u_m when $L = L_0$.

8. Consider the Lotka–Volterra predator–prey system (see Chapter 3, Volume I, Section 3.1) with diffusion given by

$$u_t = u(1 - v) + Du_{xx}, \quad v_t = av(u - 1) + Dv_{xx}$$

in the domain $0 \leq x \leq 1$ with zero flux boundary conditions. By multiplying the first equation by $a(u-1)$ and the second by $(v-1)$ show that

$$S_t = DS_{xx} - D\sigma^2,$$
$$S = au + v - \ln(u^a v), \quad \sigma^2 = a\left(\frac{u_x}{u}\right)^2 + \left(\frac{v_x}{v}\right)^2 \geq 0.$$

Determine the minimum S for all u and v. Show that necessarily $\sigma \to 0$ as $t \to \infty$ by supposing σ^2 tends to a nonzero bound, the consequences of which are not possible. Hence deduce that no spatial patterns can be generated by this model in a finite domain with zero flux boundary conditions.

(This result can also be obtained rigorously, using maximum principles; the detailed analysis is given by Murray (1975).)

9. The amoebae of the slime mould *Dictyostelium discoideum*, with density $n(x, t)$, secrete a chemical attractant, cyclic-AMP, and spatial aggregations of amoebae start to form. One of the models for this process (and discussed in Section 11.4, Volume I) gives rise to the system of equations, which in their one-dimensional form, are

$$n_t = D_n n_{xx} - \chi(na_x)_x, \quad a_t = hn - ka + D_a a_{xx},$$

where a is the attractant concentration and h, k, χ and the diffusion coefficients D_n and D_a are all positive constants. Nondimensionalise the system.

Consider (i) a finite domain with zero flux boundary conditions and (ii) an infinite domain. Examine the linear stability about the steady state (which intro-

duces a further parameter here), derive the dispersion relation and discuss the role of the various parameter groupings. Hence obtain the conditions on the parameters and domain size for the mechanism to initiate spatially heterogeneous solutions.

Experimentally the chemotactic parameter χ increases during the life cycle of the slime mould. Using χ as the bifurcation parameter determine the critical wavelength when the system bifurcates to spatially structured solutions in an infinite domain. In the finite domain situation examine the bifurcating instability as the domain is increased.

Briefly describe the physical processes operating and explain intuitively how spatial aggregation takes place.

10. Consider the dimensionless reaction anisotropic diffusion system

$$\frac{\partial u}{\partial t} = \gamma f(u, v) + d_1 \frac{\partial^2 u}{\partial x^2} + d_2 \frac{\partial^2 u}{\partial y^2},$$

$$\frac{\partial v}{\partial t} = \gamma g(u, v) + d_3 \frac{\partial^2 u}{\partial x^2} + d_4 \frac{\partial^2 u}{\partial y^2}.$$

In the absence of diffusion the steady state $\mathbf{u} = (u_0, v_0)$ is stable. By carrying out a linear analysis about the steady state by looking for solutions in the form $\mathbf{u} - \mathbf{u_0} \propto e^{\lambda t + i(k_x x + k_y y)}$, where k_x and k_y are the wavenumbers, show that if

$$H(k_x^2, k_y^2) = d_1 d_3 k_x^4 + p_1 k_x^2 k_y^2 + d_2 d_4 k_y^4 - \gamma p_2 k_x^2 - \gamma k_y^2 p_3 + \gamma^2 (f_u g_v - f_v g_u),$$

where

$$p_1 = d_1 d_4 + d_2 d_3, \quad p_2 = d_3 f_u + d_1 g_v, \quad p_3 = d_4 f_u + d_2 g_v$$

is such that $H < 0$ for some $k_x^2 k_y^2 \neq 0$ then the system can be diffusionally unstable to spatial perturbations. The maximum linear growth is given by the values k_x^2 and k_y^2 which give the minimum of $H(k_x^2, k_y^2)$. Show that the minimum of H is given by

$$\begin{bmatrix} k_x^2 \\ k_y^2 \end{bmatrix} = -\gamma \frac{(d_1 d_4 - d_2 d_3)}{(d_1 d_4 - d_2 d_3)^2} \begin{bmatrix} -d_4 f_u + d_2 g_v \\ -d_1 g_v + d_3 f_u \end{bmatrix}.$$

For a spatial pattern to evolve we need real values of k_x, k_y which requires, from the last equation, that

$$(d_1 d_4 - d_2 d_3) \begin{bmatrix} -d_4 f_u + d_2 g_v \\ -d_1 g_v + d_3 f_u \end{bmatrix} < \begin{bmatrix} 0 \\ 0 \end{bmatrix}.$$

By considering the two cases $(d_1 d_4 - d_2 d_3) < 0$ and $(d_1 d_4 - d_2 d_3) > 0$ show that the minimum of H does not lie in the first quadrant of the $k_x^2 - k_y^2$ plane and that diffusion-driven instability will first occur, for increasing ratios d_3/d_1, d_4/d_2 on one of the axial boundaries of the positive quadrant.

By setting k_x^2, k_y^2 equal to 0 in turn in the expression for H show that the conditions for diffusion-driven instability are

$$d_4 f_u + d_2 g_v > 0, \quad d_3 f_u + d_1 g_v > 0$$
$$(d_4 f_u - d_2 g_v)^2 + 4 d_2 d_4 f_v g_u > 0, \quad (d_3 f_u - d_1 g_v)^2 + 4 d_1 d_3 f_v g_u > 0$$

so for it to occur $(d_3/d_1) > d_c$ and/or $(d_4/d_2) > d_c$ where

$$d_c = -\frac{1}{f_u^2}\left[(2 f_v g_u - f_u g_v) + [(2 f_v g_u - f_u g_v)^2 - f_u^2 g_v^2]^{1/2}\right].$$

Now consider the rectangular domain $0 < x < a, 0 < y < b$ with zero flux boundary conditions with a, b constants with a sufficiently greater than b so that the domain is a relatively thin rectangular domain. Show that it is possible to have the first unstable mode 2 bifurcation result in a striped pattern along the rectangle if the diffusion coefficient ratio in one direction exceeds the critical ratio. (Such a result is what we would expect intuitively since if only one ratio, $d_4/d_2 > d_c$, then the diffusion ratio in the x-direction is less than the critical ratio and we would expect spatial variation only in the y-direction, hence a striped pattern along the rectangle. A nonlinear analysis of this problem shows that such a pattern is stable. It further shows that if both ratios exceed the critical ratio a stable modulated (wavy) stripe pattern solution can be obtained along the rectangle.)

11. Suppose that a two-species reaction diffusion mechanism in u and v generates steady state spatial patterns $U(x)$, $V(x)$ in a one-dimensional domain of size L with zero flux boundary conditions $u_x = v_x = 0$ at both boundaries $x = 0$ and $x = L$. Consider the heterogeneity functions defined by

$$H_G(w) = \frac{1}{L}\int_0^L w_x \, dx, \quad H_S(w) = \frac{1}{L}\int_0^L [w_x - H_G(w)]^2 \, dx.$$

Biologically the first of these simply measures the gradient while the second measures the deviation from the simple gradient. Show that the heterogeneity or energy integral

$$H(t) = \frac{1}{L}\int_0^L (U'^2 + V'^2) \, dx = [H_G(U)]^2 + [H_G(V)]^2 + H_S(U) + H_S(V).$$

(Berding 1987)

12. Show that the reaction diffusion mechanism

$$\mathbf{u}_t = \mathbf{f}(\mathbf{u}) + D\nabla^2 \mathbf{u},$$

where the concentration vector $\mathbf{u}$ has n components, D is a diagonal diffusion matrix with elements d_i, $i = 1, 2, \ldots, n$ and $\mathbf{f}$ is the nonlinear kinetics, linearises about a positive steady state to

$$\mathbf{w}_t = A\mathbf{w} + D\nabla^2\mathbf{w},$$

where A is the Jacobian matrix of $\mathbf{f}$ at the steady state.

Let k be the eigenvalue of the problem defined by

$$\nabla^2\mathbf{W} + k^2\mathbf{W} = 0, \quad (\mathbf{n}\cdot\nabla)\mathbf{W} = 0 \quad \mathbf{r} \text{ on } \partial B.$$

On setting $\mathbf{w} \propto \exp[\lambda t + i\mathbf{k}\cdot\mathbf{r})$ show that the dispersion relation $\lambda(k^2)$ is given by the solutions of the characteristic polynomial

$$P(\lambda) = |\, A - k^2 D - \lambda I \,| = 0.$$

Denote the eigenvalues of $P(\lambda)$, with and without diffusion, by λ_i^+ and λ_i^- respectively. Diffusion-driven instability occurs if $\mathrm{Re}\,\lambda_i^- < 0, i = 1, 2, \ldots, n$ and at least one $\mathrm{Re}\,\lambda_i^+ > 0$ for some $k^2 \neq 0$.

From matrix algebra there exists a transformation T such that

$$|\, A - \lambda I \,| = |\, T^{-1}(A - \lambda I)T \,| = \prod_{i=1}^{n}(\lambda_i^- - \lambda).$$

Use this result and the fact that $\mathrm{Re}\,\lambda_i^- < 0$ to show that if $d_i = d$ for all i then $\mathrm{Re}\,\lambda_i^+ < 0$ for all i and hence that a necessary condition for diffusion-driven instability is that at least one diffusion coefficient is different from the rest.

13. The linearisation of a reaction diffusion mechanism about a positive steady state is

$$\mathbf{w}_t = A\mathbf{w} + D\nabla^2\mathbf{w},$$

where A is the Jacobian matrix of the reaction kinetics evaluated at the steady state.

If the matrix $A + A^T$, where T denotes the transpose, is stable this means that all of its eigenvalues λ are real and negative. Show that $\mathbf{w}\cdot A\mathbf{w} < -\delta\mathbf{w}\cdot\mathbf{w}$, for some $\delta > 0$.

[Hint: By considering $\mathbf{w}_t = A\mathbf{w}$ first show that $(\mathbf{w}^2)_t = 2\mathbf{w}A\mathbf{w}$. Then show that $\mathbf{w}_t^T\cdot\mathbf{w} = \mathbf{w}^T A^T\mathbf{w}$ and $\mathbf{w}^T\cdot\mathbf{w}_t = \mathbf{w}^T A\mathbf{w}$ to obtain $(\mathbf{w}^2)_t = \mathbf{w}^T(A + A^T)\mathbf{w}$. Thus deduce that $\mathbf{w}A\mathbf{w} = (1/2)\mathbf{w}^T(A^T + A)\mathbf{w} < -\delta\mathbf{w}\cdot\mathbf{w}$ for some $\delta > 0$.]

Let k^2 be the eigenvalues of the eigenvalue problem

$$\nabla^2\mathbf{w} + k^2\mathbf{w} = 0.$$

By considering dE/dt, where

$$E(t) = \int_B \mathbf{w}\cdot\mathbf{w}\, d\mathbf{r}$$

with B the spatial domain, show that $\mathbf{w}^2 \to 0$ as $t \to \infty$ and hence that such reaction diffusion systems cannot generate spatial patterns if the Jacobian matrix is of this particular form.